U.PORTO

PROGRAMA DOUTORAL
BIOLOGIA BÁSICA E APLICADA

Contribution of human iPSCs to the study of neuron development and disease modelling *in vivo*

Raquel Real

D
2019

Raquel Real. Human iPSCs and disease modelling *in vivo*

Contribution of human iPSCs to the study of neuron development and disease modelling *in vivo*

Raquel Maria Coelho Real

D.ICBAS **2019**

SEDE ADMINISTRATIVA

INSTITUTO DE CIÊNCIAS BIOMÉDICAS ABEL SALAZAR
FACULDADE DE CIÊNCIAS
FACULDADE DE MEDICINA

RAQUEL MARIA COELHO REAL

Contribution of human iPSCs to the study of neuron development and disease modelling in vivo

Tese de Candidatura ao grau de Doutor em Biologia Básica e Aplicada submetida ao Instituto de Ciências Biomédicas Abel Salazar da Universidade do Porto

Orientador – Doutor Vincenzo De Paola
Categoria – Group Leader
Afiliação – Institute of Clinical Sciences, Faculty of Medicine, Imperial College London, UK

Coorientador – Doutor João Carlos Bettencourt de Medeiros Relvas
Categoria – Investigador Principal
Afiliação – Instituto de Biologia Molecular e Celular / Instituto de Inovação e Investigação em Saúde, Universidade do Porto

Raquel Real was supported by a PhD fellowship (PD/BD/52198/2013) awarded by Fundação para a Ciência e Tecnologia (FCT). This work was funded by the Medical Research Council, Alzheimer's Research UK and the Rosetrees Trust.

Acknowledgments

I would like to thank:

My supervisor Vincenzo De Paola, for receiving me in the Synaptic Plasticity and Repair Group and giving me the opportunity to work on this project.

My co-supervisor João Relvas, for the wise advice and encouragement.

Rick Livesey and Manuel Peter, for enthusiastically entering this collaboration.

My mentor Richard Festenstein, for the very helpful career talks.

My lab mates Shabana Khan and Maria Tortora, for their precious help in the final stages of this project and their friendship.

Joana Dopp, for being the best research assistant ever.

Cher Bass, for the helpful discussions on calcium imaging analysis.

Marta and Theresa, the best flatmates anyone could wish for. Thank you for the night-long conversations and the amazing trips together!

The amazing members of the GABBA team, Rita, Delfim and Elsa, for their infinite support.

The GABBA Programme and FCT, for believing in me and giving me the opportunity to pursue my dreams.

The Rosetrees Trust, for the additional funding to support this project.

Helen Figueira, for the talent to solve admin and logistics nightmares.

And finally, my family, who always stood by me.

Contributions

Manuel Peter (The Gurdon Institute, University of Cambridge, UK) conducted the human iPSC-derived neuron differentiation protocol, lentiviral vector preparation and transductions. **Ayiba Momoh** (The Gurdon Institute, University of Cambridge, UK) developed the new Ts21 iPSC line used in this study. **Samuel J. Barnes** (Dementia Research Institute, Imperial College London, UK) developed customised MATLAB software and analysed in vivo calcium time series images. **Mark A. Smith** (Institute of Clinical Sciences, Imperial College London, UK) performed electrophysiological recordings in acute brain slice preparations. **Chad Whilding** (Microscopy Facility, MRC London Institute of Medical Sciences, UK) developed a customised ImageJ (NIH) script for confocal microscopy image analysis. **Graham Knott** (BioEM Facility, EPFL, Switzerland) performed the electron microscopy. **Alessio Strano** (The Gurdon Institute, University of Cambridge, UK) performed the gene expression experiment, the short tandem repeat microarray and the genome-wide SNP array (with Illumina, Inc.). **Emanuela Volpi** (University of Westminster, UK) analysed fluorescent in situ hybridization signals. **Prof Gordon Stamp** (The London Clinic, UK) analysed the histology material stained with Haematoxylin-Eosin for the presence of teratoma. **Shabana Khan** and **Maria Tortora** (Institute of Clinical Sciences, Imperial College London, UK) assisted with the analysis of a subset of confocal immunohistochemistry images. **Joana Dopp** (Institute of Clinical Sciences, Imperial College London, UK) assisted with hNCAM stainings. **Antonio Trabalza** (Institute of Clinical Sciences, Imperial College London, UK) helped with the initial in vivo imaging and surgeries.

Table of contents

RESUMO **4**

ABSTRACT **6**

LIST OF PUBLICATIONS **8**

LIST OF FIGURES **9**

LIST OF TABLES **11**

LIST OF ABBREVIATIONS **12**

CHAPTER 1. INTRODUCTION **14**

1.1 Human induced pluripotent stem cells as model systems for central nervous system development and disease 14

1.2 Neural induction of hiPSCs recapitulates human neurogenesis 15

1.3 hiPSCs generate functional neurons and neural networks 16

1.4 In vivo transplantation of human PSC-derived neurons 17

1.5 Neurons derived from hPSC as model systems of disease 19

1.6 Human iPSCs and Down syndrome 20

1.7 Down syndrome brain phenotypes 21

1.8 Insights from animal models of Down syndrome 22

1.9 iPSCs in the study of Down syndrome 26

CHAPTER 2. METHODS **31**

2.1 Generation of a new Ts21 iPSC line 31

2.2 Animals 31

2.3 Surgical procedures 31

2.4 Live imaging 32

2.5 Two-photon image analysis 33

2.6 Electrophysiology 35

2.7 Immunohistochemistry 35

2.8 Histology 36

2.9 Retrograde trans-synaptic tracing 37

2.10 In situ hybridization 37

2.11 Electron microscopy 38

2.12 Gene expression analysis 38

2.13 Copy number variation detection 39

2.14 Short tandem repeat assay 39

2.15 Statistics and data presentation 39

CHAPTER 3. IN VIVO MODELLING OF HUMAN NEURON DYNAMICS 42

3.1 Cellular characterization of transplanted human grafts 42

3.2 In vivo characterization of human neuron structural development 49

3.3 Functional characterization of transplanted human grafts connectivity 57

3.4 In vivo development of neural network activity in transplanted human grafts 61

CHAPTER 4. IMAGING HUMAN NEURON STRUCTURAL AND FUNCTIONAL DYNAMICS IN DOWN SYNDROME 63

4.1 In vivo modelling of Down syndrome diseases with hiPSC-derived neurons 63

4.2 Ts21 neurons transplanted in vivo recapitulate aspects of the cortical neurogenesis defect in Down syndrome 65

4.3 Ts21 neurons exhibit normal developmental neurite refinement 68

4.4 Ts21 neurons have increased structural synaptic stability 71

4.5 Ts21 neurons show no evidence of major functional defects 75

4.6 In vivo calcium imaging reveals impaired network synchronization in Ts21 neurons 80

CHAPTER 5. DISCUSSION 83

5.1 Transplanted human iPSC-derived neurons as a model system for the study of human neural development 83

5.2 Transplanted human iPSC-derived neurons as a model system for human neurodevelopmental disorders 87

5.3 Concluding remarks 89

REFERENCES 92

APPENDIX 105

Resumo

O estudo dos mecanismos celulares que regulam o desenvolvimento neuronal humano esteve até recentemente praticamente inacessível, mas a descoberta na década passada que células somáticas de dadores podem ser reprogramadas *in vitro* para células estaminais pluripotentes induzidas (iPSCs) permitiu a criação de diversos tipos celulares, incluindo várias classes de neurónios e células da glia. Estas células têm a vantagem de serem facilmente acessíveis e de não estarem sujeitas aos mesmos constrangimentos éticos que o uso de células derivadas de células estaminais embrionárias humanas. Estudos *in vitro* com recurso a neurónios corticais humanos derivados de iPSCs permitiram aprofundar de forma inédita o conhecimento dos processos fundamentais do neurodesenvolvimento humano. No entanto, a longevidade e o potencial de maturação neuronal *in vitro* são limitados, presumivelmente devido à ausência de interações celulares complexas em culturas celulares em monocamada e à ausência de vascularização em culturas tridimensionais de organóides cerebrais. Consequentemente, os sistemas *in vitro* não permitem uma caracterização plena da sequência de eventos que ocorre durante o desenvolvimento neuronal humano. Tal conhecimento é fundamental para compreender as especificidades do desenvolvimento do cérebro humano, e que o distinguem dos cérebros de outros mamíferos. Adicionalmente, o conhecimento detalhado dos processos celulares que caracterizam o normal desenvolvimento neuronal em humanos é fundamental para compreender as múltiplas doenças que afetam o desenvolvimento cerebral em fases precoces da vida, geralmente com consequências devastadoras. No sentido de ultrapassar as limitações dos sistemas *in vitro*, células neuroprogenitoras e neurónios excitatórios prosencefálicos derivados de iPSCs foram transplantados no córtex somato-sensitivo de ratos adultos, nos quais uma janela craniana foi implantada em simultâneo para permitir microscopia multi-fotão intravital. Esta estratégia permitiu efetuar o estudo dinâmico da neuritogénese e sinaptogénese, assim como o desenvolvimento de redes neurais, ao longo de vários meses, no contexto de um microambiente multicelular complexo e vascularizado. Estes estudos revelaram que neurónios humanos em fases precoces do desenvolvimento adquirem plasticidade sináptica estrutural e conectividade, com um padrão de actividade neural de carácter oscilatório e dinâmica espaço-temporal complexa.

A abordagem acima delineada foi ainda utilizada no estudo da síndrome de Down, um distúrbio do neurodesenvolvimento comum e uma causa importante de deficiência intelectual congénita. O progresso no conhecimento dos mecanismos celulares e moleculares

subjacentes à síndrome de Down tem sido dificultado pela disponibilidade limitada de modelos que recapitulem esta complexa condição cromossómica. A compreensão do espectro de fenótipos celulares que caracterizam a síndrome de Down requer um modelo que interrogue todas as fases do desenvolvimento neural, o que torna os estudos em tecidos cerebrais humanos *post mortem* necessariamente incompletos, uma vez que estes apenas permitem observar fenótipos de forma estática. As células estaminais embrionárias humanas, por outro lado, são relativamente inacessíveis e o seu uso limitado por considerações éticas. Os modelos murinos permitem recapitular todas as fases do desenvolvimento neural e dissecar os mecanismos patogénicos da síndrome de Down. Consistentemente, estes modelos têm sido extremamente úteis para aprofundar o conhecimento da patogénese da síndrome de Down, mas existem limitações importantes que importa reconhecer. Em primeiro lugar, na maioria dos modelos murinos nem todos os genes do cromossoma 21 (Hsa21) estão presentes em triplicado. Em segundo lugar, a homologia entre os cromossomas murinos e o Hsa21 é apenas parcial. Finalmente, a regulação genética do Hsa21 é diferente da regulação genética dos cromossomas ortológos em células murinas. Consequentemente, a reprogramação de células somáticas de indivíduos com síndrome de Down em células estaminais pluripotentes induzidas constitui uma preciosa ferramenta para dissecar mecanismos patogénicos nesta síndrome cromossómica complexa. Células neuroprogenitoras, neurónios e astrócitos derivados de iPSCs humanas portadoras de trissomia 21 (Ts21) podem recapitular as fases iniciais do desenvolvimento neural de modo longitudinal. Adicionalmente, a sua transplantação no cérebro murino tem o potencial de revelar fenótipos inéditos, que não são evidentes nos sistemas *in vitro*. De facto, imagiologia multi-fotão de neurónios portadores de trissomia 21 transplantados, provenientes de dois dadores independentes com síndrome de Down, revelou que as estruturas sinápticas são menos dinâmicas nestes neurónios, e que os circuitos neurais nos transplantes com trissomia 21 são muito menos síncronos que os transplantes euploides. Ambos estes fatores têm o potencial de contribuir para os defeitos cognitivos características da síndrome de Down, o que ilustra a potencialidade das técnicas de microscopia *in vivo* de neurónios derivados de doentes para o estudo de distúrbios do neurodesenvolvimento.

Abstract

The study of cellular mechanism of human neuron development has until recently been largely inaccessible, but the discovery in the past decade that somatic donor cells can be reprogrammed in vitro to induced pluripotent stem cells (iPSCs) has enabled the generation of large pools of diverse cell types, including several classes of neurons and glial cells that are readily accessible and not subject to the same ethic constraints as the use of cells derived from human embryonic stem cells. In vitro studies using human iPSC-derived cortical neurons as a model system have advanced our understanding of basic neurodevelopmental processes in a remarkable way. However, there are limitations to the longevity and maturation potential of neurons in vitro, either due to a lack of more complex cell-cell interactions in monolayer neuronal cultures or of inner vascularization in three-dimensional brain organoid cultures. Consequently, in vitro systems are unable to fully characterize the sequence of events that occurs during the development of human neurons. Such knowledge is fundamental to understand the specificities of human brain development that set it apart from other mammalian brains. In addition, an in-depth understanding of the cellular processes that characterize normal neural development in human cells is necessary to comprehend the multiple disorders that affect early brain development, often with devastating consequences.
To overcome the limitation of in vitro systems, human cortical neural progenitor cells (NPCs) and excitatory neurons of forebrain identity derived from iPSCs were transplanted into the somatosensory cortex of adult mice, in which a cranial window was simultaneously implanted for longitudinal multiphoton intravital imaging. This strategy has allowed the dynamic study of neuritogenesis, synaptogenesis and the development of neural network activity over several months, in a multicellular and highly vascularized complex microenvironment, highlighting that human cortical neurons in early stages of development undergo structural synaptic rewiring and acquire circuit connectivity with an oscillatory pattern of neural activity and complex spatiotemporal dynamics.

Down syndrome (DS) is a common neurodevelopmental disorder and a major cause of congenital intellectual disability. Advances in our understanding of the underlying cellular and molecular mechanisms of DS have been hampered by the limited availability of model systems that recapitulate this complex chromosomal condition. Elucidation of the full spectrum of cellular phenotypes of DS requires a model system that interrogates all stages of neural development, which precludes the usefulness of human post-mortem and foetal brain tissue that provide only discrete snapshots of the disease phenotypes. Human embryonic stem cells

are relatively inaccessible and there are often ethical limitations to their use. Animal models can recapitulate all stages of neural development and enable the dissection of the pathogenic mechanisms of DS. These have been extremely useful to our understanding of disease pathogenesis, but there are important caveats. First, triplication of chromosome 21 (Hsa21) genes is incomplete in most DS mouse models. Second, there is only partial mouse-human homology of Hsa21 regions. Finally, Hsa21 genes are differentially regulated in a mouse cellular context and in human cells. Therefore, iPSCs reprogrammed from somatic cells of DS individuals represent a valuable tool to dissect disease mechanisms in this complex disorder. Human iPSC-derived NPCs, neurons and astrocytes that harbour trisomy of chromosome 21 (Ts21) can longitudinally recapitulate the early stages of neural development in DS, and its transplantation into the mouse brain has the potential to uncover new disease phenotypes not evident in in vitro systems. Indeed, longitudinal multiphoton imaging of transplanted Ts21 neurons derived from two independent individuals with DS has uncovered that synaptic structures are less dynamic in Ts21 neurons and that Ts21 neural circuits are much less synchronous. Both these factors could contribute to the cognitive deficits characteristic of DS and illustrate the potential of in vivo imaging of patient-derived neurons for disease modelling.

List of Publications

The work described in this dissertation is included in the following peer-reviewed publication:

Raquel Real*, Manuel Peter*, Antonio Trabalza*, Shabana Khan, Mark A. Smith, Joana Dopp, Samuel J. Barnes, Ayiba Momoh, Alessio Strano, Emanuela Volpi, Graham Knott, Frederick J. Livesey and Vincenzo De Paola. In vivo modeling of human neuron dynamics and Down syndrome (2018). Science *362*, eaau1810. doi: 10.1126/science.aau1810.

List of Figures

Figure 1.1 Human corticogenesis…… 16

Figure 1.2 Human chromosome 21 and mouse models of Down syndrome …… 25

Figure 1.3 Strategies to obtain isogenic disomic Ts21-iPSC lines …… 30

Figure 2.1 Schematic of experimental procedures and timeline …….... 34

Figure 3.1 Ongoing neurogenesis in transplanted human grafts …… 44

Figure 3.2 Vascularization and complex cytoarchitecture of the human graft ……..... 45

Figure 3.3 Host cell identity within the human graft …… 46

Figure 3.4 Minimal recruitment of host-derived microglia to the human graft …… 47

Figure 3.5 Ultrastructure of human grafts reveals immature neural tissue …… 48

Figure 3.6 No teratomas developed in the human grafts …….. 48

Figure 3.7 In vivo two-photon imaging of human cortical grafts reveals cellular mechanisms of pruning ……... 51

Figure 3.8 Human neurons project to known target areas of the somatosensory cortex …… 52

Figure 3.9 Developing dendritic synaptic structures are characterized by highly dynamic restructuring and balanced rates of gains and losses …… 54

Figure 3.10 Developing axonal synaptic structures mirror the events in dendritic synaptic structures …….. 56

Figure 3.11 Human neurons are excitable and have functional synaptic input …… 58

Figure 3.12 Synaptic input to the human graft is mainly from other human neurons … 60

Figure 3.13 Synchronized spontaneous neural activity emerges early and has a defined spatiotemporal order …… 62

Figure 4.1 Fluorescent in situ hybridization assay …… 64

Figure 4.2 Neurogenesis in Ts21 human cortical grafts …….. 67

Figure 4.3 Quantification of cell populations in Ts21 grafts …… 68

Figure 4.4 In vivo neurite development is normal in Ts21 neurons 70
Figure 4.5 Ts21 neurons show decreased dendritic spine plasticity 73
Figure 4.6 Axonal synaptic structures in Ts21 neurons have enhanced stability 74
Figure 4.7 Ex vivo electrophysiological characterisation of Ts21 and control neurons 77
Figure 4.8 Transplanted Ts21 and control neurons have similar synaptic input 78
Figure 4.9 Reduced I_h activation in Ts21 neurons 79
Figure 4.10 Ts21 neurons exhibit decreased burst activity 81
Figure 4.11 Reproducibility of calcium dynamics in an independent control line 82

List of Tables

Table 1 Lentiviral vectors used for cell transduction 40

Table 2 Cell lines used to generate transplanted cortical neurons 40

Table 3 Antibodies used for immunofluorescence 41

Table 4 Biophysical properties of WT and Ts21 neurons 76

List of Abbreviations

2P	Two-photon
AD	Alzheimer's disease
AMPA	α-amino-3-hydroxy-5-methyl-4-isoxazolepropionic acid
APP	Amyloid precursor protein
Aβ	Amyloid-β
CD31	Cluster of differentiation 31
ChR2	Channelrhodopsin-2
CNS	Central nervous system
CTIP2	COUP-TF-interacting protein 2
DAPI	4',6-Diamidino-2-phenylindole dihydrochloride
DNA	Deoxyribonucleic acid
DS	Down syndrome
DSCR	Down syndrome critical region
DXC	Doublecortin
EEG	Electroencephalogram
EM	Electron microscopy
EnvA	Envelope glycoprotein of avian sarcoma/leukosis virus subtype A
EPB	*En passant* bouton
FISH	Fluorescent in situ hybridization
GABA	Gamma-aminobutyric acid
GAD67	Glutamate decarboxylase 1
GECI	Genetically encoded calcium indicator
GFAP	Glial fibrillary acidic protein
GFP	Green fluorescent protein
GΩ	Gigaohm
hESCs	Human embryonic stem cells
hiPSCs	Human induced pluripotent stem cells
hNu	Human nuclei
Hsa21	Human chromosome 21
hSYN	Human synapsin
I_h	Hyperpolarization-activated cation current
IBA1	Ionized calcium binding adaptor molecule 1
LV	Lentivirus

mEPSC	Miniature excitatory postsynaptic current
mIPSC	Miniature inhibitory postsynaptic current
Mmu10	Mouse chromosome 10
Mmu16	Mouse chromosome 16
Mmu17	Mouse chromosome 17
MRI	Magnetic resonance imaging
mV	Millivolt
NBQX	2,3-Dioxo-6-nitro-1,2,3,4-tetrahydrobenzo[*f*]quinoxaline-7-sulfonamide
NCAM	Neural cell adhesion molecule
NPC	Neural progenitor cell
NSG	NOD scid gamma
NuMA	Nuclear mitotic aparatus
OLIG2	Oligodendrocyte transcription factor
PAX6	Paired Box 6
PBS	Phosphate buffered saline
PDGFRα	Platelet-derived growth factor receptor α
pF	Picofarad
PFA	Paraformaldehyde
ROI	Region of interest
ROS	Reactive oxygen species
RV	Rabies virus
RV-ΔG	Glycoprotein-deleted rabies virus
SATB2	Special AT-rich sequence-binding protein 2
SNAP	Synaptosomal nerve-associated protein
SNP	Single nucleotide polymorphism
SD	Standard deviation
SEM	Standard error of the mean
SSC	Saline sodium citrate
TBR1	T-box, brain 1
TOR	Turnover ratio
Ts21	Trisomy of chromosome 21
TVA	Tumour virus receptor A
VGLUT1	Vesicular glutamate transporter 1
WT	Wild type

Chapter 1. Introduction

1.1 Human induced pluripotent stem cells as model systems for central nervous system development and disease

Animal models have been the preferred model system to study the development of the central nervous system and its many disorders. Due to the array of sophisticated genetic engineering tools currently available for mice, this species has been the most widely used to model human brain disorders. However, not only is the neurodevelopmental process much faster in rodents than in human, rodents also lack the structural complexity of the human brain, particularly in the cortex. Cortical areas associated with higher-order cognitive functions, such as prefrontal and temporal cortices, are particularly well developed in the human brain compared to mice. These interspecies differences account for the limited validity of rodent models to recapitulate human brain development and diseases (Ardhanareeswaran et al., 2017). Alternatives include post-mortem human brain tissue, which lack a temporal dimension, primary human brain cells, which are difficult to access and are not expandable, and human embryonic stem cells (hESCs), which have the advantage of being pluripotent and can be differentiated into brain cells in vitro, making them the ideal model to study neurodevelopmental and disease mechanisms at distinct developmental stages. However, the use of hESCs in research is hampered by ethical and accessibility issues.

In 2007, two independent groups reported the generation of induced pluripotent stem cells (iPSCs) from adult human somatic cells, by the ectopic introduction of a defined set of pluripotency-related transcription factors into somatic cells (Takahashi et al., 2007; Yu et al., 2007). The most commonly used combination of transcription factors includes the so-called Yamanaka factors: Oct3/4, Sox2, Klf4 and c-Myc. These cells closely resemble human embryonic stem cells, as they express hESC surface markers, are capable of self-renewal and are pluripotent (i.e., they have the potential to differentiate into cell types from the three germinal layers). It is known that hiPSCs partially retain the epigenetic memory of the somatic cells they originate from, which leads to a differentiation bias towards the original cell type (Ohi et al., 2011). In addition, the study of gene expression profiles of hESCs and iPSCs revealed unique gene expression and epigenetic signatures in iPSCs (Chin et al., 2009; Ruiz et al., 2012). Extended in vitro culture partially corrected the differences in gene expression between hiPSCs and hESCs (Chin et al., 2009), but whether these residual molecular differences have any physiological significance is still a matter of debate. Nonetheless, hiPSCs are widely considered to be hESC-like cells (Choi et al., 2015; Guenther et al., 2010). In addition to

transcriptomics comparing the two types of pluripotent stem cells, multiple studies have generated different subtypes of neuronal cells from hESCs and hiPSCs in parallel, without distinction in differentiation potential or efficiency, developmental time course, or morphological and functional properties of the mature neurons (Kim et al., 2011; Shi et al., 2012a; Song et al., 2013). However, unlike hESCs, the generation of hiPSCs from somatic cells for research is not subject to the same ethical concerns and legal restrictions. Additionally, hiPSCs are more readily available in large numbers and from a wider pool of individuals than hESCs, which is particularly relevant when studying complex and multigenic disorders. Therefore, hiPSCs have emerged in the neuroscience field as an essential research tool for understanding human brain development, identification of disease mechanisms and drug discovery (Liang et al., 2018).

1.2 Neural induction of hiPSCs recapitulates human neurogenesis

During neural induction of hiPSCs, exposure to appropriate concentrations and gradients of specific morphogens that are normally expressed during brain development leads to the generation of different subtypes of neurons. Protocols have been developed for the in vitro generation of cortical glutamatergic excitatory neurons (Shi et al., 2012b), GABAergic inhibitory interneurons (Nicholas et al., 2013), midbrain dopaminergic neurons (Chambers et al., 2009; Soldner et al., 2009), hippocampal granule neurons (Yu et al., 2014) and spinal motor neurons (Chambers et al., 2009; Dimos et al., 2008). Importantly, in vitro differentiation of hiPSCs into cortical neurons has been shown to recapitulate many aspects of in vivo human cortical development. The human cortex is composed of six layers of neurons that contain a majority of glutamatergic excitatory neurons generated in the ventricular zone, and approximately 20% of GABAergic interneurons that are formed in the medial ganglionic eminence of the ventral telencephalon and migrate into the cortex during development (Molyneaux et al., 2007). The glutamatergic neurons destined for each cortical layer are born in a defined temporal order over several weeks, with deep layer neurons generated earlier than upper layer neurons, followed by the late production of astrocytes. It has been revealed that the generation of cortical neurons from both hESC- and hiPSC-derived neural progenitor cells (NPCs) follows the same temporal pattern (i.e., deeper layer neurons form earlier than upper layer neurons) (Espuny-Camacho et al., 2013; Shi et al., 2012a). Additionally, the extended time-course of human neurogenesis and neuronal maturation is preserved in vitro, as hiPSC-derived neurons require prolonged periods in culture to achieve morphological and electrophysiological patterns of maturity (Shi et al., 2012a) (**Figure 1.1**). Interestingly, transplantation of hESCs into the rodent brain did not accelerate the timing of neurogenesis and neuronal maturation (Espuny-Camacho et al., 2013), which suggests that developmental

processes are intrinsically regulated in a species-specific manner (van den Ameele et al., 2014). Similar observations of a protracted timeline akin to human embryonic development were made in the differentiation and maturation of forebrain GABAergic interneurons in vitro (Nicholas et al., 2013).

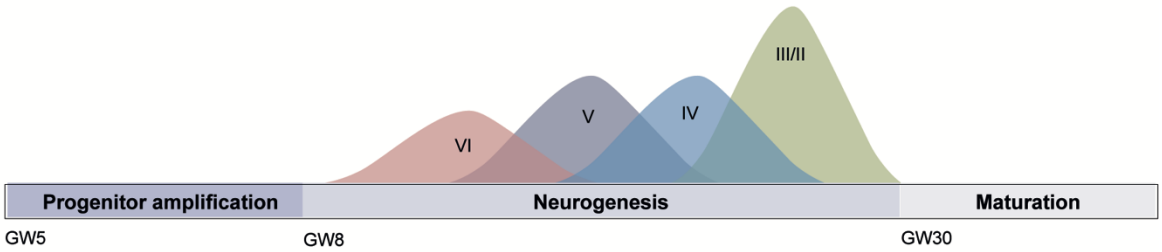

Figure 1.1 Human cortical neurogenesis.

In vitro generation and maturation of cortical neurons from hiPSCs recapitulates the time-course and temporal patterning of in vivo cortical neurogenesis, with deeper layer neurons being generated before upper layer neurons over several months. GW, gestational week. Adapted from van den Ameele et al., 2014.

1.3 hiPSCs originate functional neurons and neural networks

Several studies have addressed the fundamental question of whether hiPSC-derived neurons are able to achieve a state of functional maturation analogous to human neurons in vivo. Neural progenitor cells cultured in vitro have been shown to progressively develop passive and active membrane properties resembling mature human neurons (Niclis et al., 2017; Prè et al., 2014; Song et al., 2013). Whole-cell patch-clamp recordings of forebrain neurons derived from hiPSC performed over time reveal the appearance of voltage-dependent sodium and potassium currents and a progressive increase in the proportion of cells that fire trains of action potentials in response to current injection, indicating the gradual addition of ionic channels to the membrane and the intrinsic excitability of these neurons (Prè et al., 2014; Shi et al., 2012a). Moreover, the characteristics of the action potentials evolve over time, from relatively immature spiking phenotypes to more mature firing properties, including an increase in spike amplitudes, faster spikes and lower thresholds for action potential generation. Also, neurons derived from hiPSCs in vitro eventually develop spontaneous miniature excitatory and inhibitory postsynaptic currents (mEPSCs and mIPSCs, respectively) that increase in frequency and amplitude over time, a hallmark of functional synapses. Importantly, the temporal profile of functional maturation and synaptogenesis in hiPSC-derived neurons is protracted relative to rodent neurons, suggesting neural progenitor cells derived from hiPSCs follow an intrinsic species-specific developmental programme lasting several months (Avaliani et al., 2014; Niclis et al., 2017).

Spontaneous neural electrical activity has been documented in several mammalian species during development and has been linked to many essential developmental processes, including neuronal differentiation and migration, synaptogenesis and synaptic plasticity (Khazipov and Luhmann, 2006). In addition, spontaneous oscillatory patterns of synchronized electrical activity have been shown to play a key role in early neural network development. Importantly, hESC- and hiPSC in vitro also exhibit spontaneous activity transients that mature over time, in parallel to increased morphological complexity and progressive maturation of membrane properties (Heikkilä et al., 2009; Kirwan et al., 2015; Prè et al., 2014). Given that calcium activity reflects neuronal activity and the size of a calcium transient directly correlates with the number of repetitive action potentials fired (Smetters et al., 1999), Kirwan and colleagues have monitored the development of calcium transients longitudinally to ascertain whether hiPSC-derived cortical neurons can form neuronal networks in vitro (Kirwan et al., 2015). Indeed, hiPSC-derived neurons in vitro are not only functional and synaptically connected, but they also develop glutamatergic-dependent calcium transients that mature over time in a stereotypical manner reminiscent of cortical neural network development in vivo (Khazipov and Luhmann, 2006). Thus, neurons derived from hiPSCs constitute a very useful tool to model human neuron and neural network development in vitro.

1.4 In vivo transplantation of human PSC-derived neurons

hPSC-based in vitro systems can provide significant insights into human-specific features of brain development. However, monolayer neuronal cultures lack the spatial organisation and complex cytoarchitecture of the human brain, which limit its usefulness to model the full complexity of neurodevelopmental processes. In addition, cultures of ESC/iPSC-derived neurons are limited by short-term survival and incomplete neuronal maturation (Korecka et al., 2016). Under specific culturing conditions, hiPSC-derived neural progenitors and neurons in vitro have the intrinsic ability to self-organise into three-dimensional (3D) multi-layered cortical structures (Mariani et al., 2012). These 3D cortical structures exhibit a gene expression profile typical of the early embryonic telencephalon, recapitulating the transcriptional programs that are active during human cortical development. The generation of 3D multicellular culture systems (or organoids) has been an important development in the field of hiPSCs. Lancaster and colleagues were the first to develop a hiPSC-derived brain organoid, a structure that contains several identifiable brain regions and cortex-like layered structures (Lancaster et al., 2013). The cellular composition, gene expression profiles and epigenomic signatures of cerebral organoids are remarkably similar to those of the human foetal tissue (Camp et al., 2015; Luo et al., 2016). Therefore, brain organoids constitute an important tool for modelling human neurodevelopment, in a multicellular context that more

closely mimics human physiology. The multicellular environment of organoids enables cells to achieve a functionally more mature state than in 2D cultures, and the interaction between different cell types within the organoid allows for the study of non-cell autonomous aspects of disease pathology. Despite the obvious advantages, the organoid technology still has limitations, the most significant of which is the lack of vascularisation that limits growth and maturation. To circumvent this issue, brain organoids generated in vitro from hESCs have recently been transplanted into the brains of mice, which resulted in organoid vascularisation in vivo and prolonged survival (Mansour et al., 2018). The transplantation of dissociated hESC/iPSC-derived neurons in the central nervous system of rodents has also been shown to enhance the survival and accelerate the functional maturation of neurons (Espuny-Camacho et al., 2013; Niclis et al., 2017), and substantial efforts are under way to fully elucidate if hESC/iPSC-derived neurons can form synapses and functionally integrate into the host neural circuitry. This is significant, due to the prospect of cell replacement therapy using patient-specific iPSC-derived neurons following injury or in the context of disease. In a landmark study, mouse embryonic neurons transplanted in the primary visual cortex of adult mice after a lesion in the same cortical area extended axons and received input from host neurons in a target-specific manner (Falkner et al., 2016). More importantly, by labelling the transplanted neurons with a genetically encoded calcium indicator and performing in vivo imaging of stimulus-evoked responses, it was demonstrated that transplanted neurons respond to visual stimuli, indicating full integration within the host visual circuitry. It is well established that neurons derived from both hESCs and hiPSCs are also able to grow long-range axonal projections along white matter tracts of the host brain (Espuny-Camacho et al., 2013; Niclis et al., 2017; Steinbeck et al., 2012). Importantly, the innervation patterns of grafted hESC-derived neurons have been shown to be target-specific and to mimic the endogenous host patterns of axonal projections (Espuny-Camacho et al., 2013; Steinbeck et al., 2012). However, whether hESC/iPSC-derived axonal projections into the host brain are functionally connected to the host neural circuitry is less obvious. Several studies have tried to demonstrate host-to-graft functional connectivity through different strategies. Using an optogenetic approach, Avaliani and colleagues demonstrated that graft neurons receive synaptic afferents originating from the host. This study, in which neural progenitors derived from hiPSCs were transplanted into the hippocampus of adult rats after AAV-mediated expression of Channelrhodopsin-2 (ChR2) in host neurons, revealed evoked postsynaptic currents in human neurons upon ChR2 activation of the host hippocampal neurons (Avaliani et al., 2014). An independent study has also shown a small subset of grafted cortical hiPSC-derived neurons responding to light stimulation of host ChR2-expressing thalamic neurons (Tornero et al., 2017). In the same study, hiPSC-derived neurons exhibited electrophysiological responses to physiological sensory stimuli, providing further evidence

that host afferent synaptic inputs to human neurons are functional and that transplanted human neurons integrate into the host neural microcircuitry, in a target-specific manner. Furthermore, motor benefits observed after hESC-derived mesencephalic dopaminergic (mesDA) neurons were transplanted into the striatum of a Parkinson's disease mouse model, were reversibly abolished by using optogenetics to selectively silence the activity of the transplanted neurons (Steinbeck et al., 2015), which again indicates that transplanted neurons derived from either hESCs or hiPSCs can establish functional connections within the host circuitry. Using a combination of acute brain slice electrophysiology and optogenetics, Steinbeck and colleagues were also able to demonstrate that grafted hESC-derived mesDA neurons modulate glutamatergic synaptic transmission onto the host striatum, an indication that transplanted neurons can influence the activity of endogenous host functional networks. Similarly, light activation of ChR2-expressing hESC-derived neurons induced postsynaptic currents in mouse neurons, both in vitro and after transplantation, suggesting hPSC-derived neurons can integrate in established neural networks (Weick et al., 2011).

1.5 Neurons derived from hPSC as model systems of disease

The finding that hESC/iPSC-derived neurons can integrate in the host neural circuits is an exciting prospect, not only from the perspective of cell replacement therapies, but also because many of the fundamental questions regarding the biology of neural connectivity were until now restricted to non-human models. Animal models of complex neurological diseases often do not recapitulate the full extent of human phenotypes, and have limited value for disease modelling and drug discovery. The generation of chimeric human-rodent models of neurological diseases is thus a step forward, providing a valuable tool to investigate human specific phenotypes and disease mechanisms. A possible approach is to transplant hESC/iPSC-derived neurons from healthy individuals into animal models of disease. In a recent study, the transplantation of non-affected hESC-derived neurons in a well characterized mouse model of Alzheimer's disease (AD) led to the development of AD pathology in the human graft, including neuronal loss and the appearance of pathological tau species, features that were not observed in the host brain (Espuny-Camacho et al., 2017). An alternative approach is the use of iPSC-derived neurons from patients with specific neurological disorders, which provides insights into the cell autonomous factors contributing to disease phenotypes. The use of chimeric human-rodent models of disease is especially relevant to uncover neuronal maturation defects, as well as synaptic and neural circuitry dysfunction. In this context, the combination of in vivo morphological and calcium imaging, optogenetic stimulation, and electrophysiological recordings of transplanted human neurons can elucidate

cellular and network connectivity phenotypes, helping to understand the mechanisms underlying complex human brain diseases.

1.6 Human iPSCs and Down syndrome

Down syndrome (DS) is the most common genetic cause of congenital intellectual disability, estimated to occur in approximately 1 in 750 live births (Antonarakis et al., 2004). It is caused by trisomy of human chromosome 21 (Hsa21), which results in overexpression of many of the genes encoded on this chromosome (**Figure 1.2**). The genetic cause of DS was identified 60 years ago (Lejeune et al., 1959), but the precise pathogenic mechanisms are still largely unknown. Several hypotheses have been put forward to explain how an extra copy of Hsa21 contributes to disease-related phenotypes. The 'gene dosage effect' hypothesis states that the DS phenotypes are a direct consequence of a gene dosage imbalance resulting in overexpression of specific protein-coding genes (Dierssen, 2012). Furthermore, the identification of individuals with rare segmental duplications of Hsa21 who share a common region of triplicated genes, led to the hypothesis that genes located on this overlap region (**D**own **S**yndrome **C**ritical **R**egion, DSCR) were sufficient to produce DS phenotypes when present in three copies (Delabar et al., 1993). However, only some of the Hsa21 genes are likely to be dosage-sensitive and the concept of a DSCR has been discredited by the recognition that partial trisomy of other segments of the Hsa21 not overlapping with the DSCR are also associated with a diagnosis of DS (Korbel et al., 2009; Korenberg et al., 1994). Increasing evidence indicates that the presence of an extra copy of Hsa21 leads to a genome-wide transcriptome dysregulation that affects the expression of genes outside of Hsa21, which will ultimately contribute to the disease phenotype (Letourneau et al., 2014). The proposed mechanisms by which the presence of an extra copy of Hsa21 causes widespread gene expression dysregulation include the overexpression of regulatory coding and non-coding elements in Hsa21, including transcription factors and microRNAs, and chromatin modifications brought about by the overexpression of one or more Hsa21 candidate genes (Dierssen, 2012; Letourneau et al., 2014). While it is possible that some aspects of DS may be due primarily to the effects of single dosage-sensitive Hsa21 genes, the most likely scenario that explains the full complexity of DS phenotypes is one of genomic instability that leads to altered expression of whole chromosomal domains (Gardiner et al., 2010). In addition, the incidence and severity of many of the disease-related phenotypes is highly variable among DS individuals, suggesting phenotypes are modified by the genetic background of each affected individual and by gene-environment interactions (Roper and Reeves, 2006).

1.7 Down syndrome brain phenotypes

Although DS phenotypes are not restricted to the brain, cognitive manifestations of the disorder are the most prevalent and severe. Several imaging and post-mortem anatomical human studies have identified the many structural anomalies present in the brains of individuals with DS from foetal to adult age. A persistent finding is the overall reduction in brain size that can be detected from early developmental stages (Guihard-Costa et al., 2006; Pinter et al., 2001; Raz et al., 1995). While neuronal cell density determined by quantification of neuronal specific enolase in foetal cortical samples appears to be normal during early development (Weitzdoerfer et al., 2001), stereological quantification of total cell numbers reveals that hypocellularity is present in the neocortex (Larsen et al., 2008), hippocampus and parahippocampal gyrus (Guidi et al., 2008), and cerebellum (Guidi et al., 2011) of foetuses aged between 17 and 21 weeks of gestation, as well as postnatally (Wisniewski KE, 1990). Additionally, cortical lamination has been shown to be compromised in the temporal neocortex of foetuses with DS (Golden and Hyman, 1994). Another major anatomical defect in DS is the altered development of dendritic structures. Golgi studies have demonstrated that starting in early infancy, the DS brain exhibits dendritic hypotrophy, with reduced dendritic branching and length, reduced dendritic spine density and alterations in spine morphology in cortical pyramidal neurons (Becker et al., 1986; Takashima et al., 1981, 1994), which predict an impaired synaptic function and information processing within neuronal networks (Dierssen and Ramakers, 2006). Consistent with impaired synaptogenesis, there is significantly reduced expression of synaptic proteins such as drebrin, a neuron-specific F-actin binding protein that regulates spine morphology, and the **S**ynaptosomal **N**erve-**A**ssociated **P**roteins αSNAP and SNAP 25, which participate in neurotransmitter release from the presynaptic terminal, in the brain of foetuses with DS (Weitzdoerfer et al., 2001).

In addition to these morphological defects, there is evidence that neurogenesis is severely impaired in numerous regions of the foetal DS brain. The density of proliferating cells was found to be severely reduced in the ventricular germinal matrix (Contestabile et al., 2007), which originates neuronal and glial cells destined to form neocortical layers, and in the neurogenic zones of the hippocampal region (Guidi et al., 2008) of foetal tissue aged between 17 and 21 weeks of gestation. The proportion of proliferating cells was also significantly reduced in the neurogenic regions of the foetal cerebellum (Guidi et al., 2011). These findings point to a widespread reduction in the proliferation potency of precursor cells in neurogenic areas during critical stages of brain development, which is likely to be an essential determinant of the generalized hypocellularity that characterizes the DS brain from early life. An impairment in cell proliferation was also confirmed in vitro by a nucleotide analogue incorporation assay

in DS foetal fibroblasts (Gimeno et al., 2014) and in neural progenitors obtained from the cortical ventricular zone of 18 weeks old foetuses (Lu et al., 2012). Of note, apoptosis markers have not been found to be consistently elevated across all regions of the foetal brain (Guidi et al., 2011), suggesting a defect in neurogenesis plays a more crucial role in the reduction of brain size and hypocellularity observed in individuals with DS. In contrast to reduced neurogenesis, the number of astrocytes has been shown to be greatly increased both in developing and adult DS brains (Griffin et al., 1998; Guidi et al., 2008; Zdaniuk et al., 2011). Astrocytes form the largest population of cells in the mammalian brain and its many functions include the maintenance of the blood-brain barrier, regulation of neurotransmitter concentrations in the extracellular fluid, ion homeostasis, promotion of myelination, and regulation of synapse formation and plasticity (Lee et al., 2016). While the exact consequences of the increased number of astrocytes in the DS brain are still unclear, this finding suggests that a bias towards the acquisition of an astrocytic phenotype could underlie a reduction of neuronal precursor specification, which could further justify the reduced neuronal densities observed in the DS brain (Stagni et al., 2018).

Furthermore, trisomy of chromosome 21 (Ts21) is also a significant risk factor for neurodegeneration later in life, as all individuals with Down syndrome develop neuropathological features consistent with Alzheimer's disease (AD) between the third and fourth decades of life, and approximately 60% will develop AD-like dementia by the age of 65 (Ballard et al., 2016).

1.8 Insights from animal models of Down syndrome

Anatomical studies of foetal and post-mortem human brain tissue, as well as structural and functional imaging studies of individuals with DS, have elucidated many of the brain phenotypes of this disorder. However, these studies do not allow for the dissection of disease mechanisms and the interrogation of gene-phenotype correlations. Murine models have for a long time been the best available tool for dissecting the function of individual Hsa21 genes and for understanding the genetic contributions to DS phenotypes. The major advantages of mouse models are the accessibility to developing tissues and the amenability to genetic engineering, making it possible to directly test the contribution of specific genes to disease phenotypes (Briggs et al., 2013a). The mouse genome contains three large chromosome fragments that are syntenically conserved with most of Hsa21 (**Figure 1.2 A**). The largest syntenic region is located on mouse chromosome 16 (Mmu16), which contains ~102 orthologous protein-coding genes. The second syntenic region is located on mouse chromosome 17 (Mmu17) and corresponds to a region of ~19 orthologous protein-coding

genes on Hsa21. Finally, the third syntenic region is located on mouse chromosome 10 (Mmu10) and contains ~37 orthologous protein-coding genes (Gupta et al., 2016). In addition, 75 non-coding orthologous genes are distributed across all three mouse chromosomes.

The first DS mouse model to be developed was trisomic for the complete Mmu16 (Gropp et al., 1975), but its value to investigate the pathogenesis of DS was limited by the fact that Ts16 mice die *in utero* and Mmu16 also contains many genes with human orthologues located in other chromosomes other than Hsa21. Several mouse models trisomic for segments of Mmu16 were subsequently developed, the best characterised of which is the Ts65Dn model (Davisson et al., 1990). This mouse model is trisomic for a large telomeric fragment of Mmu16 fused to the pericentromeric region of Mmu17. The duplicated region of Mmu16 is syntenic to most of 21q and contains ~90 protein-coding genes orthologous to Hsa21. Ts65Dn mice recapitulate the human DS phenotype to some extent – they have impaired learning and memory, decreased long-term potentiation and several of the neuroanatomical defects found in DS brains, such as cerebellar hypoplasia, delayed expansion of the neocortex during embryogenesis, reduced cortical cell density, increased number of astrocytes in the hippocampus, atrophy of the dendritic tree, reduced dendritic spine density and aberrant spine morphology (Bartesaghi et al., 2011). However, this mouse model also contains an additional Mmu17 region syntenic to Hsa6 that corresponds to 35 protein-coding orthologous genes (Gupta et al., 2016). The fact that approximately 25% of the trisomic genes in this mouse model are non-Hsa21 orthologues is likely to have confounding phenotypic consequences that impair the interpretation of experimental findings. Additional segmental trisomies have been subsequently generated (**Figure 1.2 B**). Significantly, a triple trisomy mouse model that spans the entire Hsa21 syntenic regions across Mmu16, Mmu17 and Mmu10, without additional contribution of non-Hsa21 orthologous genes, was developed (Ts1Yey;Ts2Yey;Ts3Yey), which recapitulates most of the phenotypes also found in Ts65Dn mice (Yu et al., 2010). This is the most complete DS mouse model developed so far, but it is still not an accurate representation of the genetic complexity of the human condition. In an attempt to generate a mouse model that more closely resembles the human chromosomal disorder, transchromosomic Tc1 mice were constructed, containing an almost complete copy of Hsa21 (O'Doherty et al., 2005). Despite the theoretical advantage of this model, DNA sequencing of the Hsa21q revealed numerous deletions and rearrangements within the human chromosome, leaving intact only 83% of Hsa21 genes. In addition, Tc1 mice are mosaic for Hsa21 due to random loss of the human chromosome in a subset of cells from all tissues. The degree of mosaicism is variable between animals, which confounds the analysis of phenotypical consequences of the trisomy.

Collectively, murine models have contributed to our understanding of the mechanistic relationship between triplicated genes and DS phenotypes, but there are several important limitations that need to be acknowledged. First, some of the developmental processes that are affected in DS differ significantly between the two species (e.g., neurogenesis), which contributes to the inadequacy of mouse models to fully recapitulate the complexity of the human phenotype. Second, there are differences in the regulation of gene expression between species, which might influence the genome-wide consequences of increased expression of Hsa21 genes (Liu et al., 2011). Third, gene-phenotype correlations depend on the genomic context, and the fact that Hsa21 orthologous genes in mice are distributed across three different chromosomes likely affects functional gene interactions (Gupta et al., 2016). This is relevant because individual gene contributions to a given phenotype might be modest and become apparent only when multiple genes that act on the same pathway or complex are affected. Finally, Gardiner and colleagues have compared the gene content of Hsa21 with orthologous mouse genomic regions and found species-specific genes: 98 human transcripts had no orthologues in the mouse genomic sequence, while 38 mouse transcripts had no identifiable human orthologue (Gardiner et al., 2003). Therefore, no animal model generated so far accurately recapitulates the exact genomic content and functional consequences of Ts21.

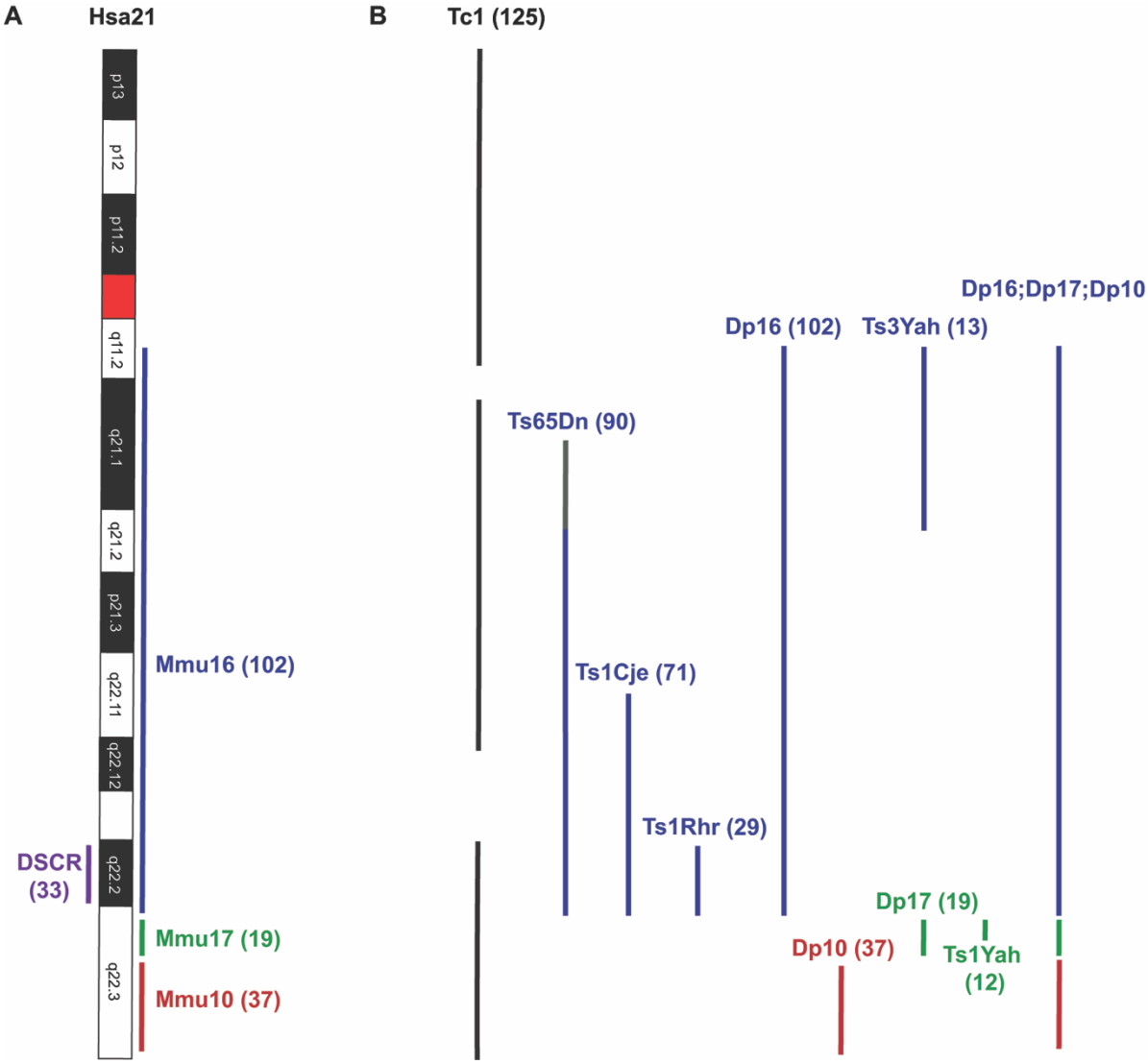

Figure 1.2 – Human chromosome 21 and mouse models of Down syndrome.

(**A**) The human chromosome 21 is the smallest of the somatic chromosomes, with 222 protein coding and 325 non-protein coding genes. The DSCR contains 33 protein coding dosage-sensitive genes. The syntenic regions on the mouse genome are represented, as well as the number of orthologous genes (in brackets).

(**B**) Mouse models of DS. Tc1 is a chimeric transchromosomic mouse model, containing a copy of Hsa21 with a 4.9 Mb pair deletion comprising approximately 19 genes; it contains appriximately 80% of the Hsa21 encoded genes. All the other models contain duplications of mouse regions that are orthologous to Hsa21. Numbers in brackets indicate the number of conserved protein coding genes that are trisomic. Note that the Ts65Dn model contains a pericentromeric region of Mmu17 that is syntenic to a region on Hsa6 containing 35 protein coding genes. Ts1Cje consists of a mouse model with a shorter fragment of Mmu16, containing only 67% of the orthologous genes that are triplicated in Ts65Dn. The Ts1Rhr model is trisomic for the syntenic region on Mmu16 that contains DSCR orthologous genes. Dp16, Dp17 and Dp10 contain a duplication of the entire Mmu16, Mmu17 and Mmu10 syntenic segments, respectively, without additional contribution of non-Hsa21 orthologous genes. Ts3Yah and Ts1Yah are mouse models with trisomy of partial syntenic segments of Mmu16 and Mmu17, respectively. The triple trisomy mouse model results from the combination of the duplicated regions of Dp16, Dp17 and Dp10, producing a model that is trisomic for all mouse orthologs of Hsa21. Adapted from Gupta et al., 2016.

1.9 iPSCs in the study of Down syndrome

After the development of iPSC technology, it was immediately apparent that the capability to generate disease-specific cells offered immense opportunities to understand disease mechanisms in complex genetic disorders. This is even more relevant in the face of the difficulty in obtaining tissue from human embryos for research purposes that precludes access to human embryonic stem cells. Several studies have reported the generation of trisomy 21 iPSC lines (Ts21-iPSCs) using different reprogramming strategies (Briggs et al., 2013b; Chou et al., 2012; Li et al., 2012; Mou et al., 2012; Park et al., 2008; Weick et al., 2013). Importantly, these studies have recapitulated multiple aspects of Down syndrome pathology, which reiterates the advantage of disease-specific iPSCs as model systems for complex genetic disorders. Ts21-iPSCs have confirmed that the presence of an extra copy of Hsa21 is associated with a global transcriptional deregulation (Briggs et al., 2013b; Hibaoui et al., 2014; Weick et al., 2013). In addition, some of the Ts21-iPSC studies conducted so far have provided evidence for neurodevelopmental phenotypes such as defective neurogenesis (Hibaoui et al., 2014; Jiang et al., 2013) and synaptogenesis (Hibaoui et al., 2014; Weick et al., 2013), a shift from neuronal to astroglial and oligodendroglial phenotypes (Briggs et al., 2013b; Hibaoui et al., 2014), a deficit in the proliferation of neural progenitor cells (Hibaoui et al., 2014; Murray et al., 2015), an increased susceptibility to cell death (Briggs et al., 2013b; Hibaoui et al., 2014; Shi et al., 2012c), and morphological defects such as reduced neurite branching and length (Hibaoui et al., 2014).

Individuals with DS have a very high incidence of early-onset dementia with neuropathological features of Alzheimer's disease, including the presence of amyloid-β (Aβ) plaques. This has been attributed to the triplication of the *APP* gene that is located in Hsa21. Shi and colleagues were the first to model AD pathology in DS using iPSC-derived neurons (Shi et al., 2012c). In this study, increased production of Aβ peptides by Ts21 cortical neurons was observed after only 70 days of in vitro differentiation, and a decline in the $A\beta_{40}/A\beta_{42}$ ratio was indicative of a disproportionate increase in the secretion of the pathogenic $A\beta_{42}$ peptide. In accordance to this finding, $A\beta_{42}$-containig aggregates (a hallmark of AD pathology) were found intra- and extracellularly in Ts21 neuronal cultures. Furthermore, there was hyper-phosphorylation of tau protein in aberrant subcellular compartments, compatible with previously well-described AD pathology. An independent study in Ts21 neurons derived from two clones of iPSCs from an individual with DS also showed an increase in Aβ-containing aggregates in Ts21 neuronal cultures (Murray et al., 2015), which substantiates the assertion that AD pathogenesis can be reproduced in cortical neurons generated from Ts21-iPSC. Additionally, Shi and colleagues found that the pharmacological inhibition of δ-secretase, one of the proteases that processes

APP to generate Aβ peptides, significantly reduced the production of $A\beta_{40}$ and $A\beta_{42}$, which highlighted the potential of disease-specific iPSC-based models to test candidate disease-modifying drugs. In another example, Briggs and colleagues found that the increased sensitivity of Ts21 neural cultures to oxidative stress could be reversed by treatment with *N*-acetylcysteine, an antioxidant drug (Briggs et al., 2013b), suggesting antioxidants might be of benefit to DS individuals. Finally, a study looking at the interactions between astroglia and neurons revealed that several of the neuronal phenotypes observed in Ts21 neurons are mediated by the secretome of Ts21 astroglia. Importantly, these astroglia-mediated effects (i.e., impaired neurogenesis, shorter neurite length, increase cell death and impaired synapse formation) could be partially corrected by treatment with the clinically available antibiotic minocycline, a drug with antioxidant and anti-inflammatory properties (Chen et al., 2014). In addition to drug screening, one of the aspects that is most appealing in an iPSC-based model system is the possibility of genetic or pharmacological manipulation of disease-specific iPSCs, which has great potential for the study of causative links between individual genetic factors and disease phenotypes. In a remarkable example, Hibauoi and colleagues were able to rescue several neurodevelopmental defects in Ts21 neural progenitors and neurons after either pharmacological or short hairpin RNA (shRNA)-induced inhibition of the *DYRK1A* gene (Hibaoui et al., 2014). This strongly suggests that overexpression of *DYRK1A*, a gene located in Hsa21 that encodes a dual serine/threonine and tyrosine kinase which phosphorylates multiple targets that have been implicated in several DS-associated phenotypes (Wiseman et al., 2009), is a main contributor to impaired neurogenesis in DS. Similarly, Huo and colleagues were able to partially rescue a migration deficit in Ts21 GABAergic interneurons in vitro by pharmacologic inhibition of PAK1, a protein involved in the regulation of the actin cytoskeleton that has been shown to be important for neural migration during corticogenesis in mice (Huo et al., 2018). Not surprisingly, *PAK1* gene is also located on Hsa21 and its expression is significantly increased in DS. Finally, Chen and colleagues inhibited the expression of *S100β* in Ts21 astroglia by transfection of small interfering RNA (siRNA), thus normalising the production of reactive oxygen species (ROS) in Ts21 astroglia and partially rescuing the deleterious effects of Ts21 astroglia on neurons (Chen et al., 2014). Again, *S100β* gene is located on Hsa21 and its expression is significantly increased in Ts21 astroglia. Although previous studies had already established a link between overproduction of S100β and impaired neurogenesis, this study demonstrated that overexpression of the *S100β* gene in Ts21 astroglia plays an essential role in mediating the toxic interactions between Ts21 astroglia and NPCs/neurons, through non-cell autonomous effects.

It is important to note that there is no absolute agreement between the neurodevelopmental phenotype observed in the different studies mentioned, which highlights that some of these phenotypes might be at least partly dependent on cell culture conditions, the reprogramming process itself and/or the specific genetic background of each DS individual from which the iPS cell lines originate, underlying complex interactions between Ts21 and other genetic and epigenetic factors that vary across individuals. In fact, there is significant clinical phenotypic variability in Down syndrome, which might also be present at the cellular level. In an attempt to counteract the genomic variability between individuals, and even between different iPSC lines reprogrammed from the same somatic cell, that could potentially confound the interpretation of disease-related phenotypes, studies using disease-specific iPSCs normally require multiple cell lines derived from unrelated healthy and age-matched affected individuals. Alternatively, the use of isogenic Ds21-iPSCs and Ts21-iPSCs limits the need to generate several iPSCs lines, by eliminating any theoretical genomic differences between disomic and trisomic lines, apart from the supernumerary copy of Hsa21 (Hibaoui and Feki, 2015). There are several strategies to generate isogenic lines reported in the literature (**Figure 1.3**). In 1-3% of DS cases, individuals exhibit mosaicism for Ts21, which allows the generation of both Ds21-iPSCs and Ts21-iPSCs from the same individual (Briggs et al., 2013b; Weick et al., 2013). In very rare cases, monozygotic twins can be discordant for trisomy 21, which constitutes another potential source of isogenic iPSCs (Hibaoui et al., 2014). Occasionally, a subclone of Ts21-iPSCs in culture will spontaneously lose one copy of Hsa21 during passaging, leading to mixed cultures of Ds21-iPSCs and Ts21-iPSCs that can then be isolated by clonal expansion (Chen et al., 2014; Maclean et al., 2012). Alternatively, loss of the extra copy of Hsa21 can be induced by AAV-mediated insertion of the *TKNEO* transgene into one copy of Hsa21, followed by negative selection against *TKNEO*-expressing cells (Li et al., 2012). More recently, insertion of an inducible *XIST* transgene in Ts21-iPSCs using zinc finger nucleases corrected Hsa21 gene expression to near normal disomic levels, reverting a proliferation deficit and a delay in neuronal maturation in vitro (Jiang et al., 2013). XIST is a non-coding RNA that is normally exclusively produced from the inactive X chromosome in mammalian females, and induces heterochromatin modifications that transcriptionally silence the inactive X chromosome. XIST-induced silencing of Hsa21 not only provides a means to accurately dissect the cellular pathologies directly due to Ts21, but also represents the first step towards a potential chromosome therapy for DS. Independently of the strategy, isogenic Ds21-iPSCs and Ts21-iPSCs are now the gold standard to study the effects of human trisomy 21, without the confounding effects of genomic variability.

Most of the studies using Ts21 neurons derived from iPSCs have been conducted in vitro. In a recent in vivo study, Huo and colleagues transplanted iPSC-derived GABAergic progenitors

from two DS individuals in the medial septum of adult mice. Both Ds21 and Ts21 GABAergic progenitors generated cortical interneurons with equal efficiency in vivo. However, Ts21 interneurons exhibited reduced soma size, neurite length and branch complexity compared with euploid interneurons. Interestingly, transplanted GABAergic interneurons derived from Ts21-iPSCs also demonstrated a migratory defect from the medial septum to the olfactory bulb and hippocampus. These findings largely confirmed previous in vitro observations, demonstrating that the cellular phenotypes described in vitro were intrinsic to Ts21 GABAergic interneurons and not an artefact of culture conditions (Huo et al., 2018). Similarly, Chen and colleagues transplanted Ts21 astroglia in the lateral ventricles of neonatal mice, to confirm that the negative effects of Ts21 astroglia on neurogenesis and neuronal cell death that had already been detected in vitro could be replicated in the host (Chen et al., 2014). However, it is plausible that neurons in culture cannot capture the full complexity of cellular phenotypes observed in DS and, further to validation of in vitro findings, transplantation of iPSC-derived neural progenitors and neurons could potentially uncover disease phenotypes that are not apparent in vitro. The aim of the present study is therefore to explore the possible contributions of in vivo hiPSC-based studies to the understanding of human neural development and disease modelling. The transplantation into the rodent brain of healthy and disease-specific hiPSC-derived cortical excitatory neurons, followed by subsequent longitudinal intravital imaging, is expected to: (i) enhance the knowledge of dynamic processes such as neuritogenesis, synaptogenesis and neural network formation in human neurons; and (ii) uncover new cellular phenotypes associated with DS that could be relevant to the cognitive impairment characteristic of this condition.

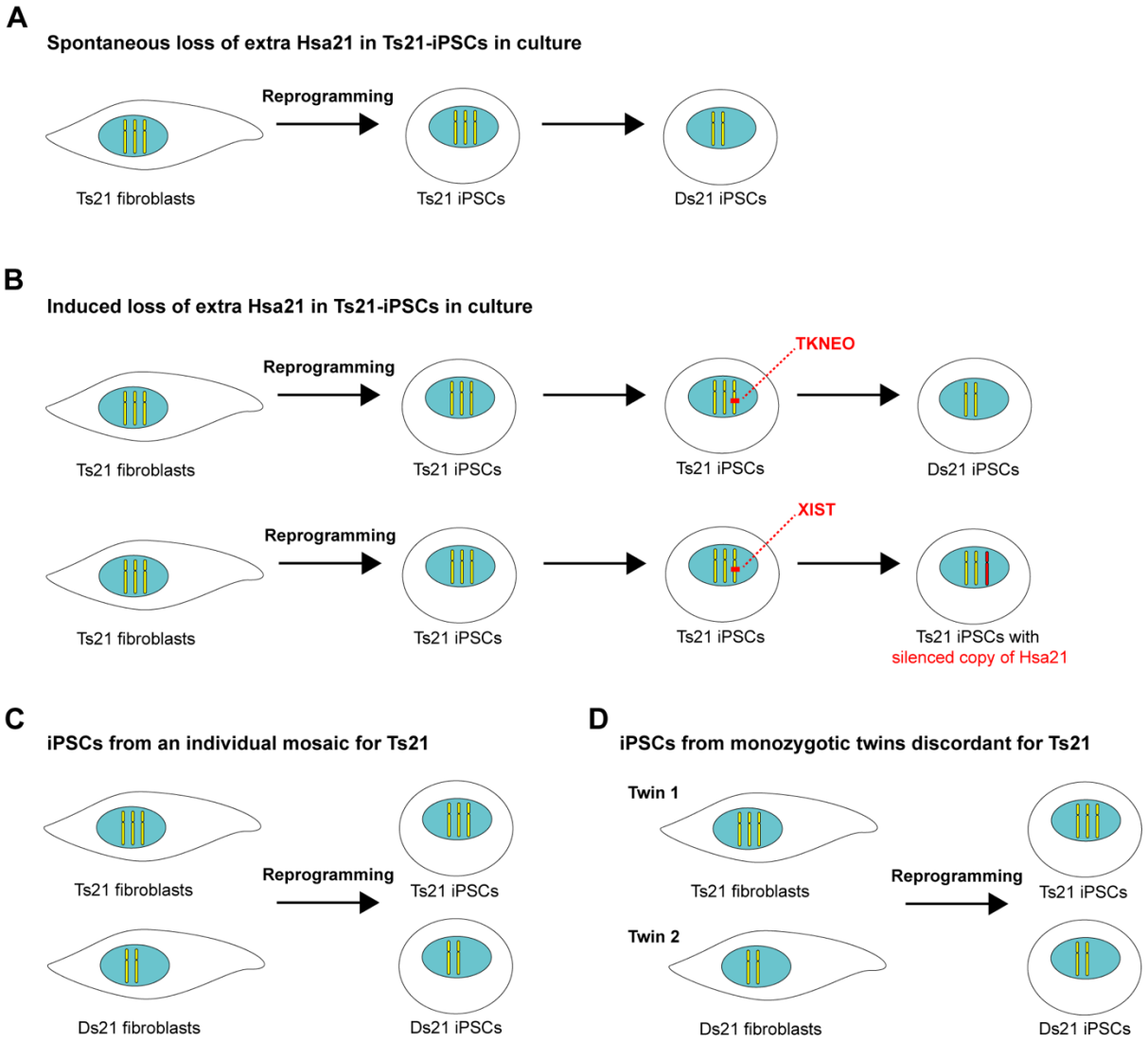

Figure 1.3 Strategies to obtain isogenic disomic Ts21-iPSC lines.

(**A**) A clone of Ts21-iPSCs can on occasion spontaneously lose one extra copy of Hsa21 *in vitro*, leading to a mosaic culture. Euploid clones can be isolated to obtain pure Ds21 and Ts21-iPSCs cultures (Weick et al., 2013; Briggs et al., 2013; Huo et al., 2018).

(**B**) Strategies have been developed to induce the loss or silencing of one extra copy of Hsa21, originating isogenic disomic controls. The introduction of a *TKNEO* fusion gene into the *APP* gene of one copy of Hsa21 in Ts21-iPSCs, followed by negative selection against *TKNEO*, led to a spontaneous chromosome loss in culture (Li et al., 2012). Alternatively, the introduction of the *XIST* transgene in the *DYRK1A* locus of one copy of Hsa21 in Ts21-iPSCs led to a chromosome-wide transcriptional silencing of that Hsa21 (Jiang et al., 2013).

(**C**) Constitutional mosaicism in DS individuals occurs in 1-3% of cases. Isolation and expansion of individual clones from the same tissue generates isogenic iPSCs, identical in every respect except for the extra copy of Hsa21 (Murray et al., 2015).

(**D**) Isogenic iPSCs have been generated from foetal fibroblasts of monozygotic twins discordant for Ts21 (Hibaoui et al., 2013). Adapted from Hibaoui and Feki, 2015.

Chapter 2. Methods

2.1 Generation of a new Ts21 iPSC line

Following approval from the Cambridgeshire Research Ethics Committee, skin biopsies were collected from donors with Down syndrome by the Department of Psychiatry, University of Cambridge, with informed consent from the donor or representative. Samples were cultured at 37°C in 5% CO_2 in DMEM with GlutaMAX™ (Thermo Fisher Scientific), supplemented with 10% foetal calf serum, penicillin (50 U/ml), streptomycin (50 μg/ml) and sodium pyruvate (1 mM), until fibroblast outgrowth was observed. When plates were confluent, fibroblasts were trypsinized and transferred to T75 cell culture flasks for further expansion. Cellular reprogramming of fibroblasts was performed using a CytoTune™-iPS 2.0 Sendai Reprogramming Kit (Thermo Fisher Scientific), according to the manufacturer's protocol. iPSCs were expanded as feeder free cultures in Essential 8™ Medium (Thermo Fisher Scientific) on Geltrex™ matrix-coated plates (Thermo Fisher Scientific) and maintained at 37°C in 5% CO_2 in a humidified incubator. Neuronal induction was performed as previously described (Shi et al., 2012b).

2.2 Animals

All experiments were performed using adult immunosuppressed NOD.Cg-*Prkdc*^{scid} *Il2rg*^{tm1Wjl}/*SzJ* male and female mice (JAX™ NSG, Charles River) aged between 3-5 months. Animals were exposed to 12-hour light/dark cycles and given access to diet and water *ab libitum*. All animal experiments were conducted in accordance with the Animals (Scientific Procedures) Act 1986, UK.

2.3 Surgical procedures

Stereotaxic cell injection and cranial glass window implantation (**Figure 2.1 A)** were performed under general anaesthesia, consisting of a combination of ketamine (83 μg/g of body weight) and xylazine administered intraperitoneally (7.8 μg/g of body weight), as previously described (Holtmaat et al., 2009). Before surgery began, mice were given subcutaneous bupivucaine (1 mg/kg of body weight) and intramuscular dexamethasone (2.5 mg/kg of body weight) to prevent pain and inflammation, respectively. Mice were placed on a heating pad and fitted into a stereotaxic frame (World Precision Instruments). The skin overlying the surgical field was

thoroughly cleaned with povidone-iodine solution. The scalp was then removed and topic lidocaine (1% solution) was applied to the skull prior to a 3-4 mm craniotomy being performed on the right parietal bone, using a high-speed drill. Neural cortical progenitors were allowed to differentiate for 31 days (Shi et al., 2012a), before being transduced with a lentiviral vector carrying either GFP or GCaMP6s plus tdTomato genes, under the control of the human Synapsin-1 promoter (**Table 1**). Between days 35 and 38, cells were dissociated with Accutase® (Sigma) and injected into the right somatosensory cortex with a customised glass needle fitted into a Hamilton syringe, using a micro syringe pump (UMP-3, World Precision Instruments), at the following stereotactic coordinates: anterior-posterior = -1.8 mm; medial-lateral = +2.8 mm; dorsal-ventral = -0.5 mm from bregma. Between 20,000-40,000 cells were injected in 1 µl of sterile cortex buffer solution (NaCl 125 mM, KCl 5 mM, glucose 10 mM, HEPES 10 mM, $MgSO_4$ 2 mM, $CaCl_2$ 2 mM, pH adjusted to 7.4). The needle was left in place 5 minutes after the injection, to avoid reflux of the injected cells. The cranial window was sealed with a 5-mm diameter glass coverslip using cyanoacrylate (Vetbond™, 3M). The exposed skull was covered with dental acrylic and a metal plate fixed on the left side, for positioning at the two-photon microscope stage. Post-operative anaesthesia consisted of carprofen (5 mg/kg of body weight), a non-steroid anti-inflammatory agent, or buprenorphine (0.05 mg/kg of body weight), administered as needed. **Table 2** lists all cell lines used in this study to generate the transplanted cells.

2.4 Live imaging

Three weeks after transplantation and cranial window implantation, animals were imaged in a custom built two-photon laser scanning microscope (Prairie Technologies) using a tunable Ti:Sapphire laser (Coeherent) and PrairieView acquisition software. Mice were lightly anaesthetized using isoflurane mixed with oxygen (1.5% isoflurane for structural imaging, and between 0.5-1% for calcium imaging). Eye ointment (Lacri-Lube®) was applied to the eyes to prevent dehydration and body temperature was maintained by a heat pad. Animals were tightly head-fixed to the microscope stage by securing the head-plate onto a custom-made head-plate holder. For structural imaging of neurites and synaptic structures, GFP was excited using a 920 nm pulsed laser bean and z-stacks acquired with either a 20x NA 1.2 (for neurites, 512 x 512 pixels, 149.42 x 149.42 μm) or 60x NA 0.9 (for synaptic structures, 512 x 512 pixels, 50.46 x 50.46 μm) water-immersion Olympus objective. For calcium imaging, transplanted cells were first identified by the tdTomato signal using a 1040 nm laser bean, and single plane images were taken. GCaMP6 was then excited using a 920 nm pulsed laser bean, and five-minute time lapse movies were acquired at 3 Hz in a single plane using a 20x water-immersion

Olympus objective (256 x 256 pixels, 298.86 x 298.86 μm). Data was acquired for approximately 60 minutes per animal.

2.5 Two-photon image analysis

Neurites were imaged at 3, 6 and 12 weeks post-transplantation (**Figure 2.1 B**). At each time point, the same neurites were imaged at T_{0h}, T_{8h} and T_{24h}. Two-photon z-stack images were pre-processed in FIJI (NIH) using the StackReg plugin (Thevenaz et al., 1998) and background subtraction. Neurite length measurements were performed by manually tracing neurites from clear fiducial points in maximum intensity projection images. Length measurements were exported and analysed in Microsoft Excel. Speed of growth and retraction at 8h and the proportion of neurites growing, retracting and stable at 24h were calculated for each time point.

Dendritic spines and axonal *en passant* boutons (EPBs) were imaged at 3 and 4 months post-transplantation. At each time point, the same dendrites and axons were imaged at 48h intervals for a maximum of 2 to 6 days. Dendritic spines were manually annotated and correlated between sessions using a MATLAB custom-made spine analysis software (Holtmaat et al., 2009). EPBs were analysed using EPBscore, a semi-automated software written in MATLAB (Grillo et al., 2013; Song et al., 2016). To be included in the analysis, EPBs had to be at least 1.90 times brighter than the axonal backbone in at least one session. Further analysis was performed using Microsoft Excel. Density of EPBs/spines was defined as Density (*a*) = N(*a*) / Length, where N is the total number of EPBs/spines present at any given time point *a*. The turnover ratio (TOR) was defined as TOR = (nG + nL) / (2*N), where nG and nL are the number of EPBs/spines gained and lost in a defined time interval, respectively, and N is the total number of EPBs/spines present in the same time interval. The fraction of EPBs/spines gained and lost between sessions *a* and *b* were defined as Gains = nG(*b*-*a*) / N(*a*+*b*) and Losses = nL(*b*-*a*) / N(*a*+*b*), respectively, where N(*a*+*b*) is the total number of EPBs/spines present in sessions *a* and *b*. The survival fraction (Fr) was defined by the fraction of the cumulative sum of EPBs/spines that survive at each time point, divided by the total number of EPBs/spines present in the first session.

In vivo calcium time-series were pre-processed in FIJI (NIH) using the moco plugin (Dubbs et al., 2016) for registration, followed by the application of a 3D median filter. For analysing the calcium activity of single cells, neurons were manually selected on the mean normalized maximum intensity projection of the data. Nuclei were excluded from the selection.

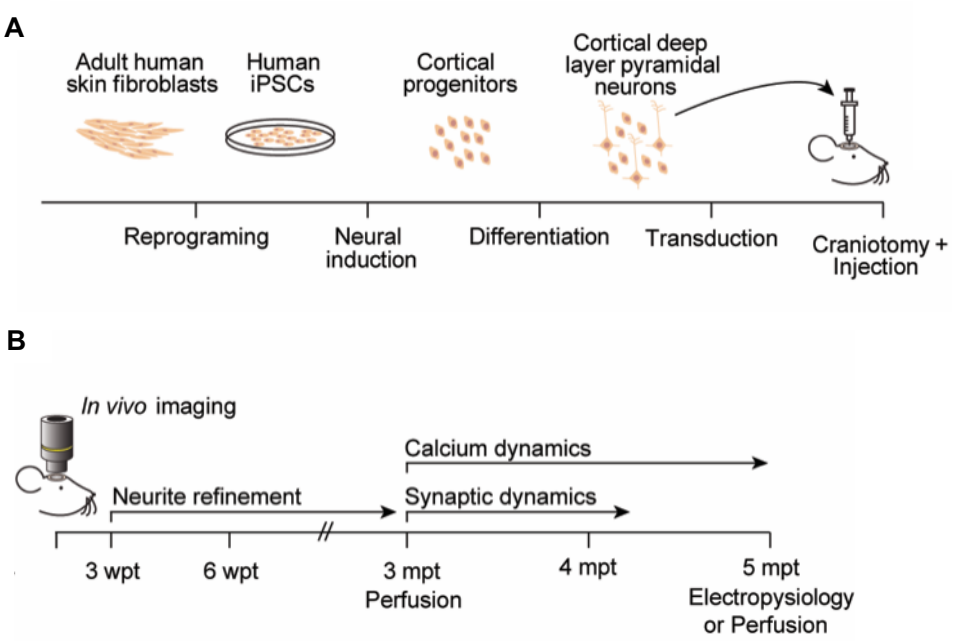

Figure 2.1 Schematic of experimental procedures and timeline.

(**A**) Cells obtained from skin biopsies were reprogrammed to iPSCs and differentiated into excitatory cortical neurons according to Shi et al. (2012b). Neurons were then transduced with lentiviral vectors carrying GFP (for structural imaging) or GCaMP6s + tdTomato (for calcium imaging). At ~36-38 days, cortical neural progenitors and neurons were transplanted in the somatosensory cortex of adult immunodeficient mice, and a cranial window implanted for long-term intravital microscopy.

(**B**) Imaging began 3 weeks after surgery. Neurites were imaged at 3, 6 and 12 wpt (weeks post-transplantation), synaptic dynamics was monitored at 3 and 4 mpt (months post-transplantation) and calcium dynamics at 3 and 5 mpt. Animals were either perfused at 3 or 5 mpt. A subset of animals was sacrificed at 5 mpt and the brains used for ex vivo electrophysiology experiments.

Fluorescence traces were calculated as the average fluorescence of pixels lying within the cell in each frame. To eliminate slow changes in raw fluorescence traces, the 15th percentile value of the fluorescence distribution was subtracted from the raw fluorescence signal. $\Delta F/F_0$ signals were calculated by dividing the raw fluorescence signal by the median of each cell fluorescence distribution, and normalizing to the background calcium signal. Cellular activity was calculated using the integrated fluorescence with a 15% $\Delta F/F_0$ threshold (Barnes et al., 2015). Activity was then normalized to the duration of the imaging paradigm in seconds. For analysing the global calcium activity of the entire region of interest (including the neuropil), the same protocol was applied but activity was measured in the whole region of interest instead of in individual cells. Bursts of calcium activity were defined as global events where > 95% of the peak pixel intensity was above the threshold defined above. All regions were visually inspected to confirm the presence of global events. To determine directionality of burst events,

images were divided into a 3 x 3 grid. For each burst event, the peak of the first derivative of the $\Delta F/F_0$ transient was calculated at 8 spatial positions (excluding the central square). The time of the peak derivative value at each of the 8 spatial positions during a calcium event was also annotated. Polar plots were calculated by taking the difference of each time point from the earliest time. Analysis of calcium signals was performed in MATLAB.

2.6 Electrophysiology

Coronal acute brain slices (350 µm) were maintained at room temperature (22-25 °C) in external solution (NaCl 125 mM, KCl 2.5 mM, NaH_2PO_4 1.25 mM, $NaHCO_3$ 25 mM, $CaCl_2$ 2 mM, $MgCl_2$ 1 mM, D-glucose 10 mM and D-mannitol 15 mM, pH adjusted to 7.4 and equilibrated with 95% O_2 and 5% CO_2). Human neurons were identified in the somatosensory cortex by excitation of GFP. Whole-cell current-clamp recordings were performed at 35 °C using borosilicate glass micropipettes with a resistance of 4-8 MΩ filled with intracellular solution (K^+ gluconate 130 mM, KCl 10 mM, EGTA 0.5 mM, NaCl 1 mM, $CaCl_2$, 0.28 mM, $MgCl_2$ 3 mM, Na_2ATP 3 mM, GTP 0.3 mM, phosphocreatine 14 mM and HEPES 10 mM, pH adjusted to 7.2). Current-voltage relationships were evoked by stepwise current injection from -80 up to +50 pA in steps of 10 pA. Whole-cell voltage-clamp recordings were performed at -70 mV using a modified internal solution (in which CsCl 130 mM was used instead of K^+ gluconate). Slices were bathed in (+)-bicuculline (20 µM) for miniature excitatory currents (mEPSC) or NBQX for miniature inhibitory currents (mIPSC). Synaptic kinetic analysis was performed on cells with at least 40 recorded events only.

2.7 Immunohistochemistry

At the end of the live imaging experiments, animals were anesthetized with an overdose of ketamine and xylazine, and then perfused intracardially with PBS, followed by 4% paraformaldehyde (PFA) solution in PBS. Brains were fixed overnight in 4% PFA and embedded in 4% agar in PBS. Sections were cut at 40 µm in a vibratome (Leica VT1000S) and stored free-floating in PBS with 0.01% NaN_3. For the cellular characterization of the graft, consecutive sections containing the graft were blocked in a 10% donkey serum with 0.5% Triton X-100 in PBS solution for 1h at room temperature, and then incubated overnight with primary antibodies at 4°C (**Table 3**). Sections were then incubated with appropriate secondary antibodies (1:1000, Alexa Fluor®, Thermo Fisher Scientific) for 2h at room temperature. All antibody incubations were performed in 5% donkey serum with 0.1% Triton X-100 in PBS solution. Nuclei were counterstained with DAPI (1:1000, Thermo Fisher Scientific) for 10

minutes, followed by extensive washing with PBS. Sections were then transferred to glass slides and mounted using ProLong® Gold Antifade Mountant (Thermo Fisher Scientific). All sections stained with anti-NuMA antibody required a sodium citrate (10 mM, pH 6) heat-mediated antigen retrieval procedure. Brain sections were imaged with a Leica TCS SP5 or SP8 confocal laser scanning microscope, using a 20x (NA 0.75) or an oil-immersion 40x objective (NA 1.45). Regions of interested were randomly selected within the graft area. A customized semi-automated ImageJ script was used to analyse images with nuclear markers. Briefly, nuclei were segmented and intensity values of segmented objects measured across all channels after background subtraction. Threshold levels were set to define positive objects. The criteria for threshold selection was elimination of type I error while minimizing the occurrence of type II error. Astrocytes ($GFAP^+$) and oligodendrocyte progenitors ($PDGFR^+$) were manually counted in FIJI (NIH). Microglia was analysed using a custom Cell Profiler pipeline (Bloomfield et al., 2018).

To obtain maps of axonal projections from the graft into the host brain, every other free-floating 70 µm section was selected across the entire brain (*n* = 2). Sections were stained with anti-human NCAM antibody (**Table 3**) as detailed above. Sections were imaged with an epifluorescence microscope (Olympus IX70) using a 20X objective (NA 0.5). The Allen Mouse Brain Atlas (Franklin and Paxinos, 2008) was used to identify brain areas of interest and axons were quantified in each region by manual counting of fibres using ImageJ (NIH).

2.8 Histology

Free-floating 40 µm brain sections were mounted on glass slides and allowed to air-dry at room temperature. Sections were then stained with the Haematoxylin and Eosin Stain Kit (Vector Labs) according to manufacturer protocol. Tissue sections were covered with Mayer's Haematoxylin for 4 minutes and then rinsed under running tap water to remove the excess stain. Sections were then covered with Bluing Reagent for 15 seconds, after which they were rinsed again. Slides were dipped in 100% ethanol for 10 seconds, and the excess blotted off. Eosin Y solution was applied to completely cover the brain sections for 2 minutes. Sections were again dipped in 100% ethanol for 10 seconds, followed by dehydration in three changes of 100% ethanol for 1 minute each. Finally, sections were cleared using a Xylene substitute (Sigma-Aldrich) and coverslipped with DPX mounting medium (Sigma-Aldrich). Sections were then analysed by an experienced pathologist, to exclude the formation of teratoma in the grafts.

2.9 Retrograde trans-synaptic tracing

TVA expressing lentivirus was produced using the pBOB-SynP-HTB plasmid (Addgene plasmid #30195). Neurons in culture were infected with the lentivirus expressing rabies glycoprotein (G), TVA receptor and nuclear GFP at day 30. The medium was changed the following day to remove the virus and the cells stereotactically injected into the somatosensory cortex of adult NSG mice, as previously described. After 5 months, an EnvA-pseudotyped, G-deleted mCherry expressing rabies virus (EnvA+RV-ΔG-mCherry) was injected in the same location. Animals were perfused 7 days later with 4% PFA intracardially, and the brains fixed overnight in 4% PFA. Coronal brain sections were cut at 50 µm in a vibratome (Leica VT1000S), and stained with anti-human nuclei (hNu), anti-GFP and anti-DsRed antibodies (**Table 3**), as described above. All regions of interest containing mCherry positive cells were imaged with a Leica TCS SP5 confocal laser scanning microscope using a 20x objective (NA 0.7), and quantifications of mCherry+/hNu+ and mCherry+/hNu- cells were performed by manual counting using Fiji (NIH). The EnvA pseudotyped rabies virus was a kind donation from Dr Marco Tripodi (MRC Laboratory of Molecular Biology, Cambridge, UK).

2.10 In situ hybridization

Brain sections were incubated in distilled water for 5 minutes, followed by dehydration in an ethanol series (30% and 50% for 10 minutes each, followed by 70% for another 30 minutes). Sections were allowed to air dry at room temperature for 1 day. Sections were then re-hydrated in PBS for 15 minutes and permeabilised in PBS with 0.5% Triton X-100 for 20 minutes. Heat-mediated antigen retrieval with sodium citrate buffer (10 mM, pH 6) was performed. Slides were transferred to 2x SSC, and afterwards equilibrated in a 2x SSC with 50% formamide solution for at least 4 hours, at room temperature. After mounting the Hsa21 probe (XL 21q22/XCP 21, Metasystems) and applying a 22x22 mm^2 coverslip sealed with rubber cement, slides were allowed to rest for 1h at room temperature, to allow the infiltration of the section with the probe. Slides were incubated at 80 °C for 5 minutes, to allow for denaturation of both cellular DNA and probe, and then at 37 °C in a dark humidified chamber for 2 days, to allow hybridization to occur. Slides were washed in 2x SSC at 37 °C, and then counterstained with DAPI (1:1000, Thermo Fisher Scientific). Sections were mounted using ProLong® Gold Antifade Mountant (Thermo Fisher Scientific) and imaged with a Leica SP5 confocal laser scanning microscope using an oil-immersion 63x (NA 1.45) objective.

Quantification of FISH signals was performed manually in ImageJ (NIH). Nuclei that appeared to be incomplete, damaged, overlapped with other nuclei, or that showed significant

background ‘noise’ were excluded from the analysis. A minimum of 50 nuclei from at least two Z-stack images were scored for each cell line. Nuclei were assigned to four different categories (‘one signal’, ‘two signals’ ‘three signals’ and ‘> three signals’) based on the observed number of FISH signals.

2.11 Electron microscopy

Immediately after the last imaging session, mice were perfused with a 2.5% glutaraldehyde and 2% paraformaldehyde solution in phosphate buffer (100 mM, pH 7.4). For electron microscopy reconstruction of dendritic spines imaged in vivo, brain sections containing those regions were cut parallel to the cranial window plane at 60 μm using a vibratome (Leica VT1000S). The individual brain sections were then re-imaged at the two-photon microscope to locate the previously imaged dendrites. Next, laser marks were made in the tissue to delimitate the exact location of the dendrites imaged in vivo, allowing for its identification in the resin embedded tissue (Bishop et al., 2011). The sections were then processed at EPFL’s BioEM Facility. Briefly, sections were stained with heavy metals and embedded in resin. Blocks were made in the graft area and around the visible laser marks. Blocks containing the graft were cut at 50-nm thickness sections, which were then collected on single slot grids. These were further stained and imaged in a transmission electron microscope (Tecnai, FEI Company). Additionally, blocks containing dendrites imaged in vivo were imaged using serial block-face scanning electron microscopy (Gatan 3View and Zeiss Merlin scanning electron microscope). Serial images taken from the regions of interest were aligned using FIJI (NIH), and the dendrites reconstructed using the TrakEM2 tools. The 3D structure of the reconstructed dendrite and presynaptic boutons was created with Blender software (version 2.57, Blender Foundation).

2.12 Gene expression analysis

RNA was collected from day 35-36 cultures and profiled using a custom gene expression panel of approximately 250 genes (NanoString™). Gene counts were normalized using the mean of 6 positive control probes and 7 housekeeping genes (*CLTC*, *GAPDH*, *GUSB*, *PPIA*, *RPLP1*, *RPS15A* and *RPS9*).

2.13 Copy number variation detection

Genomic DNA was extracted from iPSC clones using DNeasy Blood and Tissue Kit (Qiagen) following the manufacturer's instructions. Genome-wide SNP analysis was performed using the Infinium HumanCytoSNP-12 BeadChip or the Infinium CytoSNP-850K BeadChip platforms (Illumina Inc.). Data was processed using GenomeStudio 2.0 and analysed using CNV Region Report plugin v2.1 (Illumina Inc.).

2.14 Short tandem repeat assay

Genomic DNA was extracted from iPSCs as previously described. DNA typing was performed using the PowerPlex® 16 HS System (Promega) according to the manufacturer's instructions. Genotype of the third allele in trisomy lines was extrapolated from the electropherogram peak height.

2.15 Statistics and data presentation

Statistical analyses were performed in GraphPad Prism (Version 7, GraphPad Software). All data are presented as the mean ± standard error of the mean (SEM), unless otherwise specified. Significance was set at $P < 0.05$. In the figures, *$P < 0.05$, **$P < 0.01$, ***$P < 0.001$ and ****$P < 0.0001$.

All image analysis was performed in the original image files. For display purposes only, two-photon images were cleared of the background in Adobe Photoshop. All figures were prepared in Adobe Illustrator CC 2018.

Table 1. Lentiviral vectors used for cell transduction

Plasmid	# Transplanted animals (WT/Ts21)
pBOB-Syn-GFP	24 (12/12)
pBOB-Syn-GCaMP6s-P2A-tdTomato	24 (12/12)
pBOB-Syn-H2B-GFP-2A-TVA receptor-2A-rabies glycoprotein	6 (6/0)

Table 2. Cell lines used to generate transplanted cortical neurons

Cell Line ID	Karyotype	Clone ID	Donor Cells	Reprogramming Method	Reference
WT-1	Euploid	NDC1.2	Fibroblasts	Retrovirus with OSKM	Israel et al., 2012
Ts21-1	Trisomy 21	DSiPS	Fibroblasts	Retrovirus with OSKM	Park et al., 2008
WT-2	Euploid	THO3B	Fibroblasts	Sendai virus with OSKM	Real et al., 2018
Ts21-2	Trisomy 21	THO3F	Fibroblasts	Sendai virus with OSKM	Real et al., 2018

O, *OCT3*/4. S, *SOX2*. K, *KLF4*. M, c-*MYC*.

Table 3. Antibodies used for immunofluorescence

Antibody	Host Species	Dilution	Reference
DsRed-Express	Rabbit	1:500	Clontech, 632496
Human Nestin	Mouse monoclonal	1:1000	R&D Systems, MAB1259
PDFG Receptor α	Rabbit	1:1000	Cell Signaling, 3164
GFP	Chicken	1:300	Novus Biologicals, NB100-1614
Doublecortin	Rabbit	1:400	Cell Signaling, 4604
Ki67	Rabbit	1:1000	Abcam, ab15580
Ki67 (clone B56)	Mouse monoclonal	1:100	BD Biosciences, 550609
Ki67 [OTI5D7]	Rat monoclonal	1:500	Abcam, ab156956
Human Nuclei	Mouse monoclonal	1:200	Millipore, MAB1281
Pax-6	Rabbit	1:300	Biolegend, 901301
NuMA	Rabbit	1:200	Abcam, ab97585
NCAM (ERIC-1)	Mouse monoclonal	1:1000	Santa Cruz Biotechnology, sc-106
Human GFAP	Mouse monoclonal	1:500	Stem123, AB-123-U-050
GFAP	Rabbit	1:1000	DAKO, Z0334
GAD67	Rabbit	1:500	Abcam, ab97739
Iba1	Goat	1:1000	Abcam, ab5076
CD31	Rat	1:200	Biolegend, 102402
TBR1	Rabbit	1:200	Abcam, ab31940
SATB2 [A4B10]	Mouse monoclonal	1:200	Abcam, ab51502
CTIP2 [25B6]	Rat monoclonal	1:300	Abcam, ab18465
OLIG2	Rabbit	1:1000	Millipore, AB9610
VGLUT1	Guinea Pig	1:1000	Millipore, AB5905

Chapter 3. In vivo modelling of human neuron dynamics

3.1 Cellular characterization of transplanted human grafts

To establish the value of an in vivo model of human neural development based on human iPSCs-derived neurons transplanted into the cortex of adult immunodeficient mice, hiPSCs previously generated from skin fibroblasts of an adult individual (Israel et al., 2012) were differentiated into cerebral cortex stem and progenitor cells by the combination of retinoid signalling and dual SMAD inhibition (Shi et al., 2012b), a protocol which has been previously shown to have very high efficiency in promoting cortical neural induction (Shi et al., 2012a). Neural stem cells thus generated were subsequently transduced with a lentiviral vector expressing fluorescent GFP under the human synapsin 1 (hSYN1) promoter, after which cells were transplanted in the somatosensory cortex of adult immunocompromised mice (NSG strain). Importantly, at the stage of transplantation, between 36-38 days after neural induction, cultures contained a combination of cortical neural progenitor cells and cortical deep layer neurons only. To confirm cell identity after transplantation, fluorescent immunohistochemistry was performed at 3 and 5 months after the transplantation procedure (**Figure 3.1**). Cortical neural progenitors ($PAX6^+$ cells) and proliferating cells ($Ki67^+$ cells) were still present at both 3 and 5 months after transplantation (25.7 ± 4.2% vs. 16.2 ± 2.4% for PAX6 and 6.8 ± 3.0% vs. 1.0 ± 0.3% for Ki67, respectively). Consistent with ongoing neurogenesis after transplantation, cortical deep layer excitatory neurons ($TBR1^+$ and $CTIP2^+$ cells) as well as cortical upper layer excitatory neurons ($SATB2^+$ cells) were present, with the proportion of the former decreasing over time (from 60.2 ± 6.4% to 25.8 ± 4.0% for TBR1 and from 46.5 ± 16.4% to 19.9 ± 5.8% for CTIP2), while the proportion of the latter increased (from 43.6 ± 18.2% to 71.2 ± 9.6%). Additionally, glial cells derived from the neuroectoderm – astrocytes ($hGFAP^+$ cells) and oligodendrocytes ($OLIG2^+$ cells) – also developed over time, which is consistent with the known temporal pattern of human cortical neurogenesis (van den Ameele et al., 2014). In addition, as previously observed with transplanted hESC-derived cortical neural progenitors (Espuny-Camacho et al., 2013), the transplantation of hiPSC-derived neurons into the rodent brain did not have an impact on the time course of neurogenesis, with the development of the different cortical cells types occurring over a protracted period of time, more consistent with human rather than mouse cortical development. This finding confirms that the developmental processes that regulate cortical neurogenesis are cell-autonomous and species-specific. The differentiation protocol used promotes the acquisition of a dorsal

telencephalic identity, therefore no GABAergic interneurons of human origin were identified in the graft, as these cells derive from the ventral telencephalon.

In addition to the various cell types that characterize the human cortex, the human grafts contained complex cytoarchitectural patterns, including the presence of rosette-like structures (**Figure 3.2**). Neural rosettes are transient multicellular structures that form in vitro when hESCs/iPSCs are differentiated into the cortical lineage (Ziv et al., 2015). The typical radial organization of neuroepithelial and radial glial cells around a lumen in neural rosettes is reminiscent of the structure of the ventricular zone of the developing mammalian cortex, where cortical neurogenesis occurs (Lui et al., 2011). Rosette-like structures were observed only in early stage tissue grafts (<2 months after transplantation) and consisted of a core of $PAX6^+$ and $Ki67^+$ cells, with early-born neurons (DXC^+) located at the periphery of the rosettes and into the rest of the graft (**Figure 3.2 A**). In addition, $Nestin^+$ processes extended radially from the core of the rosette into the periphery. Nestin is a radial glial cell marker and the observed parallel arrangement of $Nestin^+$ processes in the graft (**Figure 3.2 B**) is suggestive of the organization of radial fibres in the human foetal cortex (Lui et al., 2011). Thus, the patterns observed in the human cortical grafts are highly evocative of the structure of the ventricular zone, and indicate that neurogenesis in the grafts occurs in similar structures to in vivo. Another interesting observation was the relative segregation of lower and upper layer neurons subtypes in the human grafts (**Figure 3.2 C**); although no true cortical layering was present, neurons from different layers tended to form independent territories. Thus, human cortical progenitor cells after transplantation tend to recapitulate several aspects of cortical neurogenesis, including the organizational features of the early foetal cortex. Cerebral organoids have been developed that also recapitulate several aspects of neurogenesis and the structural features of the human brain (Lancaster et al., 2013; Mariani et al., 2015; Pasca et al., 2015; Qian et al., 2016). However, the lack of vascularization in the organoids in vitro limits their survival. It was significant that the human grafts were highly vascularized, as evident by the presence of endothelial marker CD31 (**Figure 3.2 D**). Since human cortical neurogenesis is a process that occurs over many months, the enhanced survival conferred by the transplantation of human cortical progenitors offers advantages to the study of human cortical development into later stages of maturation.

To explore the interaction between the human graft and the host brain, fluorescent immunohistochemistry was also performed to identify cell types derived from the host within the graft (**Figure 3.3**). Human grafts contained several cell types derived from the host, including cortical excitatory glutamatergic deep ($TBR1^+$ and $CTIP2^+$ cells) and upper layer ($SATB2^+$) neurons, inhibitory GABAergic interneurons ($GAD67^+$ cells), astrocytes ($GFAP^+$

cells), oligodendrocytes (OLIG2$^+$ and PDGFRα^+ cells) and microglial cells (IBA1$^+$ cells). Microglia cells derive from the mesoderm (Ginhoux et al., 2013) and therefore no human microglial cells are present in the grafts. Importantly, cell types derived from the host accounted for a minority of all cells within the human graft (**Figure 3.3 C**).

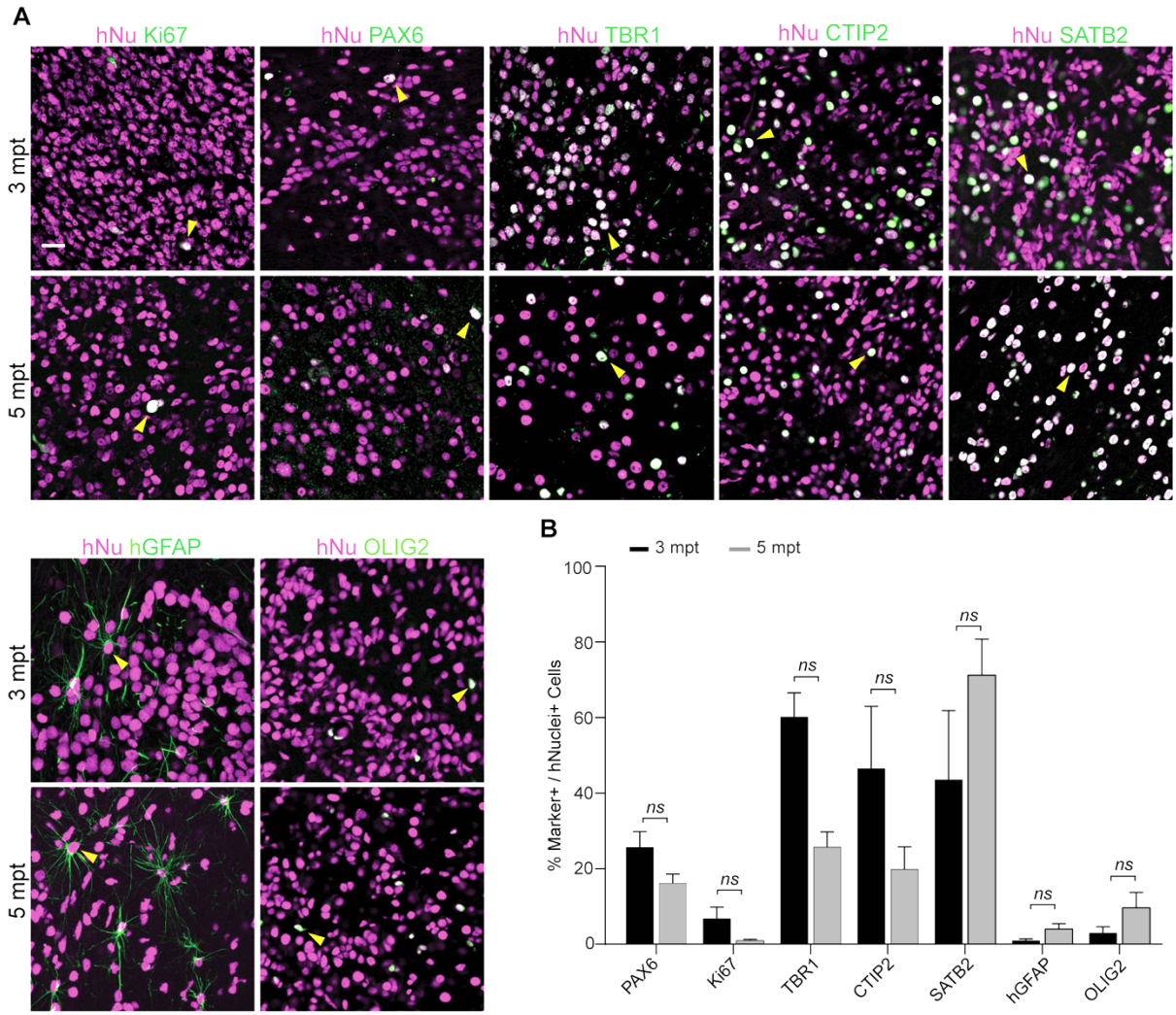

Figure 3.1 Ongoing neurogenesis in human cortical grafts.

(**A**) Representative immunostaining of human grafts 3 and 5 months after transplantation for Ki67, PAX6, TBR1, CTIP2, SATB2, GFAP and OLIG2. Arrowheads indicate examples of positive human cells. Scale bar, 20 µm.

(**B**) Quantification of cell populations in vivo at 3 and 5 months post-transplantation (*n* = 3 animals for each time point; human nuclei (hNu$^+$) sampled per cell marker 2994 ± 487 at 3 mpt and 3283 ± 245 at 5 mpt, mean ± SD). Sidak's multiple comparison test after one-way ANOVA; *ns*, not significant. Data are represented as mean ± SEM.

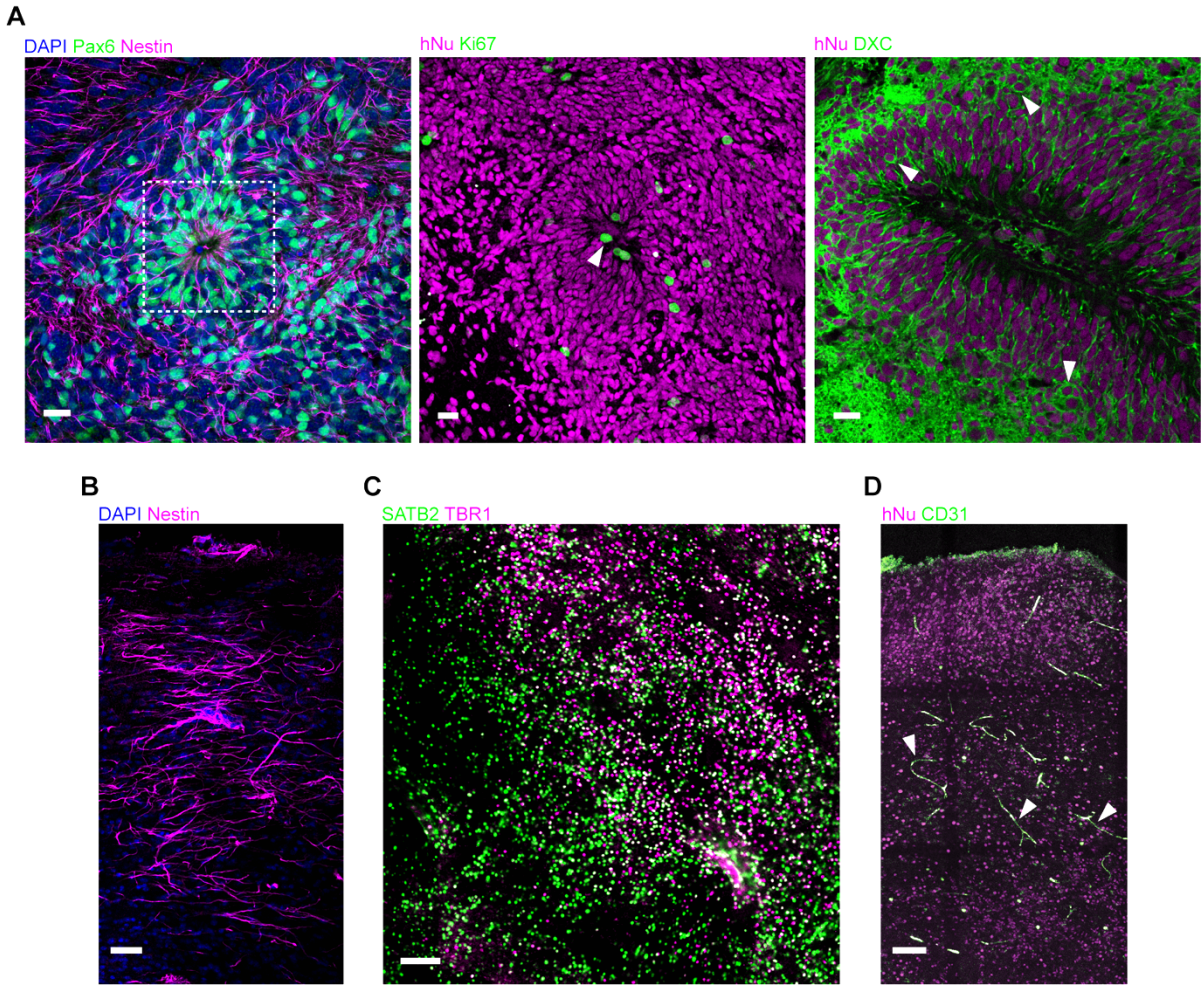

Figure 3.2 Vascularization and complex cytoarchitecture of the human grafts.

(**A**) Representative immunostaining of a neural rosette-like structure in the human graft for PAX6, Nestin, Ki67 and doublecortin (DXC), 2 months after transplantation. Arrowheads indicate positive human cells. The highlighted region in the first image (left) depicts the core at of neural rosette at its centre. Scale bars, 20 μm.

(**B**) Representative immunostaining of Nestin-positive processes in the human graft 2 months after transplantation. Scale bar, 50 μm.

(**C**) Representative immunostaining of the human graft 5 months after transplantation for SATB2 and TBR1. Note the segregation of upper and lower layer cortical neurons Scale bar, 100 μm.

(**D**) Representative immunostaining of the endothelial marker CD31 in the human graft 5 months after transplantation, denoting vascularization of the human graft (arrowheads). Scale bar, 100 μm.

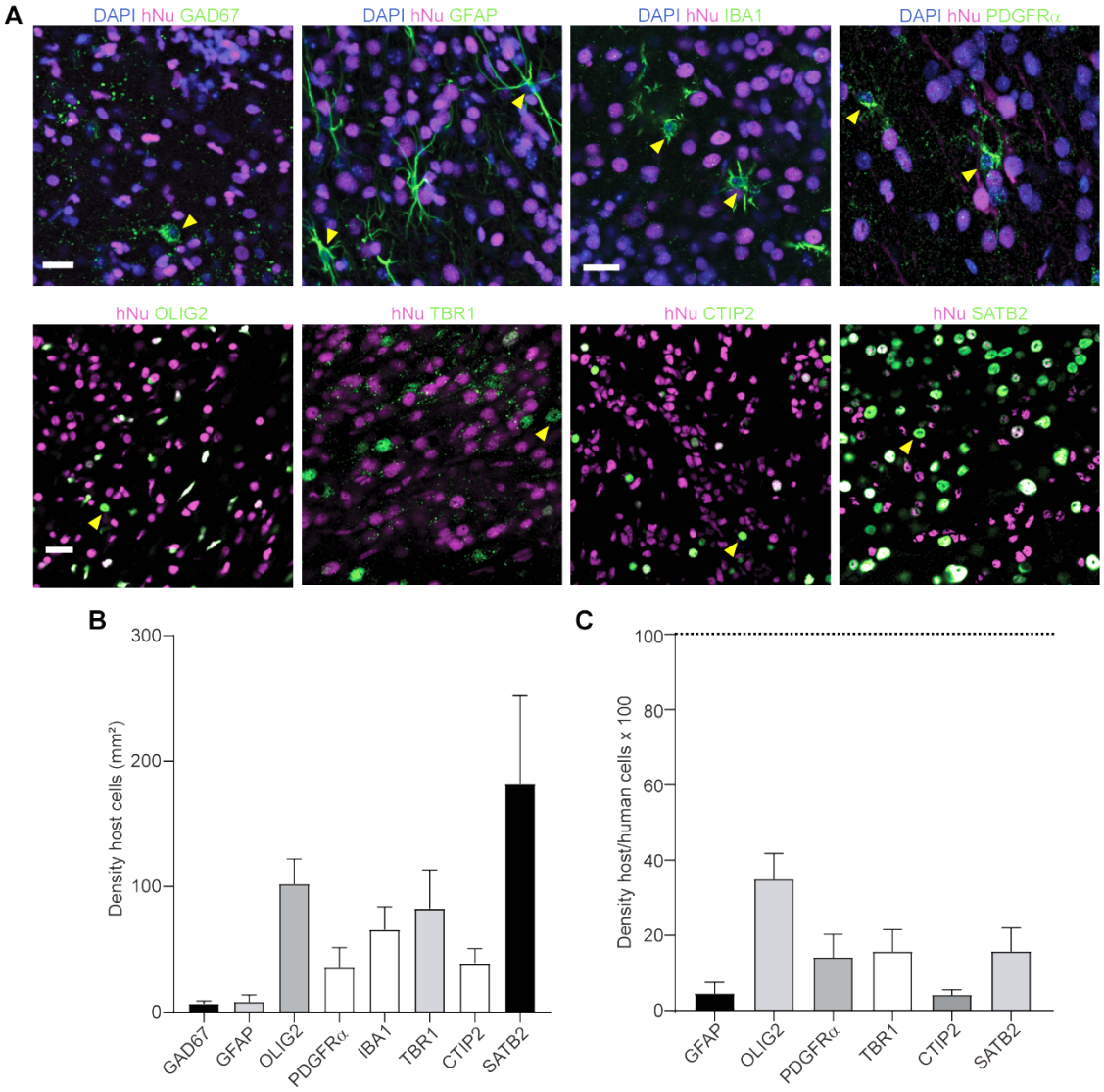

Figure 3.3 Host cell identity within the human grafts.

(**A**) Representative immunostaining of human grafts at 5 months after transplantation for GAD67, GFAP, IBA1, PDGFRα, OLIG2, TBR1, CTIP2 and SATB2. Arrowheads indicate examples of positive host cells. Scale bars, 20 µm.

(**B**) Quantification of host cell density within the graft (*n* = 3 mice; area sampled per cell marker 1.54 ± 0.03 mm^2, mean ± SD).

(**C**) Host cell density in the graft normalized to the respective human cell density (dashed line; *n* = 3 mice; area sampled per cell marker 0.80 ± 0.08 mm^2, mean ± SD). Data are represented as mean ± SEM.

To understand whether the human grafts elicited an immune response from the host, microglia was quantified in the graft and in the contralateral somatosensory cortex of the host, which was devoid of human cells. Notably, there were significantly less microglial cells in the human grafts compared to the same region in the contralateral host brain, indicating minimal recruitment of host-derived microglia to the human graft (**Figure 3.4**).

Finally, to comprehend how the human graft integrates with the host brain, electron microscopy was performed. This revealed a predominantly immature neural tissue in the graft area (i.e., reduced number of synapses and absence of myelinated fibres), consistent with the early developmental stage of the human neurons, but no apparent frontier between the graft and the host brain tissue (**Figure 3.5**). Similarly, H&E staining of brain sections also revealed a markedly immature neural tissue, with no evidence of teratoma formation (**Figure 3.6**). These findings suggest that the human grafts are structurally well integrated within the host brain, and that cellular interactions between the host and the graft are likely. Overall, these findings suggest that the adult mouse microenvironment can support the development of a multicellular and structurally complex human cortical transplant.

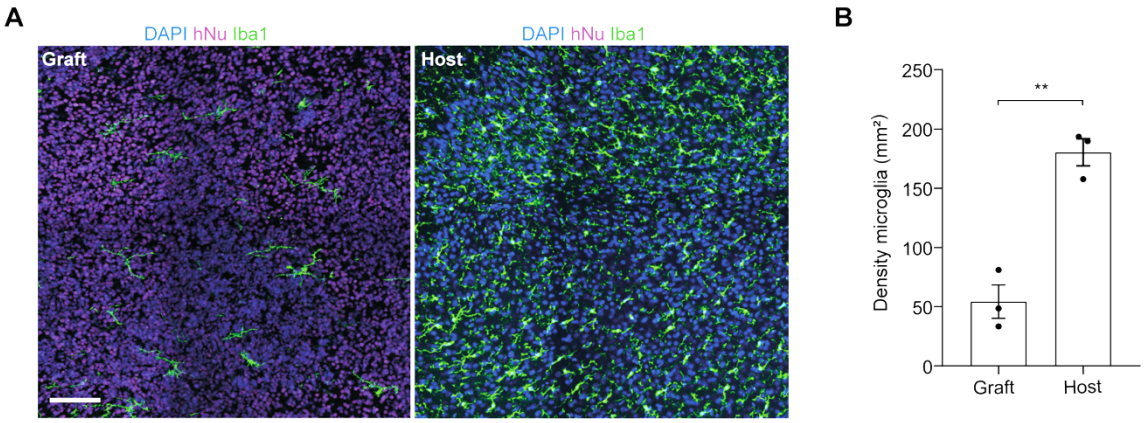

Figure 3.4 Minimal recruitment of host-derived microglia to the human graft.

(**A**) Representative immunostaining of Iba1 in the graft (left) and host cortex (right), 3 months after transplantation. Scale bar, 100 µm.

(**B**) Quantification of microglia density 3 months post-transplantation (n = 3 mice) in the graft (area sampled 5.2 ± 1.5 mm^2, mean ± SD) and respective contralateral host cortex (area sampled 2.4 ± 0.0 mm^2, mean ± SD). Paired t-test, $^{**}P < 0.01$. Data are represented as mean ± SEM. Each data point represents an animal.

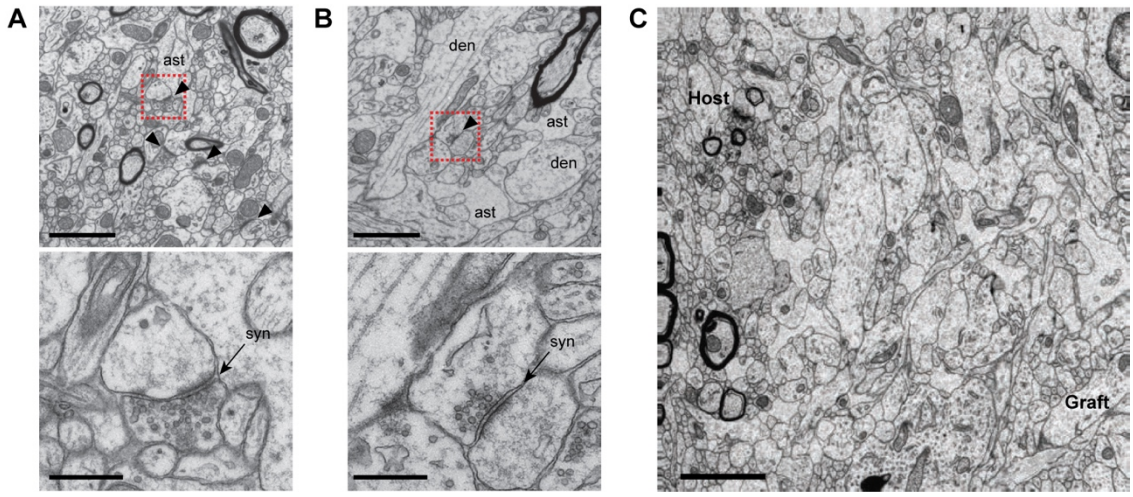

Figure 3.5 Ultrastructure of human grafts reveals immature neural tissue.

(**A**) Representative electron microscopy image of the neuropil in the host cortex immediately adjacent to the human graft. Several synapses (arrowheads) are present. The bottom panel is a magnified image of the region highlighted by the red box. Scale bars, 2 µm (top) and 0.5 µm (bottom).

(**B**) Representative electron microscopy image of the human graft. Fewer synapses (arrowhead) are present (enlarged example in bottom panel). Scale bars, 2 µm (top) and 0.5 µm (bottom). ast, astrocytic profiles. den, dendrite. syn, synapse.

(**C**) Representative electron microscopy image of the interface between the human graft and the host brain tissue. Note the presence of myelinated fibers exclusively in the host brain tissue. Scale bar, 3 µm.

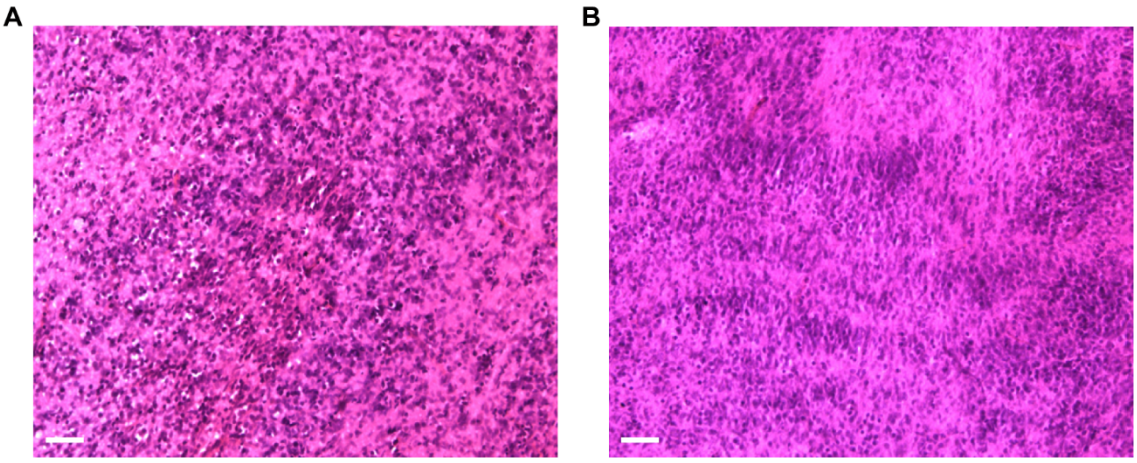

Figure 3.6 No teratomas developed in the human grafts.

(**A-B**) Representative images of human grafts stained with haematoxylin and eosin (H&E) at 3 (A) and 5 (B) months post-transplantation. There is diffuse and nodular proliferation of neural progenitor cells, intermediate size cells and focal palisading of nuclei. No other differentiating elements are present and teratoma formation was excluded in all human grafts analysed (n = 4 at 3 months and n = 10 at 5 months after transplantation). Scale bars, 100 µm.

3.2 In vivo characterization of human neuron structural development

The transplantation of human cortical progenitors and immature neurons into the cortex of mice provides a unique opportunity to study the cellular mechanisms of human neuron development in vivo. To explore the dynamics of neurite outgrowth in vivo, hiPSC-derived cortical progenitor cells and neurons were engineered to express GFP via lentiviral-mediated transduction prior to transplantation. GFP-expressing human neurons developed neurites that grew extensively outside the initial engraftment area, in bundles along vessels (**Figure 3.6 A**) and organized in layers both parallel and radially oriented below the dura mater (**Figure 3.7 B**), consistent with patterns of axon organization found in the human cortex (Edwards et al., 2018; Morawski et al., 2018). During the first three months after transplantation, neurons were still seen migrating (**Figure 3.7 C**) and developing neural processes in a highly dynamic mode (**Figure 3.7 D-G**), reflecting the very early stage of maturation of the cells present in the human grafts. Twelve weeks after the transplantation, the fate of 92 neurites from 88 cells (n = 6 mice) was followed to determine mechanisms of human neurite development and refinement. While most neurites showed net elongation over a 24h period (58.4 ± 5.5 %; **Figure 3.7 I**), intermediary pruning events were very frequent, with both axonal and dendritic arbours undergoing extensive remodelling by interchanging retraction and elongation of individual neurites in 31.0 ± 2.1% of cases. Net pruning of branches was also observed, mainly by retraction (39.7 ± 4.8%) rather than degeneration, which occurred in <1% of tracked neurites. Distinction between degeneration and retraction was established based on the presence or absence of fluorescent debris suggesting neurite fragmentation, respectively. The observed pattern of neurite refinement is consistent with pruning mechanisms described in the early development of rodents (Portera-Cailliau et al., 2005). Axonal *en passant* boutons (EPBs), one of the two types of presynaptic specialization in cortical neurons, could be observed in branches with a growth cone elongating (**Figure 3.7 G**), a finding previously described in transplanted mouse embryonic neurons (Falkner et al., 2016), again revealing conservation of basic developmental growth programs between species. Neural processes elongated for long distances (maximum neurite extension = 462.769 µm in 24h) at a speed of 10.29 ± 0.73 µm/h (**Figure 3.7 H**), which is comparable to that observed in the neonatal mouse brain (Portera-Cailliau et al., 2005).

To determine which host brain regions the human axons were projecting to, the entire brains of 3 animals were stained for hNCAM, which specifically stains the membranes of human neurons. This was performed 5 months after transplantation, to allow sufficient time for long-range axonal extension. The main target areas of the somatosensory cortex (where the human cells were implanted) were preferentially targeted, as revealed by the higher number of human

fibres in these areas compared to non-target areas (**Figure 3.8**), suggesting that axonal targeting was not a random event. Specifically, more human axons were found in the ipsilateral motor cortex, striatum, thalamus and contralateral somatosensory cortex – all known target areas of the somatosensory cortex – than in the cerebellum or substancia nigra. Similarly, the corpus callosum had more human axonal tracts than the internal capsule and the cerebral peduncles, as expected from rodent axonal tracing experiments (Zakiewicz et al., 2014). This suggests that while human axons are either not responsive or can overcome the inhibitory signals present in the adult mouse brain (Giger et al., 2010), they may be directed by persistent guidance cues or pre-existing axonal paths.

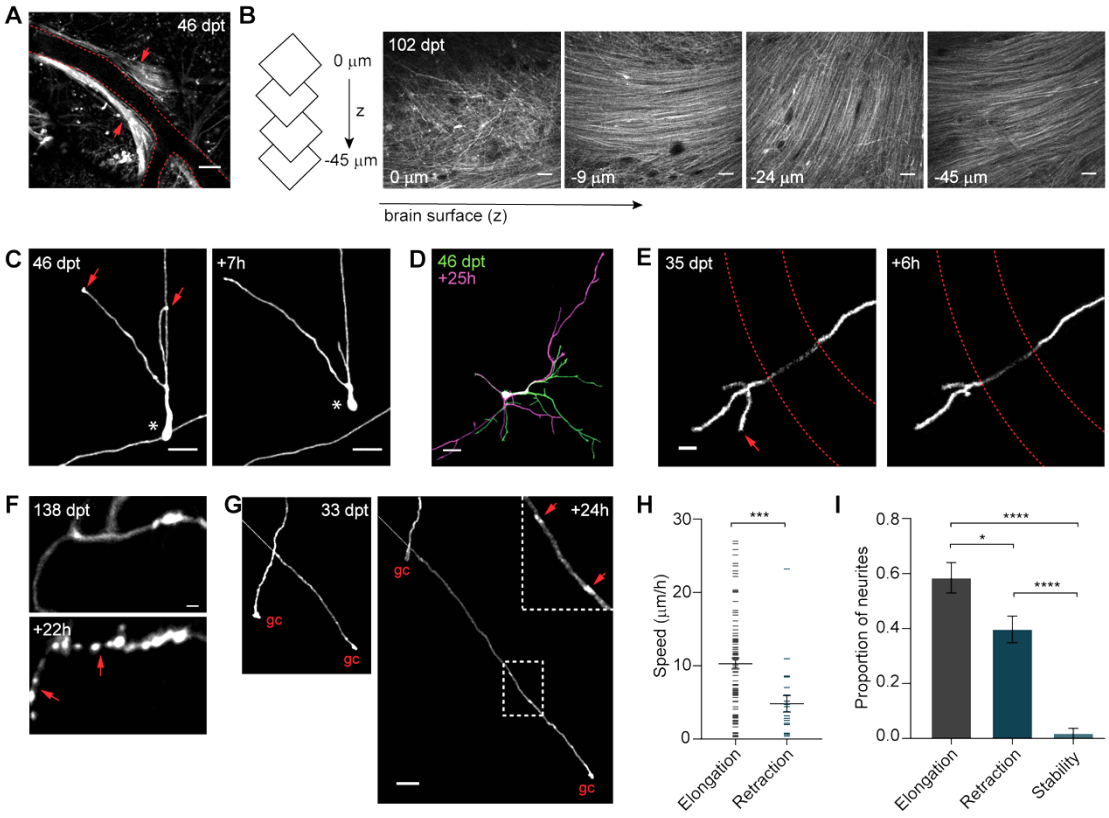

Figure 3.7 In vivo 2P imaging of human cortical grafts reveals cellular mechanisms of pruning.

(**A**) Representative example of axonal bundles (arrows) along blood vessels; dashed red lines represent a blood vessel. Scale bar, 50 µm.

(**B**) Representative example of axonal layering in the z-plane in human grafts. Scale bar, 50 µm.

(**C**) Representative example of a human neuron migrating (*) and remodelling the leading processes (arrows) over a 7h interval. Scale bar, 20 µm.

(**D**) Representative example of extensive remodelling of a dendritic arbour in a human pyramidal neuron over a 25h period. Scale bar, 20 µm.

(**E**) Pruning of an axonal branch by retraction (arrow) over 6h. Dashed red lines represent a blood vessel. Scale bar, 10 µm.

(**F**) Representative example of neurite degeneration over 22h, arrows indicate axonal fragments. Scale bar, 2 µm.

(**G**) Representative examples of axon elongation and retraction over 24h; arrows in the inset indicate EPBs. gc, growth cone. Scale bar, 20 µm.

(**H**) Quantification of speed of neurite elongation and retraction at 3 months after transplantation (n = 113 neurites from 104 cells, in 6 animals). Mann-Whitney U-test, ***$P < 0.001$.

(I) Proportion of neurites elongating, retracting and stable in 24h intervals at 3 months after transplantation (n = 92 neurites from 88 cells, in 6 animals). Bonferroni's multiple comparisons test after one-way ANOVA, $F_{2,15} = 43.74$, $P < 0.0001$; *$P < 0.05$; ****$P < 0.0001$. Data are represented as mean ± SEM.

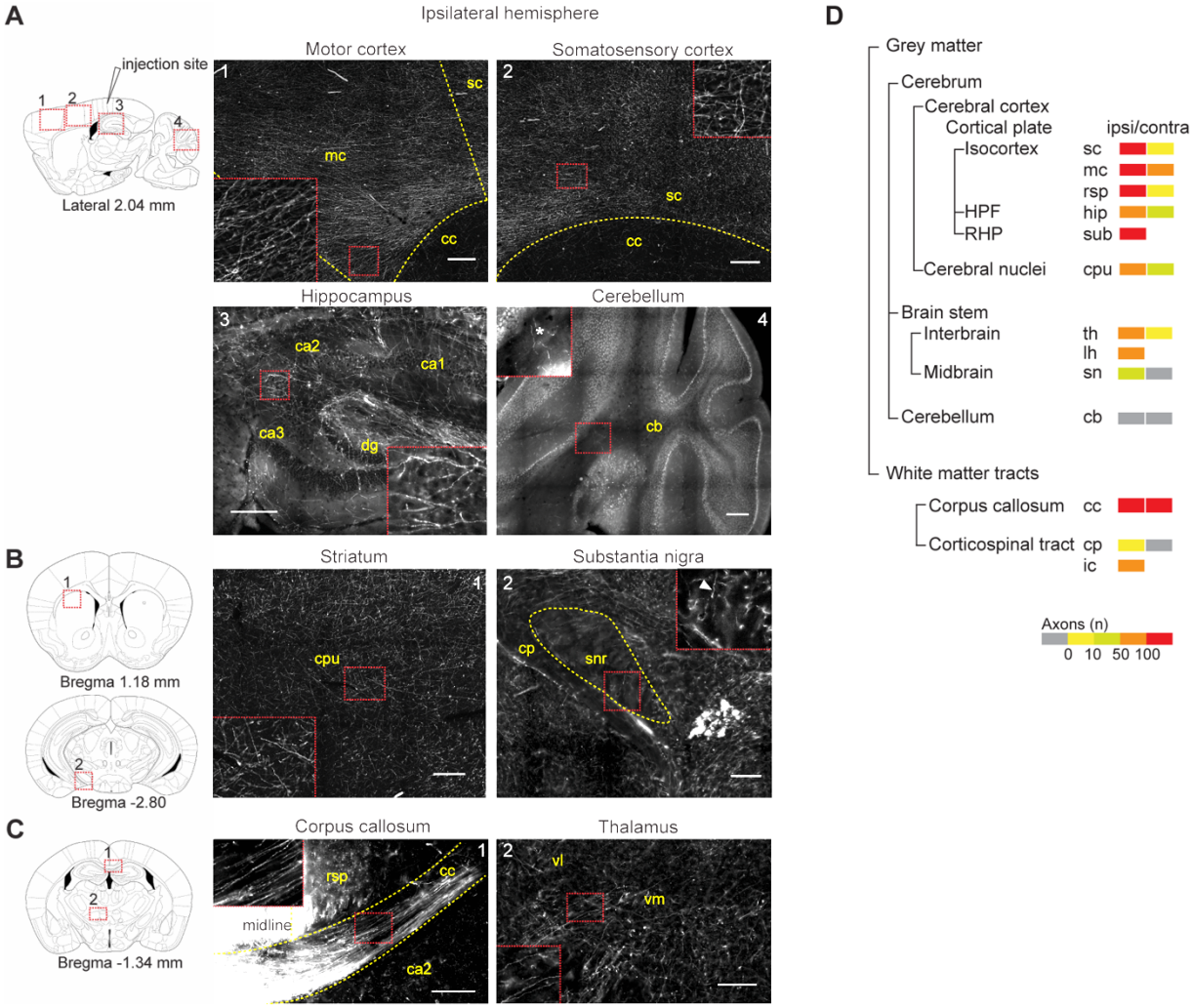

Figure 3.8 Human neurons project to known target areas of the somatosensory cortex.

(**A**) Left: schematic sagittal view of the adult mouse brain; numbered red boxes indicate the following regions: (1) somatosensory cortex adjacent to the injection site, (2) motor cortex, (3) hippocampus, and (4) cerebellum. Right: representative hNCAM immunostaining of the numbered regions shown in the schematic 5 months after transplantation; asterisk marks autofluorescence in a vessel, in the absence of hNCAM signal.

(**B**) Left: schematic coronal view of the adult mouse brain 1.18 (top) and -2.80 mm (bottom) from Bregma. Right: representative hNCAM immunostaining of the striatum, substantia nigra and cerebral peduncle 5 months after transplantation; arrowhead in the inset shows an example of an axonal fibre.

(**C**) Left: schematic coronal view of the adult mouse brain 1.34 mm from Bregma; numbered red boxes indicate the following regions: (1) corpus callosum and (2) thalamus. Right: representative hNCAM immunostaining of the regions indicated in the schematic 5 months after transplantation. Schematic brain images were adapted from Franklin and Paxinos, 2008. Dashed yellow lines mark anatomical boundaries. Red dashed boxes contain magnified insets. Scale bars, 200 µm.

(**D**) Quantification of axonal density in grey and white matter brain regions (*n* = 3 animals). Fibre density is color-coded (from grey: no human axons, to bright red: > 100 human axons).

(continued on next page)

Axonal boutons and dendritic spines are the structural correlates of mammalian excitatory synapses (Harris and Weinberg, 2012). In order to investigate the early stages of human synaptic development, EPBs and dendritic spines were monitored longitudinally in transplanted GFP-expressing human neurons (**Figure 3.9 A-B and Figure 3.10 A-B**). Dendritic filopodia or spines were first observed at 32.8 ± 5.5 days after transplantation (n = 3 animals). However, due to the initial phase of cell migration and extensive neurite remodelling, the same dendrites could not be tracked over consecutive imaging sessions during the first 3 months after transplantation. In addition, for most dendrites the density of synaptic structures was too low to quantitatively study the dynamics of dendritic spines, in accordance to the very early developmental stage of the transplanted neurons. At later time points, eight neurons had sufficient dendritic spine numbers to calculate spine density and turnover ratios. Time-lapse imaging performed at 48h intervals for up to 6 days revealed that the average spine density 3 months after transplantation was 0.043 ± 0.006 spines/µm (n = 176 in all sessions). The low spine density is consistent with the primordial developmental stage of the transplanted neurons. There was also evidence of significant dendritic spine formation and elimination, as indicated by a turnover ratio of 46.9 ± 5.3% over 4 days (**Figure 3.9 F**). Despite the highly dynamic synaptic reorganization, average spine density was kept constant over the same time interval (Kruskal-Wallis test, $P > 0.05$; **Figure 3.9 C**, red line), due to synaptic structures being added and eliminated at equal rates (Wilcoxon matched-pairs signed rank test, $P > 0.05$; **Figure 3.9 D**, red line). To investigate how spine dynamics evolves over time, the same measurements were performed after one month. Again, average spine density was constant over time (Kruskal-Wallis test, $P > 0.05$; **Figure 3.9 C**, blue line), as was the average fraction of dendritic spines gained and lost over 48h (paired two-tailed t-test, $P > 0.05$; **Figure 3.9 D**, blue line). However, the average spine density was 0.112 ± 0.024 spines/µm (n = 291 in all sessions), significantly higher than at 3 months after transplantation (two-way ANOVA, $F_{3,46} = 0.4357$, $P < 0.0001$; **Figure 3.9 C**). Consistently, the turnover ratio was significantly reduced to 27.6 ± 3.7% (Mann-Whitney U-test, $P < 0.05$; **Figure 3.9 E**) and the survival fraction also increased considerably (two-way ANOVA, $F_{3,47} = 1.513$, $P < 0.05$; **Figure 3.9 F**), suggesting that the increased spine density over one month is due to stabilization of dendritic spine dynamics within this time interval.

(continued from previous page)

Abbreviations: mc, motor cortex. sc, somatosensory cortex. rsp, retrosplenial cortex. HPF, hippocampal formation. hip, hippocampal region. ca1, ca2, ca3 indicate CA1, CA2, CA3 subfields of the hippocampus, respectively. dg, dentate girus. RHP, retrohippocampal region. sub, subiculum. cpu, caudate-putamen (striatum). th, thalamus. lh, lateral hypothalamus. sn, substantia nigra. cb, cerebellum. cc, corpus callosum. cp, cerebral peduncle. ic, internal capsule. vl, ventrolateral thalamus. vm, ventromedial thalamus.

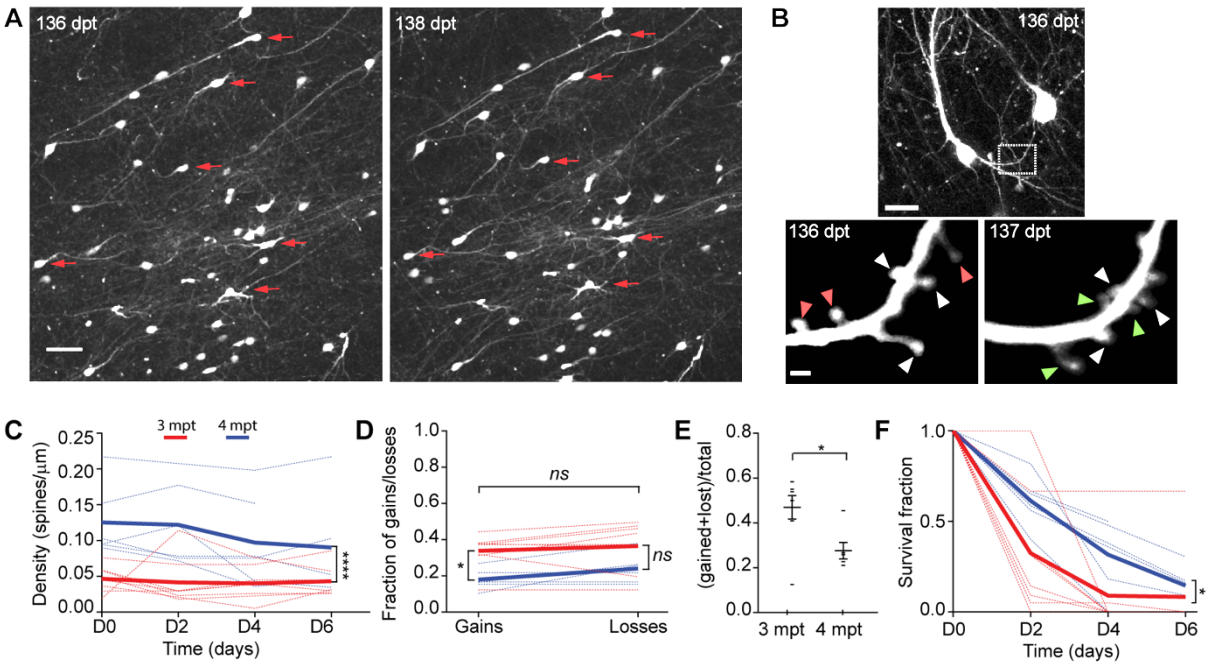

Figure 3.9 Developing dendritic synaptic structures are characterized by highly dynamic restructuring and balanced rates of gains and losses.

(**A**) Overview of the cranial window over a 2-day period; the arrows indicate examples of cells with a stable location in the indicated time interval. Scale bar, 50 µm.

(**B**) Top: representative example of a human neuron. Scale bar, 20 µm. Bottom: detail of a dendrite (white box in top panel) imaged over 24h; green, red and white arrowheads indicate gained, lost and stable dendritic spines, respectively. Scale bar, 2 µm.

(**C**) Dendritic spine density over 4-6 days at 3 (red: n = 8 cells from 3 animals, 1.40 mm total dendritic length) and 4 months after transplantation (blue: n = 6 cells from 2 animals, 0.93 mm total dendritic length). Two-way ANOVA, interaction $F_{3,46}$ = 0.4357, P = 0.7285. ****P < 0.0001.

(**D**) Average fraction of dendritic spines gained and lost over 48h at 3 (red: n = 8 cells) and 4 months after transplantation (blue: n = 6). Two-way ANOVA, interaction $F_{1,24}$ = 0.1894, P = 0.6673. Sidak's multiple comparisons test, *P < 0.05 (gains); P = 0.063 (losses). *ns*, not significant.

(**E**) Dendritic spine turnover ratio (TOR) over 4 days at 3 (n = 8) and 4 months after transplantation (n = 6 cells). Mann-Whitney U-test, *P < 0.05. Each data point represents a cell.

(**F**) Dendritic spines survival fraction at 3 (red: n = 7 cells) and 4 months after transplantation (blue: n = 6 cells). Two-way ANOVA, interaction $F_{3,47}$ = 1.513, P = 0.2235; *P < 0.05. Dashed lines represent individual cells and solid lines represent means.

Although dendritic spines were traced for only a limited time (4 weeks), the observed increase in spine density is consistent with the fact that in humans, synaptic density increases significantly during foetal life (Molliver et al., 1973) and only reaches its peak in mid-childhood (Petanjek et al., 2011).

To more thoroughly access synaptic dynamics, presynaptic terminals along eight human cortical axons were also studied (**Figure 3.10 A-B**). Time-lapse imaging performed at 48h intervals for up to 4 days revealed that the average density of axonal boutons 3 months after transplantation was 0.051 ± 0.0075 EPBs/μm (n = 145 in all sessions). As observed with dendritic spines, the density remained stable over a few days (one-way ANOVA, $F_{2,17}$ = 0.4014, P > 0.05; **Figure 3.10 C**), indicating that axonal boutons were also added and eliminated at equal rates (Wilcoxon matched-pairs signed rank t-test, P > 0.05; **Figure 3.10 F**). In addition, the turnover ratio of EPBs over 4 days was 45.1 ± 3.6% (**Figure 3.10 D**), indicating comparable dynamics between axonal EPBs and dendritic spines at 3 months after transplantation (Mann-Whitney U-test, P > 0.05).

Overall, together with EM evidence of synaptic contacts within the human grafts (**Figure 3.5 B**), the present data indicate that transplanted cortical neurons undergo synaptogenesis and that this process is highly dynamic. Synaptic structures first formed within 4 weeks of in vivo development and exhibited significant synaptic reorganization. Even though neurons balanced the rates of synaptic gain and loss over a time scale of a few days, over more prolonged time intervals the density of synaptic structures increased due to increased stabilization of synaptic structures, which is consistent with the development of the human foetal cerebral cortex (Molliver et al., 1973).

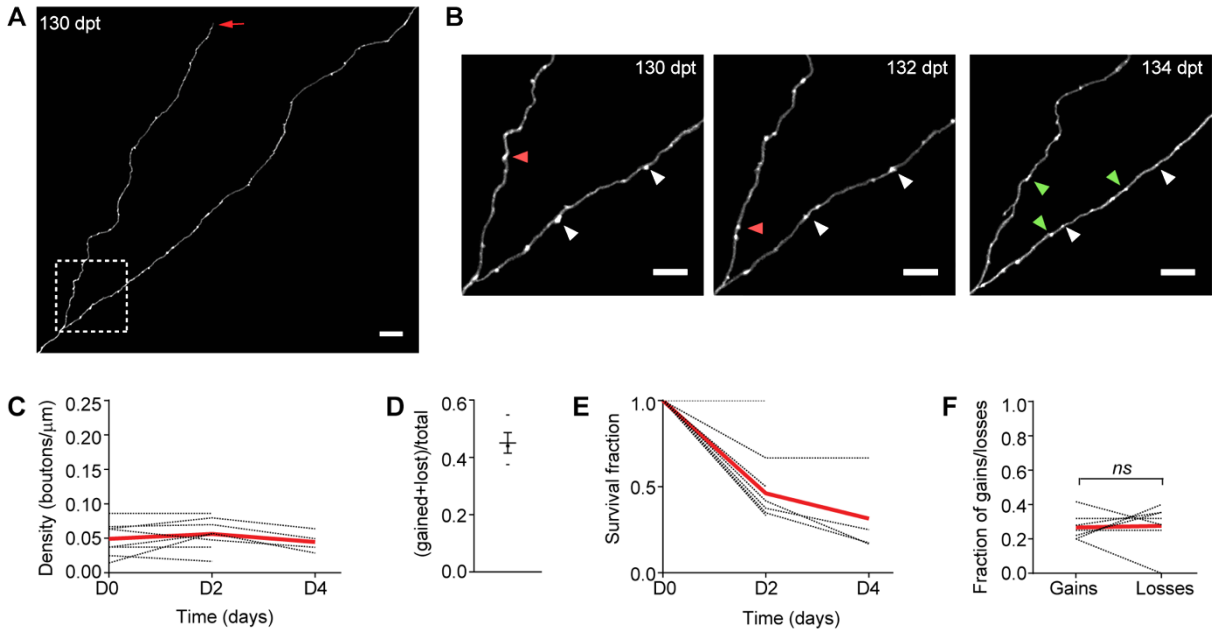

Figure 3.10 Developing axonal synaptic structures mirror the events in dendritic synaptic structures.

(**A**) Representative example of a branched human axon at 130 days after transplantation; arrow indicates a growth cone. Scale bar, 10 µm.

(**B**) Detail of axon in (A), imaged every 48h over 4 days; green, red and white arrowheads indicate gained, lost and stable EPBs, respectively. Scale bar, 5 µm.

(**C**) EPB density over 2-4 days at 3 months after transplantation (*n* = 8 cells from 3 animals, 1.3 mm total axonal length). One-way ANOVA, $F_{2,17}$ = 0.4014; *P* = 0.6756.

(**D**) Quantification of EPB TOR over 4 days at 3 months after transplantation (*n* = 4 cells). Each data point represents an axon.

(**E**) Quantification of EPB survival fraction at 3 months after transplantation (*n* = 8 cells).

(**F**) Average fraction of EPB gains and losses over 48h at 3 months after transplantation (*n* = 8 cells). Wilcoxon matched-pairs signed rank *t*-test; ns, not significant. Dashed lines represent individual cells and solid lines represent means.

3.3 Functional characterization of transplanted human grafts connectivity

To probe whether synapses were functional, animals were sacrificed and coronal brain sections immediately cut for whole-cell patch-clamping. Current-clamp recordings were made from spherical (presumably immature, *n* = 8 neurons) and pyramidal shaped somas (presumably mature, *n* = 18 neurons), as identified by differential interference contrast microscopy and expression of either GFP or tdTomato. Pyramidal 'like' neurons had a more hyperpolarized resting membrane potential (-53.8 ± 1.7 mV vs. -44.4 ± 2.3 mV, *P* <0.01), higher cell capacitance (19.4 ± 6.2 pF vs. 6.2 ± 0.6 pF, *P* <0.001) and a lower input resistance (1.4 ± 0.1 GΩ vs. 1.7 ± 0.2 GΩ, *P* <0.0001) than the spherically-shaped cells, consistent with a more mature state. While both cell types were quiescent at resting membrane potentials, depolarizing current-steps evoked action potential firing in 7 out of 8 spherical cells and in all pyramidal neurons tested. However, action potential amplitudes were larger (94.3 ± 2.6 mV, vs. 70.4 ± 4.5 pF, *P* <0.0001) and half-widths shorter (2.2 ± 0.2 ms vs. 3.3 ± 0.4 ms, *P* <0.01) in pyramidal compared to spherically-shaped cells. Additionally, within the pyramidal neuron population itself, there was a wide-spectrum of biophysical properties, with some neurons resembling the immature non-differentiated spherical cells (**Figure 3.11 A**, left) and others more akin to the low resistance cells observed in native cortical neurons (**Figure 3.11 A**, right). These data suggest that the human grafts are composed of neurons at different stages of biophysical maturation, which was expected given the transplantation of cortical progenitor cells and ongoing neurogenesis after transplantation.

Pyramidal shaped hiPSC-derived neurons in the grafts were further voltage-clamped at -70 mV. Spontaneous miniature excitatory postsynaptic currents (mEPSC) were observed at a frequency of 0.30 ± 0.05 Hz (*n* = 18 neurons), with an amplitude of 20.1 ± 3.2 pA (in 5 out of 18 neurons). This was completely blocked by NBQX, an AMPA receptor antagonist (**Figure 3.11 B**). Although synaptic events were also observed in the remaining neurons, spontaneous frequency was insufficient to acquire enough events for detailed kinetic analysis. Using a high chloride (130 mM) internal solution and in the presence of NBQX, spontaneous miniature inhibitory postsynaptic currents (mIPSC) were also observed at a frequency of 0.24 ± 0.12 Hz (*n* = 6 neurons), with an amplitude of -73.3 ± 21.0 pA (in 3 out of 6 neurons), that were completely inhibited by bicuculline, a competitive GABA A antagonist (**Figures 3.11 C**). Similar to mEPSC, inhibitory synaptic events were observed in the remaining neurons but insufficient events were acquired for detailed kinetic analysis. In summary, grafted hiPSC-derived cortical neurons are excitable and fire action potentials, and receive both excitatory and inhibitory synaptic input, suggesting functional network connectivity.

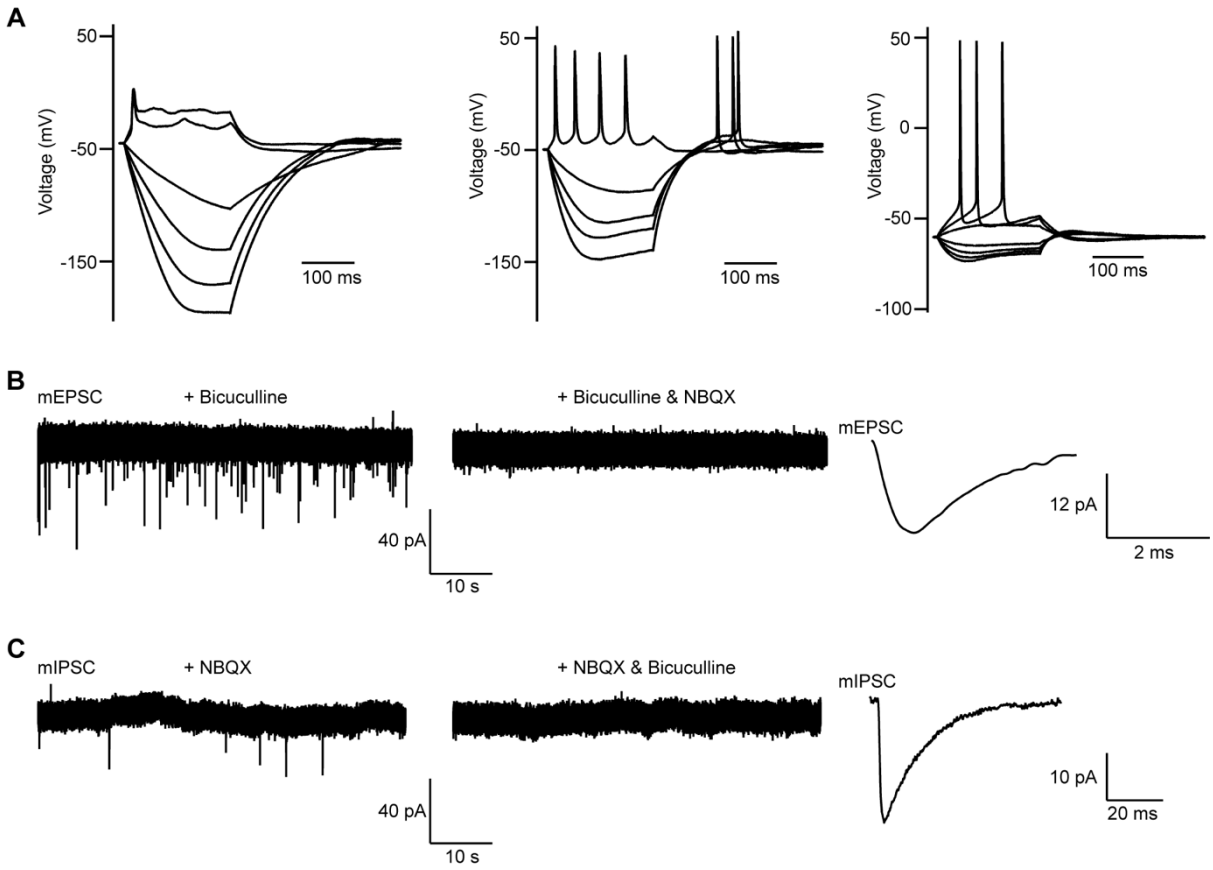

Figure 3.11 Human neurons are excitable and have functional synaptic input.

(**A**) Representative examples of current-voltage relationships of pyramidal shaped GFP-positive human iPSC-derived neurons in grafts. Action potentials are evoked by 200 ms pulses from -80 to +50 pA.

(**B**) Representative spontaneous miniature excitatory synaptic currents (mEPSC, downward deflections) recorded in voltage-clamp mode at -70 mV, in the absence (left) and presence of NBQX, an AMPA receptor antagonist (middle). Ensemble mEPSC averages from a single neuron (*n* = 60 events) shown at an expanded time scale (right).

(**C**) Representative spontaneous miniature inhibitory synaptic currents (mIPSC, downward deflections) recorded in symmetrical chloride conditions in the presence of NBQX (left). mIPSC are completely blocked by (+)-bicuculline, a GABA A receptor antagonist (middle). Ensemble mIPSC averages from a single neuron (*n* = 40 events) shown at an expanded time scale (right).

To understand where the afferent synaptic input to the functionally active neurons was coming from, monosynaptic retrograde tracing was performed, using a modified pseudotyped rabies virus (RV). RV are neurotropic and infect all neuronal cell types, spreading between synaptically connected neurons exclusively in the retrograde direction. The genome of RV encodes only five proteins, one of which is an envelope glycoprotein (G) that is essential for the trans-synaptic spreading of viral particles (Callaway and Luo, 2015). Glycoprotein-deleted rabies viruses (RV-ΔG) have been developed that lack the ability to infect presynaptic nerve terminals and thus propagate the infection between neurons, unless G is expressed in the cells of interest as a transgene (Wickersham et al., 2007a). As a consequence of G deletion, RV can only spread monosynaptically, as only cells expressing G can produce infectious particles (i.e., the starter cells). Another important modification to RV-ΔG was the introduction of an alternative envelope protein (avian ASLV type A, EnvA) to create a pseudotyped RV (Wickersham et al., 2007b). EnvA+RV-ΔG particles can only infect cells that express the avian tumour virus receptor A (TVA), which is normally absent from mammalian neurons. Thus, pseudotyped EnvA+RV-ΔG can only infect genetically defined neurons that have been engineered to express TVA. The use of pseudotyped EnvA+RV-ΔG therefore allows for the precise tracing of monosynaptic inputs to genetically selected neurons (**Figure 3.12**).

Using the approach outlined in Figure 3.11 A, human iPSC-derived cortical progenitors and neurons were transduced with a lentiviral vector containing the TVA receptor, nuclear GFP and glycoprotein G, under the control of the human synapsin promoter. Five months after transplantation, the pseudotyped mCherry expressing-rabies virus (EnvA+RV-ΔG-mCherry) was injected in the same location, and only grafted cells expressing the TVA receptor were susceptible to infection (starter cells, GFP and mCherry double positive). Cells that are monosynaptically connected to the infected human cells also become infected and express mCherry only (presynaptic input cells), allowing for accurate tracing of the neural input to the graft cells (**Figure 3.12 B**). While most of the input to the transplanted human neurons came from other human neurons (92.5% ± 1.5%), also host neurons innervate the human graft (7.5% ± 1.5%) (**Figure 3.12 C**). The traced host neurons were located within the graft, in the cortical areas adjacent to the graft, rarely in the contralateral cortex, and in the ipsilateral CA1 hippocampal region, while no traced neurons were found in other subcortical regions, namely the thalamus (**Figure 3.12 B**). This indicates limited connectivity to the host brain. Previous studies with rodent embryonic and ESC-derived neurons have revealed that axon outgrowth is very efficient when grafting into neonatal rodents or following a cortical lesion in the adult host brain (Gaillard et al., 1998, 2007; Michelsen et al., 2015), presumably because in both these conditions specific guidance cues may be present to promote growth. In contrast, the adult uninjured brain has been shown to significantly limit the ability of transplanted mouse ESC-

derived neurons to project to target areas and integrate in the host brain (Michelsen et al., 2015). In this study, the transplantation of human iPSC-derived neurons into the adult cortex in the absence of a lesion did not inhibit axon outgrowth (**Figure 3.8**), but it could potentially limit or delay the establishment of functional connectivity with the host, due to lack of a more permissive microenvironment.

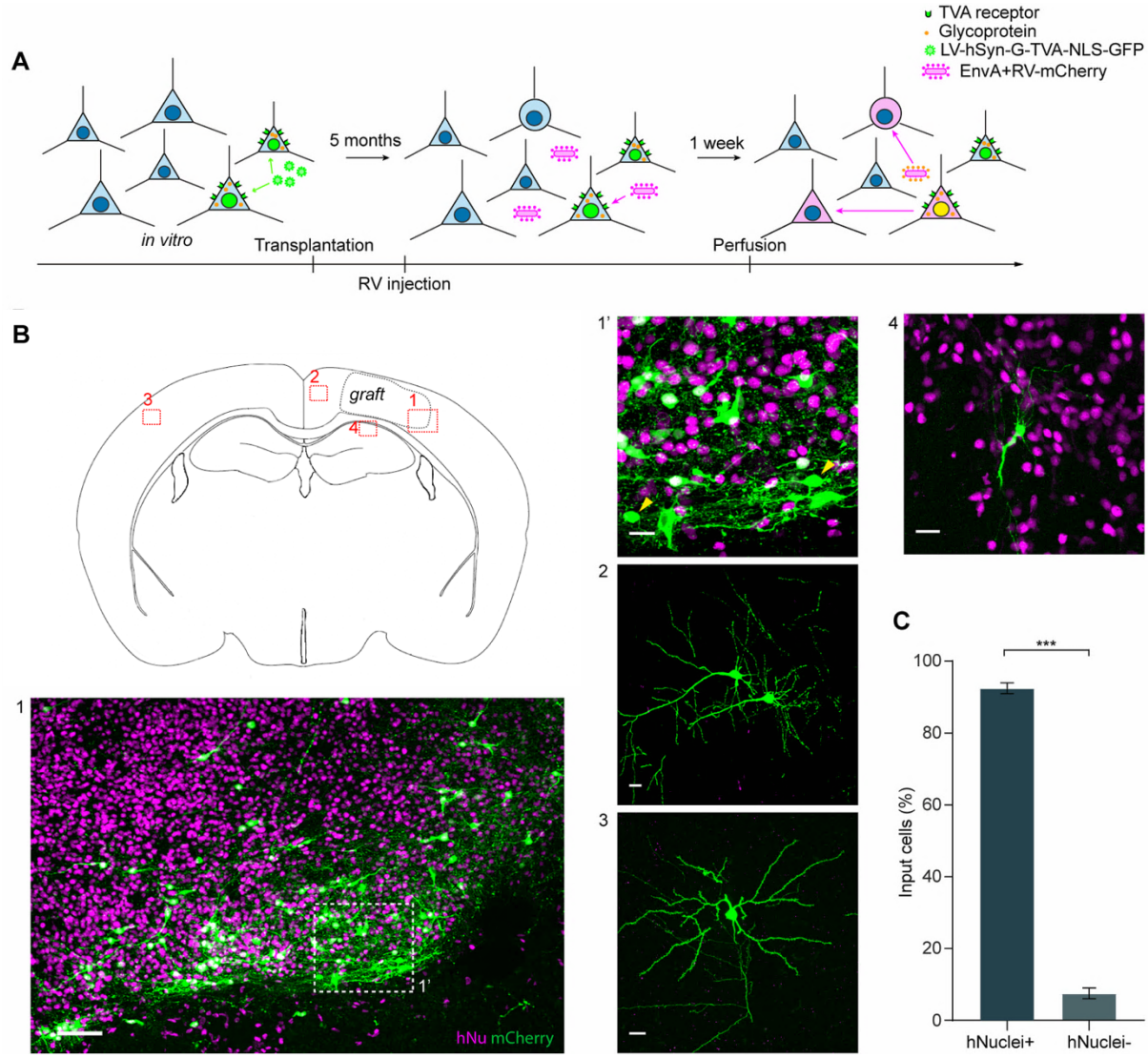

Figure 3.12 Synaptic input to the human graft is mainly from other human neurons.

(**A**) Experimental design of retrograde monosynaptic tracing of human neurons with ΔG-rabies virus.

(**B**) Location of host input cells in the periphery of the graft (1, 1'), ipsilateral cortex (2), contralateral cortex (3) and in the CA1 region of the ipsilateral hippocampus (4). Scale bars, 100 μm (1) and 20 μm (1', 2, 3 and 4).

(**C**) Quantification of human versus host input cells (n = 2 mice). Unpaired t-test, ***P < 0.001. Data are represented as mean ± SEM.

3.4 In vivo development of neural network activity in transplanted human grafts

In most neuron types, action potentials are coupled to the opening of voltage-gated Ca^{2+} channels, leading to a large increase in the concentration of intracellular free calcium. Cellular calcium imaging is therefore a sensitive method for monitoring neural activity in large populations of neurons (Peron et al., 2015). The development of genetically encoded calcium indicators (GECIs) has allowed for the non-invasive recording of neural activity in specified neuronal populations or subcellular compartments in vivo. The GCaMP family of GECIs is among the most widely used for calcium imaging due to its sensitivity in detecting intracellular calcium changes. GCaMPs consist of a circular permuted green fluorescent protein (GFP), bound on either side to the calcium-binding protein calmodulin (CaM) and to the calmodulin-binding peptide M13. In the presence of calcium, the interaction between calmodulin and the M13 peptide elicits a conformational change in the protein that results in increased emitted GFP fluorescence (Grienberger and Konnerth, 2012). Some of the most recently developed GCaMPs, including the GCaMP6 family of calcium indicators, are highly sensitive and can reliably detect individual action potentials (Chen et al., 2013).

To assess the functional development of neural networks in the human grafts, neurons were engineered to express the genetically encoded fluorescent calcium sensor GCaMP6s before transplantation, to enable the study of calcium-mediated neuronal activity in vivo. GCaMP6s is an ultrasensitive sensor with slower kinetics, but increased dynamic range and brightness upon calcium binding (Chen et al., 2013). Transplanted human neurons exhibited spontaneous, sparse activity as early as two weeks after transplantation (**Figure 3.13 A-C**). Over time, this sporadic activity evolved into complex, synchronous burst patterns (**Figure 3.13 D**), with entire regions becoming activated simultaneously across the neuropil and multiple somas in the field of view. In addition, activity bursts often had a recurrent oscillatory quality, with frequencies in the delta range, and a distinct spatiotemporal order that was constant between bursts (**Figure 3.13 E-G**). Interestingly, the same pattern of neural activity was observed in human brain organoids transplanted in the mouse cortex, highlighting the specificity of this finding (Mansour et al., 2018).

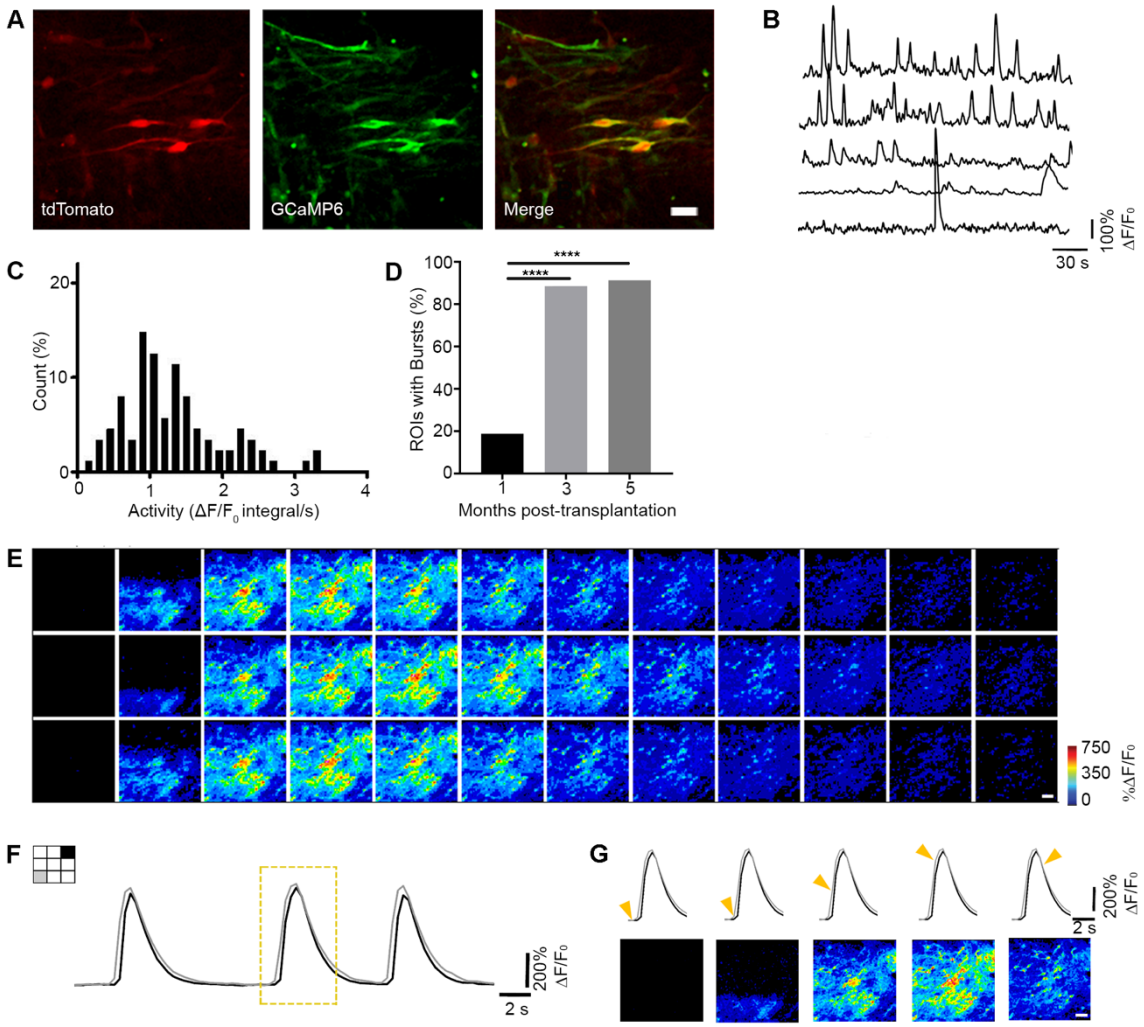

Figure 3.13 Synchronized spontaneous neural activity.

(**A**) Representative example of calcium activity in a human cortical graft at 1 month after transplantation. Neurons express both tdTomato (red), a structural marker, and GCaMP6 (green), a calcium indicator. GCaMP positive neurons are shown as an average intensity projection over a 4-minute period of spontaneous activity. Scale bar, 10 μm.

(**B**) Representative $\Delta F/F_0$ calcium traces from 5 active human neuros imaged 1 month after transplantation.

(**C**) Distribution of the spontaneous calcium activity in human cortical grafts at 1-2 months after transplantation. Activity was measured as the integral of the average $\Delta F/F_0$ signal over the entire region of interest, normalized to the total duration of the recording in seconds (*n* = 88 cells from 6 ROIs, in 3 mice).

(**D**) Quantification of ROIs that exhibit bursts at 1-2 (3/16 ROIs, *n*= 4 mice), 3 (31/35 ROIs, *n* = 5 mice) and 5 (21/23 ROIs, *n* = 3 mice) months after transplantation. Fisher's exact test, ****$P < 0.0001$.

(**E**) Individual frames from a typical recurrent burst of calcium activity. Scale bar, 20 μm.

(**F**) Example tracing of burst activity taken from two different spatial regions (grey and black, as shown in the schematic on the left) of the ROI shown in (E). Note the defined spatiotemporal order of the bursts.

(**G**) Detail of the calcium transient shown in the dashed yellow box in (F) over time (top) and corresponding image frames (bottom). Yellow arrows indicate the time of the frame. Scale bar, 20 μm.

Chapter 4. Imaging human neuron structural and functional dynamics in Down syndrome

4.1 In vivo modelling of Down syndrome diseases with hiPSC-derived neurons

Human iPSC-derived neurons transplanted into the adult cortex of mice recapitulate several aspects of human cortical development, such as the timing and order of neurogenesis, the long-range elongation of axons to relevant anatomical areas, the increase in synaptic density over time, the development of mature firing properties and the emergence of synchronized patterns of neural activity that have been described in rodents to be fundamental for several aspects of neurodevelopment, including the establishment of neural networks in the developing brain. As such, the model described thus far offers the opportunity to question the cellular mechanisms of human neurodevelopmental diseases.

Induce pluripotent stem cells lines reprogrammed from two individuals with Down syndrome were differentiated into neural progenitor cells and excitatory neurons of cortical forebrain identity, following a previously published and well established protocol (Shi et al., 2012b). Both lines (TS21-1 and Ts21-2) were confirmed to be trisomic for Hsa21 in vitro by copy number assay in a genome-wide single nucleotide polymorphism (SNP) array (**Supplementary Figure 1**), which also excluded the presence of other chromosomal abnormalities in all cell lines used in this study. This is relevant, given the propensity of many hiPSC lines to acquire aneuploidy in vitro (Mayshar et al., 2010). During the reprogramming process of Ts21-2, two disomic clones were identified (WT-2 and WT-2'). A microsatellite short tandem repeat assay demonstrated that the parental fibroblast population was not mosaic for Hsa21, and that Ts21-1, WT-2 and WT-2' were identical to the parental fibroblasts and to each other at all loci tested, apart from Hsa21 loci, thus ruling out contamination by WT clones and confirming that the disomic clones originated from the spontaneous loss of a copy of Hsa21 that led to the rescue of the trisomy (**Supplementary Figure 2**). Because it could not be ascertained which copy of Hsa21 had been lost, it was not possible to conclude that Ts21-2 and WT-2 or WT-2' are truly isogenic cell lines. However, revertant disomic cell lines generated by the spontaneous loss of a random copy of Hsa21, a phenomenon known to occur during the reprogramming of iPSCs (Chen et al., 2014; Maclean et al., 2012), are a valid and very useful control for a Ts21 cell line, highlighting phenotypes caused by an extra copy of Ts21 instead of genetic and epigenetic variability between individuals. Therefore, WT-2 was used as a disomic control for Ts21-2 in the experiments that followed.

The cortical forebrain identity of neural progenitors and neurons derived from both disomic (WT-1 and WT-2) and trisomic (Ts21-1 and Ts21-2) hiPSC lines was tested by conducting a gene expression profile analysis using a custom gene expression panel of approximately 250 genes, which revealed enrichment in cortical and excitatory markers, as expected (**Supplementary Figure 3**). Cells were transduced with a lentiviral vector expressing GFP under the control of human synapsin (**Table 1**), and then transplanted at day 36-38 into the right somatosensory cortex of immunosuppressed adult mice. As before, a small cranial window was implanted for longitudinal in vivo imaging. The Hsa21 ploidy level of all cell lines was again confirmed after in vivo engraftment using fluorescent in situ hybridization (FISH) of tissue sections containing the human graft (**Figure 4.1**).

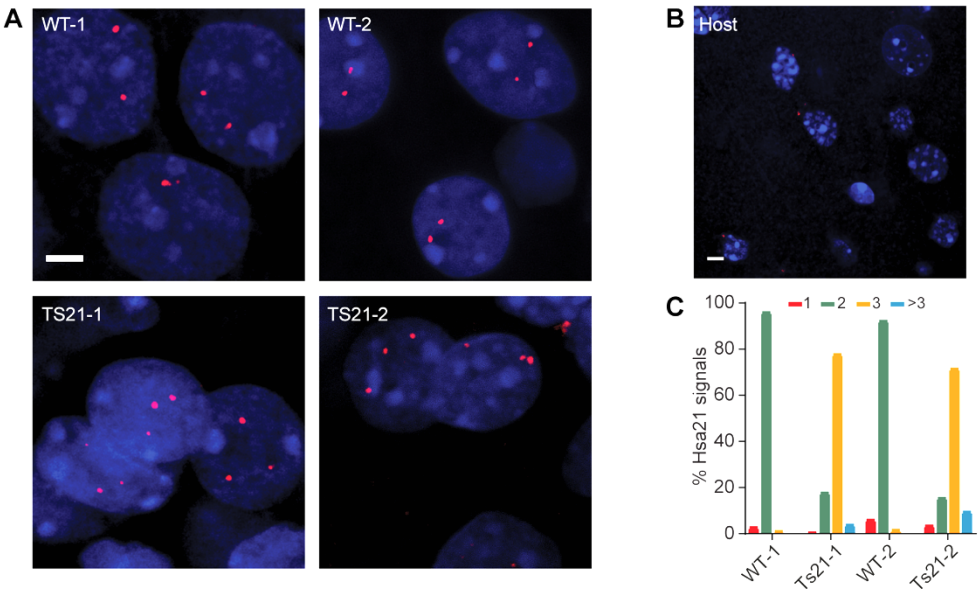

Figure 4.1 Fluorescent in situ hybridization assay.

(**A**) Representative examples of Hsa21-specific FISH signals (red) in each of the four transplanted lines. Nuclei are counterstained with DAPI (blue). Scale bar, 3 µm.

(**B**) Representative example of Hsa21-specific FISH in the contralateral host cortex (negative control). Scale bar, 5 µm.

(**C**) Quantification of the percentage of Hsa21 signals in the human grafts from each of the four transplanted cell lines.

4.2 Ts21 neurons transplanted in vivo recapitulate aspects of the cortical neurogenesis defect in Down syndrome

Ts21-1 and Ts21-2 lines generated cortical progenitors, proliferating cells and neurons similarly to control grafts 5 months after transplantation (**Figures 4.2**). Forebrain identity of transplanted neurons was again confirmed after transplantation by immunofluorescence detection of the cortical marker TBR1. Interestingly, there was a significant deficit in the production of late-born cortical neurons expressing SATB2 in both Ts21 cell lines (**Figure 4.3**). In addition, there was also an increased number of human astrocytes in the Ts21 grafts. This is relevant because it has been shown that in the human foetal DS brain there is a significant increase in the number of astrocytes (Guidi et al., 2008; Zdaniuk et al., 2011), a finding that persists into adulthood (Griffin et al., 1998; Mito and Becker, 1993).

Astrocytes play a significant role in several physiological processes and its dysfunction is thought to contribute to disease pathology (Dossi et al., 2018). In DS, astrocytes present an activated morphology and have been shown to negatively impact neurogenesis, neuritogenesis and synaptogenesis in hiPSC-derived neurons, an effect that is strongly mediated by the overexpression of the Hsa21-encoded S100β in Ts21 astroglia (Chen et al., 2014). Furthermore, the study by Chen and colleagues provides clear evidence that the interaction of Ts21 astroglia with neurons is deleterious, as Ts21 neurons derived under directed neuronal differentiation conditions, which yields low percentages of astrocytes, have morphological and electrophysiological properties similar to control neurons, but under spontaneous differentiation conditions, yielding significantly larger numbers of astrocytes, Ts21 neurons show abnormal morphology, reduced neurite growth, defective neurogenesis and increased apoptosis, defects which are restored by culturing Ts21 neurons with astroglial cell-conditioned medium collected from control rather than Ts21 astrocytes. Other studies have confirmed the developmental bias towards glial lineages in DS (Briggs et al., 2013b), which is likely to have a significant role in mediating the pathogenesis of the disease.

Interestingly, it has been shown that the increased number of glial cells occurs at the expense of neurons, suggesting there is an early commitment of DS neural progenitor cells to a glial rather than neuronal cell fate. Overexpression of several Hsa21 genes has been implicated in this premature neurogenic-to-gliogenic shift, including APP, S100β and OLIG2 (Lu et al., 2011, 2012). In addition, Dyrk1A overexpression, a gene also located on Hsa21, has been shown to lead to a premature cell cycle exit and differentiation of intermediate progenitor cells. The likely consequence of the premature differentiation and acquisition of a glial cell fate is the reduction of the neuronal progenitor pool size (Yabut et al., 2010), with the potential consequence of

limiting the number of late-born neurons generated. This would be in line with the highly significant reduction in the generation of late-born, upper-layer cortical neurons observed in this study ($SATB2^+$ cells), presumably due to an early depletion of the neuronal progenitor population. One piece of evidence argues against this hypothesis, which is the similar levels of PAX6-expressing cells, a marker of neuronal progenitor cells, in DS and control grafts. However, this could be justified by the relatively late time point at which cell quantification was performed (5 months after transplantation). A time course analysis of the relative proportions of PAX6-expressing neuronal progenitor cells, newly-born postmitotic neurons and astrocytes would assist in clarifying this point.

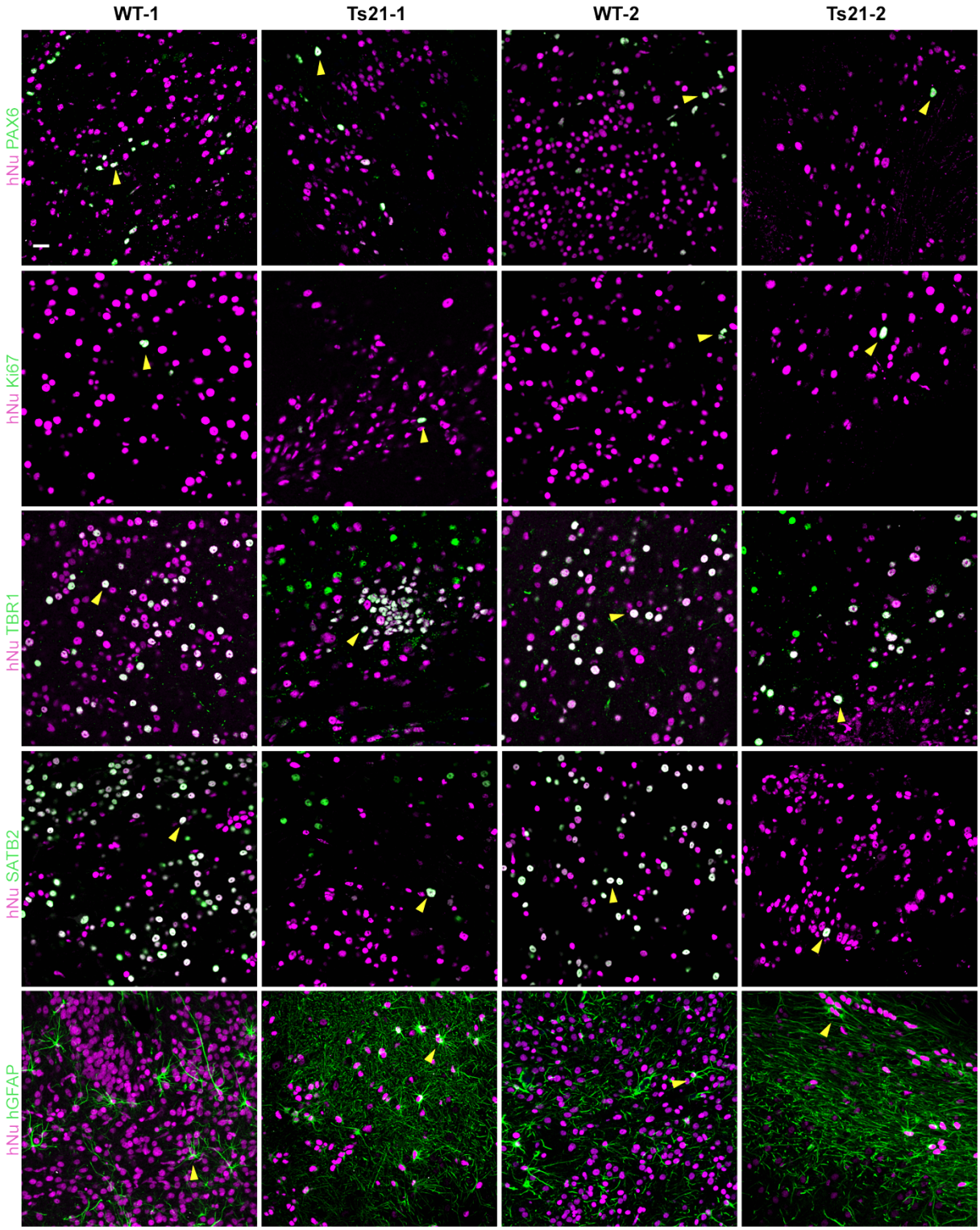

Figure 4.2 Neurogenesis in Ts21 human cortical grafts.

Representative immunostaining of WT-1, Ts21-1, WT-2 and Ts21-2 human grafts 5 months after transplantation for PAX6, Ki67, TBR1, SATB2 and GFAP. Arrowheads indicate examples of positive human cells. Scale bar, 20 μm.

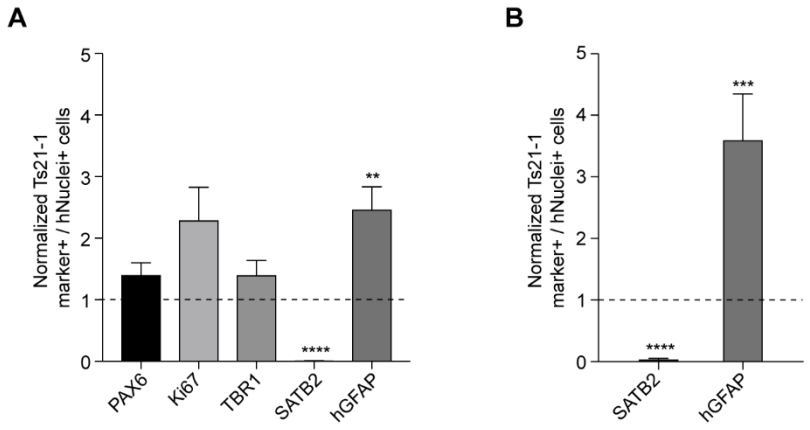

Figure 4.3 Quantification of cell populations in Ts21 grafts.

(**A**) Quantification of marker+ / hNuclei+ cells in Ts21-1 grafts (*n* = 3 mice, average number of ROIs sampled per cell marker = 67) normalized to WT-1 (dashed line, *n* = 3 mice, average number of ROIs sampled per cell marker = 37). Mann-Whitney *U*-test, ***P* < 0.01, *****P* < 0.0001. Data are represented as mean ± SEM.

(**B**) Quantification of SATB2+ / human nuclei+ cells and GFAP+ / human nuclei+ cells in TS21-2 grafts (*n* = 2 mice, average number of ROIs sampled per cell marker = 22) normalized to WT-2 (dashed line, *n* = 4 mice, average number of ROIs sampled per cell marker = 45). Mann-Whitney *U*-test, ****P* < 0.001, *****P* < 0.0001. Data are represented as mean ± SEM.

4.3 Ts21 neurons exhibit normal developmental neurite refinement

After transplantation, mice were imaged at regular intervals with a multiphoton microscope, according to the imaging protocol outlined in Figure 2.1. As with WT-1 cells, Ts21 cortical progenitors and neurons survived for the duration of the experimental timeline in the adult mouse cortex, which provided a unique opportunity to investigate aspects of neuronal development not accessible in vitro, since processes such as long-range axon growth, synaptogenesis and functional network connectivity take longer to achieve than cell culture studies will allow (Korecka et al., 2016).

Chronic in vivo imaging of GFP-expressing human neurons enabled the exploration of the dynamics of neurite outgrowth up to 3 months after transplantation. However, since at any given time point grafts contained both early and late born neurons, due to human proliferating cortical neural progenitor cells being present until the end of the experimental timeline, a comparison of neurite development dynamics between cell lines was performed at 3 weeks after transplantation, to reduce the age variability of neurons being monitored (**Figure 4.4**). As described earlier for WT-1 neurons, most neurites from Ts21 neurons exhibited net elongation over a 24h period (Ts21-1: 56.4 ± 6.0% vs. Ts21-2: 55.1 ± 8.9%; unpaired two-tailed *t*-test, *P*

> 0.05), although interchanging growth and retraction for each individual neurite could also be observed (Ts21-1: 28.2 ± 2.8% vs. Ts21-2: 41.5 ± 12.9%; unpaired two-tailed *t*-test, $P > 0.05$). Pruning events (either 24h net retraction or interchanging with periods of elongation) occurred at a rate of 55.7 ± 3.1% for Ts21-1 and 65.7 ± 12.7% for Ts21-2 neurons (unpaired two-tailed *t*-test, $P > 0.05$). Importantly, neurite outgrowth and developmental pruning were mostly preserved in neurons form two independent Ts21 lines, when compared to their respective controls (**Figure 4.4 C**). A previous in vitro study reported that growth cones from DS human foetal cortical neurons advance faster than euploid controls, albeit in certain culture conditions only (Sosa et al., 2014). In addition, some studies of iPSC-derived neurons in culture have identified a decreased neurite length in Ts21 neurons (Hibaoui et al., 2014; Huo et al., 2018), but this has not been a consistent finding (Briggs et al., 2013b). Interestingly, Chen and colleagues detected a defect in neurite outgrowth exclusively under spontaneous differentiation conditions (i.e., in the absence of neurotrophic factors), but not under directed differentiation conditions such as in the present study (Chen et al., 2014). Neurite length was not specifically looked at in this study, but transplanted human Ts21 cortical neurons derived from two independent iPSC lines had similar rates of neurite elongation and retraction to their respective controls (**Figure 4.4 D**), highlighting that early neurite development is largely unaffected in Ts21 neurons.

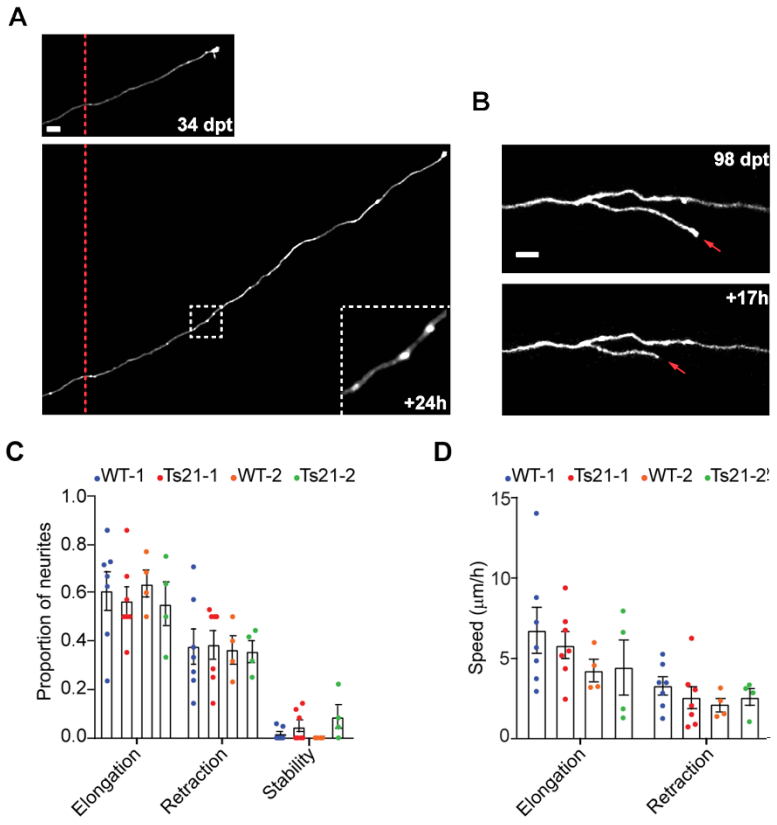

Figure 4.4 In vivo neurite development is normal in Ts21 neurons.

(**A**) Representative example of axon elongation in a Ts21-1 neuron over a 24h period. The inset highlights the presence of EPBs.

(**B**) Representative example of axonal branch retraction in a Ts21-1 neuron over 17h.

(**C**) Proportion of elongating, retracting and stable neurites in 24h intervals in WT-1 (n = 96 neurites from 79 cells in 7 grafted animals), Ts21-1 (n = 65 neurites from 60 cells in 7 grafted animals), WT-2 (n = 65 neurites from 53 cells in 4 grafted animals) and Ts21-2 (n = 60 neurites from 51 cells in 4 grafted animals) human grafts 3 weeks after transplantation. Unpaired two-tailed t-test; $P > 0.05$. Each data point represents an animal.

(**D**) Speed of neurite elongation and retraction in WT-1 (n = 96 neurites from 73 cells in 7 grafted animals), Ts21-1 (n = 62 neurites from 54 cells in 7 grafted animals), WT-2 (n = 53 neurites from 47 cells in 4 grafted animals) and Ts21-2 (n = 54 neurites from 46 cells in 4 grafted animals) human grafts 3 weeks after transplantation. Unpaired t-test; $P > 0.05$. Each data point represents an animal. Data are represented as mean ± SEM.

4.4 Ts21 neurons have increased structural synaptic stability

Several proteins relevant to synaptic formation and function are encoded in chromosome 21, and most post-mortem studies of human DS brains have identified synaptic structural defects in the neocortex and hippocampus. These include a reduced number of dendritic spines in at least some pyramidal neurons starting from early infancy, larger spine heads, thinner spines and spines of unusual length (Marin-Padilla, 1976; Suetsugu and Mehraein, 1980; Takashima et al., 1981). Consistently, some studies in DS animal models have also highlighted a reduction in synapse density in the hippocampus and neocortex of neonatal and adult Ts65Dn mice (Chakrabarti et al., 2007; Kurt et al., 2004). However, other studies failed to detect consistent changes in dendritic spine density in multiple cortical and hippocampal regions in several mouse models of DS (Belichenko et al., 2009, 2004, 2007). Similarly, in vitro studies in neurons derived from DS iPSC lines have demonstrated a reduction in the expression of pre- and post-synaptic proteins in Ts21 neurites (Hibaoui et al., 2014; Weick et al., 2013), but as with animal models this has not been a consistent finding across studies (Shi et al., 2012c).

However, the dynamics of synapse formation and elimination in developing Ts21 neurons has so far remained largely unexplored. To investigate structural synaptic plasticity in Ts21 neurons, transplanted GFP-expressing human neurons derived from iPSCs from DS individuals were imaged with a 2P microscope every 48h, for four days (**Figures 4.5 and 4.6**).

To determine whether dendritic spine development was associated with synapse formation in Ts21 neurons, a subset of dendrites from one transplant were reconstructed with electron microscopy after multiple days of in vivo imaging (**Figure 4.5 A-C**). Dendritic spines formed synapses in 41% of cases (14 out of 34 dendritic spines); interestingly, 43% of these synapses formed within 48 hours of dendritic spines first appearing, suggesting a relatively strong association between the presence of dendritic spines and the existence of an underlying synapse. Serial EM reconstructions revealed that human dendritic spines and their corresponding presynaptic terminals contained a postsynaptic density and synaptic vesicles, respectively, suggestive of complete synaptic maturation (**Figure 4.5 C**). Whether these synapses are between human cells or between human and host neurons could not be assessed, as no immune labelling was performed.

At baseline, Ts21 neurons had a significantly higher or a trend towards higher spine density than control neurons from two independent cell lines (**Figure 4.5 D**). A very high density of GFP-positive neurons in the transplants prevented a quantitative analysis of synaptic dynamics in the WT-2 neurons, but longitudinal in vivo imaging in all other three cell lines revealed that

dendritic spines in Ts21 neurons derived from two distinct individuals were more stable than in control neurons (WT-1), as demonstrated by a higher survival fraction and a reduced turnover ratio (**Figure 4.5 E-F**). Therefore, one can speculate that the higher dendritic spine density in Ts21 neurons is a consequence of increased spine survival and reduced dendritic spine turnover. Nonetheless, it is important to emphasize that although almost half of dendritic spines in Ts21 neurons form mature synapses, it is not known how this compares to control neurons. It is possible that a larger proportion of dendritic spines in Ts21 neurons do not form synapses relative to control neurons, or that more of these synapses are not functional. It is also important to note that studies of post-mortem human foetal brains have detected no change in synaptic or dendritic spine density in DS at such an early stage (Petit et al., 1984; Takashima et al., 1981), although none of these studies can inform on the dynamics of synaptic remodelling in the developing DS brain. Therefore, caution should be exercised when interpreting these results, but it is entirely plausible that decreased synaptic remodelling could be one factor contributing to cognitive impairments in DS. Indeed, functional synaptic defects have been systematically demonstrated in animal models, such as decreased plasticity at excitatory synapses, which has been suggested to result from an enhanced inhibitory tone in the brain of trisomic mice (Belichenko et al., 2007; Kleschevnikov et al., 2004; Siarey et al., 2005).

In contrast to dendritic spines, the density of presynaptic axonal *en passant* boutons in Ts21 neurons was comparable to control neurons (**Figure 4.6 B**). However, there was a similar tendency for increased EPB stability in Ts21 neurons, demonstrated by a trend towards increased EPB survival and reduced turnover ratio over four days (**Figure 4.6 C-D**). As with dendritic spines, the high density of GFP-positive human neurons prevented a quantitative analysis of presynaptic dynamics in WT-2 neurons, but the results from available cell lines support the notion of increased structural synaptic stability in Ts21 neurons.

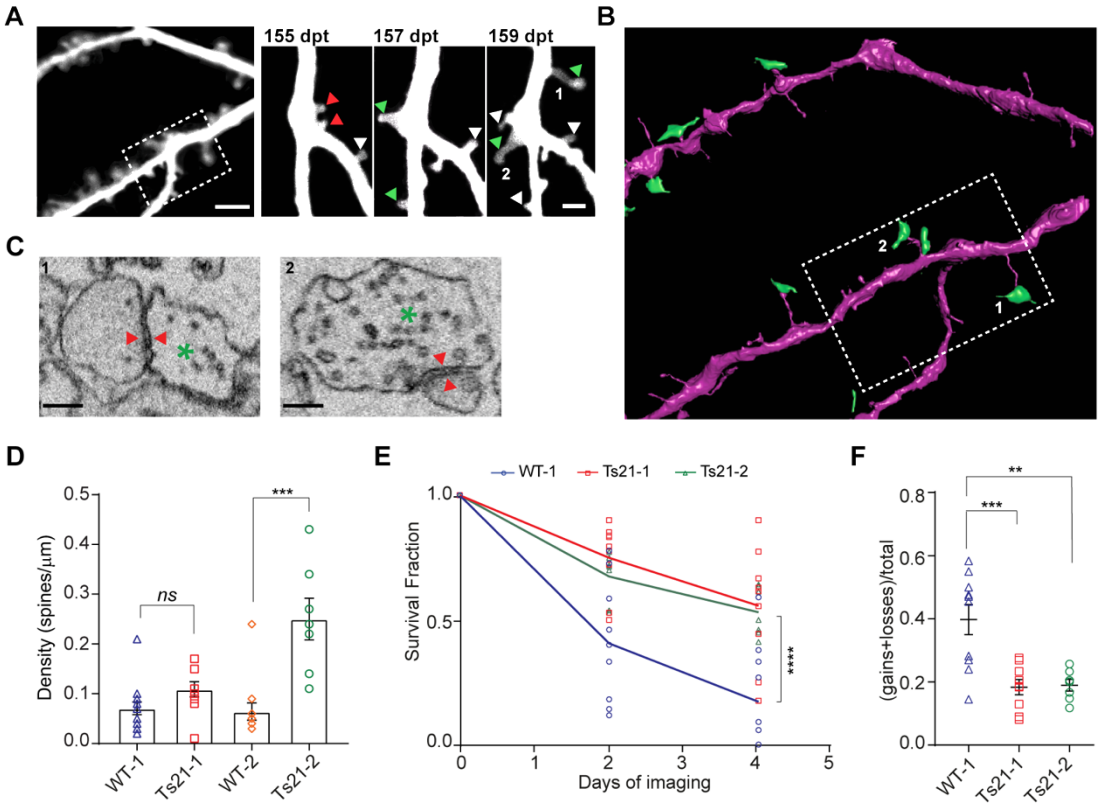

Figure 4.5 Ts21 neurons show decreased dendritic spine plasticity.

(**A**) Representative example of dendritic branches and spines on a Ts21-1 neuron, imaged at 48h intervals for 4 days; green, red and white arrowheads indicate gained, lost and stable dendritic spines, respectively.

(**B**) 3D-rendering of the same dendritic region imaged in vivo in (A), obtained from electron microscopy reconstruction. Presynaptic terminals are shown in green.

(**C**) Electron microscopic images of the dendritic spines marked with 1 and 2 in (B). Red arrows indicate the location of synapses. Green asterisk, presynaptic terminal.

(**D**) Dendritic spine density at D_0 in WT-1 (n = 14 cells from 3 animals), TS21-1 (n = 10 cells from 4 animals), WT-2 (n = 12 cells from 4 animals) and TS21-2 (n = 7 cells from 2 animals) in human grafts at 3-4 months post-transplantation. Kruskal-Wallis test, ***P < 0.001; *ns*, not significant. Each data point represents a cell.

(**E**) Dendritic spines survival fraction over 4 days in WT-1 (n = 10 cells from 2 animals), Ts21-1 (n = 9 cells from 4 animals) and Ts21-2 (n = 7 cells from 2 animals) human grafts at 3-4 months post-transplantation. Two-way ANOVA, interaction $F_{4,69}$ = 5.435, P = 0.0007; Tukey's multiple comparisons test, ****P < 0.001. Each data point represents a cell.

(**F**) Quantification of dendritic spine turnover rate over 4 days in WT-1 (n = 10 cells from 2 animals), Ts21-1 (n = 9 cells from 4 animals) and Ts21-2 (n = 7 cells from 2 animals) grafts at 3-4 months post-transplantation. Sidak's multiple comparisons test after one-way ANOVA, $F_{2,23}$ = 3.078, **P < 0.001. Each data point represents a cell. Data are represented as mean ± SEM.

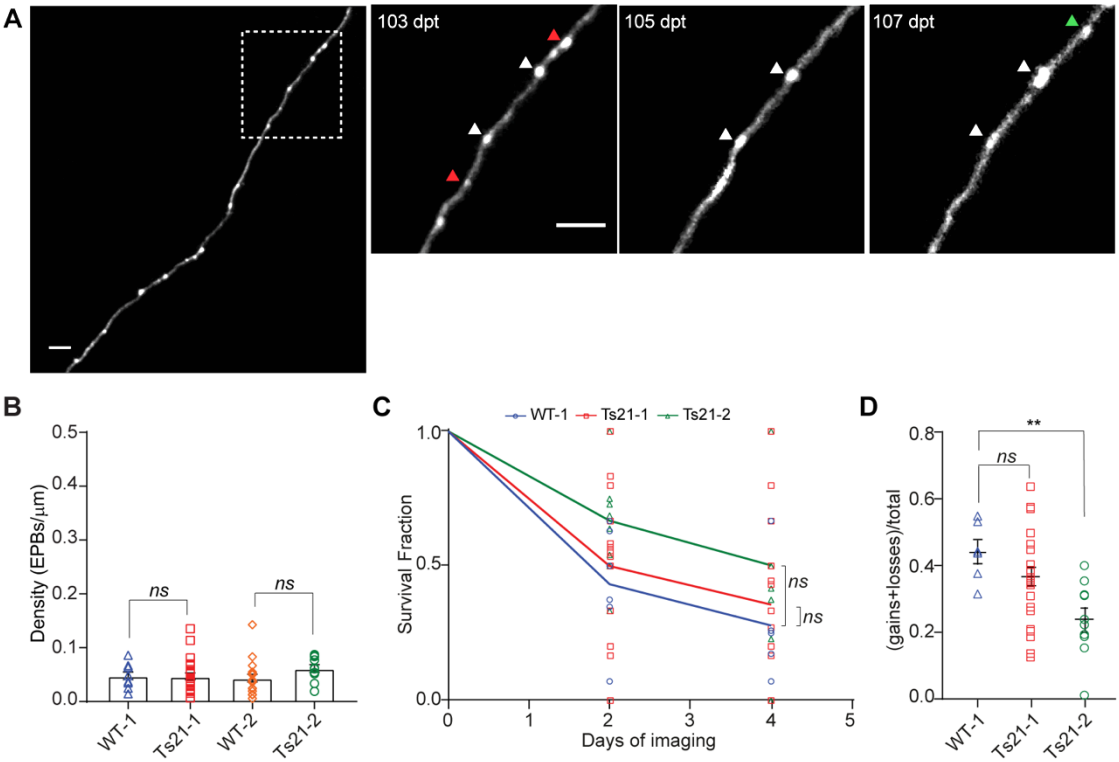

Figure 4.6. Axonal synaptic structures in Ts21 neurons have enhanced stability.

(**A**) Representative example of an axon of a Ts21-2 neuron imaged at 48h intervals for 4 days. The arrowheads in the insets indicate stable (white), new (green) and lost EPBs (red).

(**B**) Density of EPBs at D_0 in WT-1 (*n* = 10 cells from 3 animals), Ts21-1 (*n* = 10 cells from 3 animals), WT-2 (*n* = 19 cells from 4 animals) and Ts21-2 (*n* = 10 cells from 3 animals) axons in human grafts at 3-4 months post-transplantation. Kruskal-Wallis test; *ns*, not significant. Each data point represents a cell.

(**C**) EPB survival fraction over 4 days in WT-1 (*n* = 6 cells), TS21-1 (*n* = 24 cells) and TS21-2 (*n* = 10 cells) grafts at 3-4 months post-transplantation. Two-way ANOVA, interaction $F_{4,111}$ = 0.8211, *P* = 0.5144; *ns*, not significant. Each data point represents an axon.

(**D**) EPB turnover rate over 4 days in WT-1 (*n* = 6 cells), TS21-1 (*n* = 24 cells) and TS21-2 (*n* = 10 cells) grafts at 3-4 months post-transplantation. Sidak's multiple comparison test after one-way ANOVA, $F_{2,37}$ = 5.588, **P < 0.01; *ns*, not significant. Each data point represents an axon. Data are represented as mean ± SEM.

4.5 Ts21 neurons show no evidence of major functional defects

Dendritic spines and axonal boutons are the anatomical sites of synapse formation, and structural abnormalities could predict impaired synaptic function. To confirm transplanted Ts21 neurons were functionally mature and to probe their synaptic function, voltage-clamp recordings in acute brain slices containing the human grafts were performed, on average 5 months after transplantation. Human cells grafted in 4 animals per cell line were identified by fluorescence and selected for patching based on the presence of pyramidal cell morphology. Resting membrane potential was similar in all cell lines (unpaired two-tailed *t*-test, $P > 0.05$; **Table 4**). There was a trend towards increased input resistance, a measure of both cell size and membrane ion channel composition, and decreased membrane capacitance, a measure of soma size, in Ts21 neurons from two independent cell lines (**Table 4**). The frequency of evoked action potentials upon incremental steps of depolarizing current injection was similar between WT-1 vs. Ts21-1 and WT-2 vs. Ts21-2, except at -50 pA between WT-2 vs. Ts21-2 (**Figure 4.7 G**). However, evoked action potential amplitude and width were slightly reduced in Ts21 neurons (**Figure 4.7** and **Table 4**). Overall, these results point to the basic biophysical properties being largely unaffected in Ts21 neurons at early developmental stages, and are consistent with in vitro recordings of hiPSC-derived neurons (Chen et al., 2014; Shi et al., 2012c; Weick et al., 2013). The observed variability in physiological parameters between disomic and trisomic neurons is most likely attributed to differences in the degree of neuronal maturation within each individual graft rather than to phenotypic differences *per se*, with recorded Ts21 neurons probably being slightly less mature than control neurons. These results also indicate preservation of the overall excitability of Ts21 neurons, and are in contrast to in vitro electrophysiological recordings of primary hippocampal neurons from mouse models of DS, which have shown reduced number of action potentials generated in response to current injection (Stern et al., 2015).

Equally, whole-cell voltage-clamp recordings of mEPSC were unaffected in neurons from both Ts21 lines compared to their respective controls, indicating that Ts21 neurons formed functional synapses comparable to control neurons (**Figure 4.8**). A similar result was found in vitro using excitatory cortical neurons derived from the same iPSC line as Ts21-1 and using the same directed neuronal differentiation protocol (Shi et al., 2012c). Chen and colleagues highlighted the importance of an healthy astroglia in promoting synapse formation – control and DS iPSC-derived neurons cultured with astroglia-conditioned medium (ACM) collected from control astroglia exhibited spontaneous synaptic activity in 6 week-old cultures, but synaptic activity was absent when control and Ts21 neurons were cultured in ACM from Ts21 astroglia (Chen et al., 2014). In contrast, recordings from cultures containing both

glutamatergic and GABAergic neurons derived from two independent Ts21 cell lines, at 5 to 6 weeks of differentiation, revealed a trend towards a decreased fraction of neurons exhibiting spontaneous postsynaptic currents (sPSCs) that implied a reduction in synaptic activity, with no difference in the ratio of excitatory to inhibitory sPSCs between groups or in the biophysical properties of sPSCs in Ts21 neurons (Weick et al., 2013). Whether this reduced incidence of spontaneous postsynaptic currents in early Ts21 neurons is a time-dependent characteristic (i.e., delayed synaptic maturation in Ts21 neurons) is unknown, as recordings were not performed at later time points. Alternatively, it is possible that phenotypic variability between neurons derived from different iPSC cell lines is, at least partially, a reflexion of the reprogramming and differentiation methods or culture conditions used in each study, as the results from Chen and colleagues mentioned earlier seem to suggest. Finally, although cognitive impairment is a universal feature of DS, its severity varies immensely between individuals, and it cannot be excluded that neurons derived from different donors have distinct characteristics, reflecting the relative severity of the syndrome in each donor.

Table 4. Biophysical properties of WT and Ts21 neurons

Parameter (mean ± SD)	**WT-1 (*n* = 18)**	**Ts21-1 (*n* = 21)**	***P* value**
Resting membrane potential (mV)	-53.8 ± 7.2	49.3 ± 12.7	0.1926
Input resistance (GΩ)	1.39 ± 0.63	1.83 ± 1.20	0.3176
Capacitance (pF)	19.44 ± 9.41	13.06 ± 7.07	0.0086
Action potential amplitude (mV)	91.3 ± 11.1	77.0 ± 16.4	0.0098
Action potential width (ms)	2.20 ± 0.74	1.59 ± 0.48	0.0187
Parameter (mean ± SD)	**WT-2 (*n* = 27)**	**Ts21-2 (*n* = 16)**	***P* value**
Resting membrane potential (mV)	-57.1 ± 8.6	-55.3 ± 10.8	0.5381
Input resistance (GΩ)	0.97 ± 0.75	1.35 ± 1.07	0.1829
Capacitance (pF)	24.58 ± 11.96	20.9 ± 13.2	0.3095
Action potential amplitude (mV)	87.9 ± 16.0	82.7 ± 10.8	0.0929
Action potential width (ms)	2.13 ± 0.99	1.48 ± 0.42	0.0147

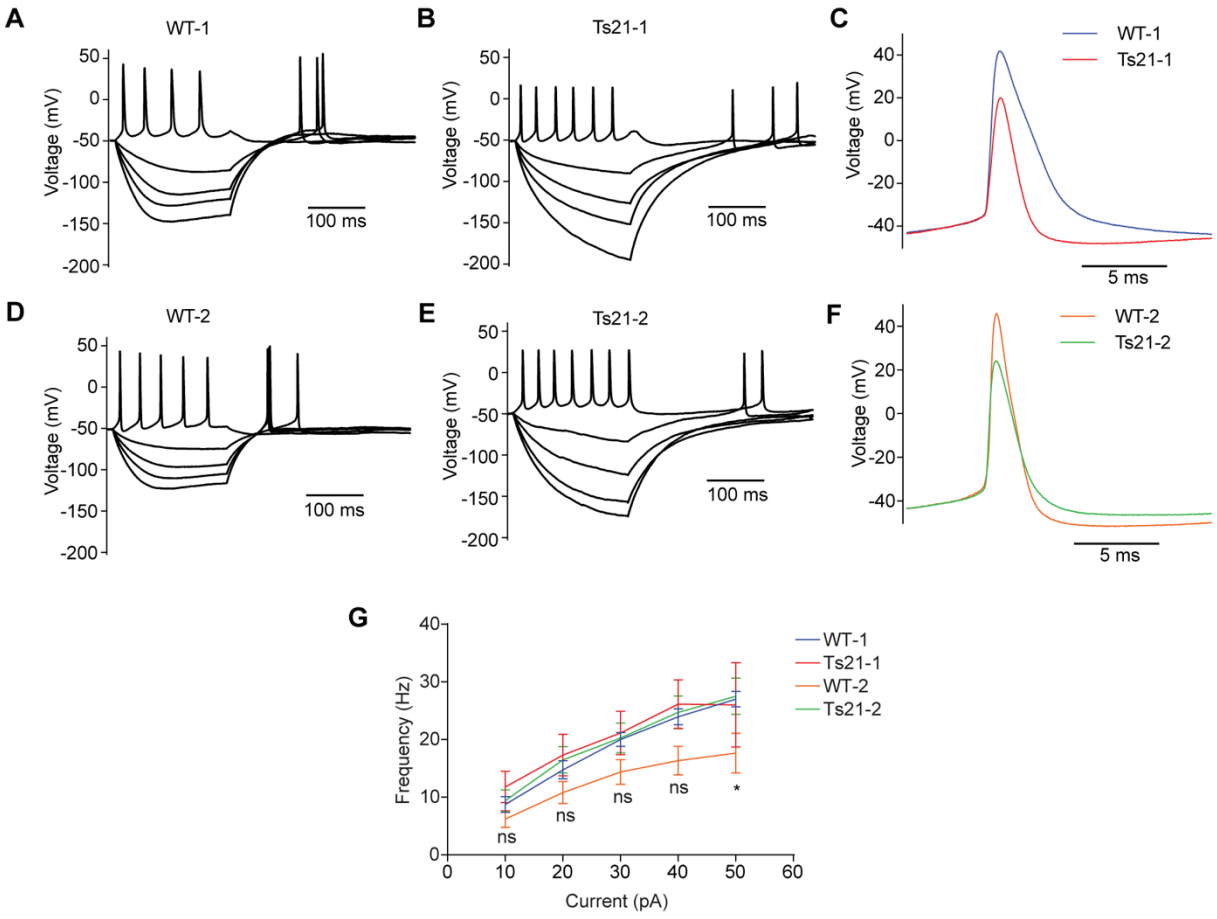

Figure 4.7 Ex vivo electrophysiological characterisation of Ts21 and control neurons.

(**A-B**) Representative current-voltage relationships in WT-1 (A) and Ts21-1 (B) neurons.

(**C**) Representative action potential in WT-1 and Ts21-1 neurons.

(**D-E**) Representative current-voltage relationships in WT-2 (D) and Ts21-2 (E) neurons.

(**F**) Representative action potential in WT-2 and Ts21-2 neurons.

(**G**) Frequency of action potentials evoked by injection of depolarizing current steps. Tukey's multiple comparisons test after two-way ANOVA, interaction $F_{12,321}$ = 0.3128, P = 9869; *P < 0.05; *ns*, not significant. Data are represented as mean ± SEM

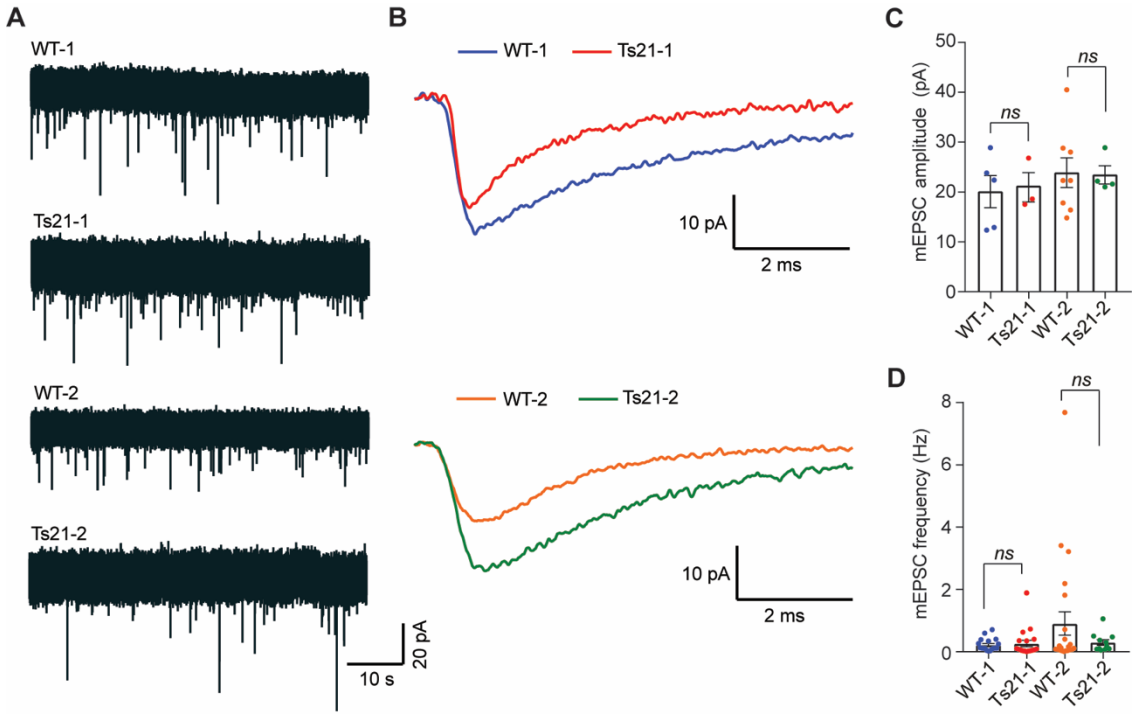

Figure 4.8 Transplanted Ts21 and control neurons have similar synaptic input.

(**A**) Representative traces of spontaneous miniature excitatory synaptic currents (mEPSCs, downward deflections) recorded from acute brain slices of human grafts, in voltage-clamp mode at -70 mV.

(**B**) Ensemble mEPSC averages from a single neuron shown at an expanded time scale from each of the four transplanted cell lines.

(**C,D**) mEPSC amplitude (WT-1: *n* = 5; Ts21-1: *n* = 3; WT-2: *n* = 8; Ts21-2: *n* = 4) and frequency (WT-1: *n* = 18; Ts21-1: *n* = 19; WT-2: *n* = 23; Ts21-2: *n* = 11) in grafted human neurons. Kruskal-Wallis test: amplitude, *P* = 0.8395; frequency, *P* = 0.2094. Each data point represents a cell. *ns*, not significant. Data are represented as mean ± SEM.

Despite normal overall excitability and synaptic activity in Ts21 neurons, injection of hyperpolarizing current steps revealed a reduction of I_h activation in Ts21 neurons, as evidenced by the significant decrease in the number of sag responses in Ts21-1 and Ts21-2 neurons (**Figure 4.9 A-C**). It was not possible to probe these hyperpolarization-activated currents pharmacologically, but the presence of a voltage sag followed by rebound depolarization is characteristic of I_h activation, which is mediated by hyperpolarization-activated cyclic nucleotide-gated (HCN) channels. In addition, the magnitude of the rebound depolarization increased with the size of the hyperpolarizing current injected (**Figure 4.11 D**), which is consistent with the activation of a hyperpolarizing-activated cation conductance and further suggests that HCN channels are indeed mediating these responses. It should be noted that membrane hyperpolarization is both necessary and sufficient to activate these channels (Benarroch, 2013).

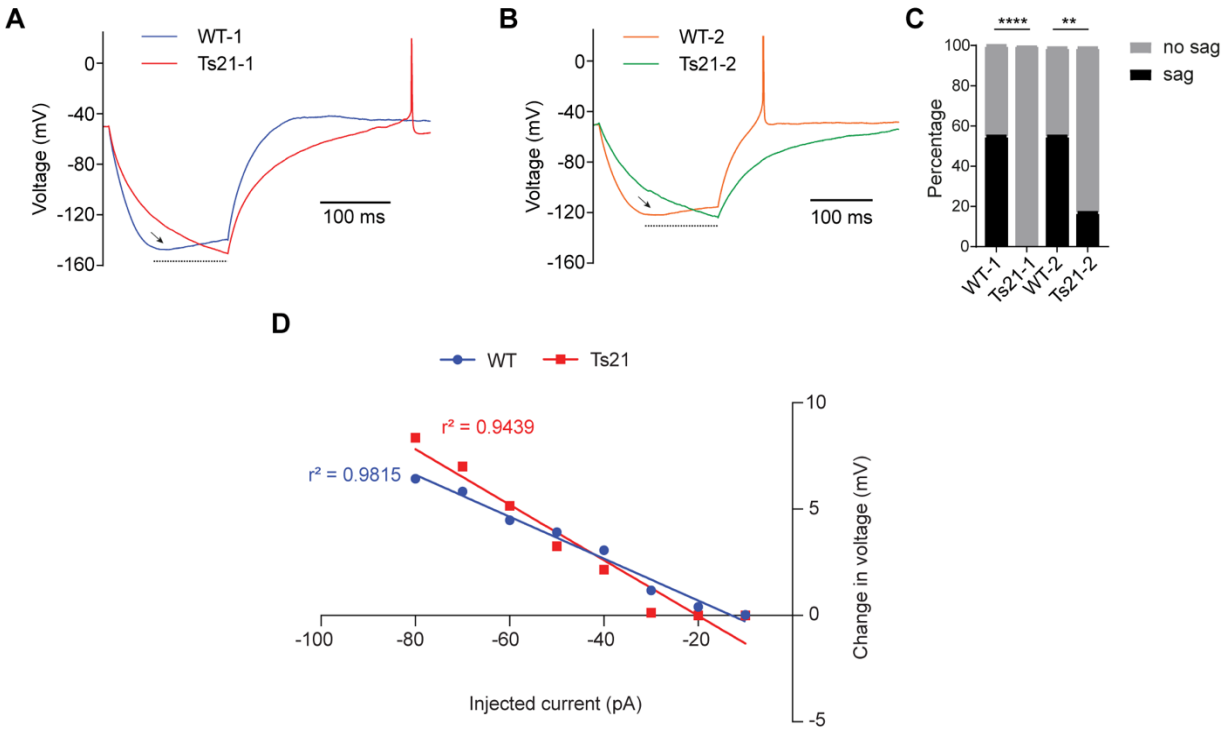

Figure 4.9 Reduced I_h activation in Ts21 neurons.

(**A,B**) Representative voltage traces showing the relationship between hyperpolarizing current injection and the change in transmembrane potential in transplanted hiPSC-derived neurons. Arrows indicate the depolarizing sag.

(**C**) Percentage of cells in which I_h activation could be elicited by injection of hyperpolarizing currents, per cell line (WT-1 55.0% vs. TS21-1 0.0%, Fisher's exact test ****$P < 0.0001$; WT-2 55.56% vs. TS21-2 17.39%, Fisher's exact test **$P < 0.01$).

(**D**) The size of hyperpolarizing current injections demonstrates a positive correlation with the magnitude of rebound depolarization, represented as a change from peak to steady-state voltage. Data is fitted with linear regression (control neurons, $r^2 = 0.9815$; Ts21 neurons, $r^2 = 0.9439$).

4.6 In vivo calcium imaging reveals impaired network synchronization in Ts21 neurons

As discussed in a previous section, transplanted disomic hiPSC-derived neurons exhibit spontaneous calcium activity that occurs in synchronous bursts of neural activation. Similar patterns have been observed in vitro (Kirwan et al., 2015) and after transplantation of hEPSC-derived brain organoids (Mansour et al., 2018). Interestingly, EEG studies of preterm neonates also revealed oscillatory rhythmic patterns of electrical activity (Khazipov and Luhmann, 2006), which strongly supports the notion that a developmental period of spontaneous synchronized burst activity is fundamental for neural network formation and refinement.

There is some evidence that individuals with DS have impaired cortical network activity and neuronal synchronization. First, EEG studies in adults with DS have shown a decrease in the amplitude of resting alpha rhythms, which are a measure of cortical neural synchronization (Babiloni et al., 2010; Katada et al., 2000). Second, functional MRI studies in adults have revealed altered patterns of whole-brain functional connectivity that denote a simplified brain network architecture in DS individuals (Anderson et al., 2013; Pujol et al., 2015). Interestingly, abnormal network activity has also been demonstrated in the neocortex and hippocampus of DS mouse models (Cramer et al., 2015; Raveau et al., 2018; Stern et al., 2015), with evidence of reduced spontaneous network oscillations. Therefore, to investigate whether transplanted human Ts21 neurons exhibited a defect in the pattern of neural network activation, neurons from both disomic (WT-1 and WT-2) and trisomic (Ts21-1 and Ts21-2) cells lines were transduced before transplantation with a lentiviral vector expressing tdTomato and the calcium reporter gene GCaMP6s. In vivo spontaneous calcium imaging of the human grafts revealed that, while neurons in all grafts had spontaneous neural activity 3 months after transplantation, there was a significant reduction in synchronized bursts and overall calcium signals in the Ts21 lines, indicating decreased synchronized neural activity across multiple somas and the neuropil (**Figure 4.10**). To exclude that this synchronization deficit was not due to a delay in the functional maturation of Ts21 networks, recordings were again repeated 5 months after transplantation, which confirmed a strong synchronization defect in trisomic neurons from two independent cell lines.

In addition, differences in spontaneous neural activity could not be explained by Ts21 neurons receiving less synaptic input, as whole-cell voltage-clamp recordings of mEPSC were unaffected in neurons from both Ts21 lines compared to their respective controls, indicating that control and Ts21 neurons were equally able to form functional synaptic connections (**Figure 4.8**). Importantly, the observed deficit in network synchronization was clearly

associated with the presence of an extra copy of Hsa21, as it was reversed by normalization of the Hsa21 copy number in the revertant disomic control (WT-2). The revertant disomic line exhibited not only the same spontaneous bursting pattern as an independent control line derived from a healthy individual (WT-1), but also showed a defined spatiotemporal profile of neural activation as observed in WT-1 (**Figure 4.11**), further supporting the validity of this cell line as an independent euploid control.

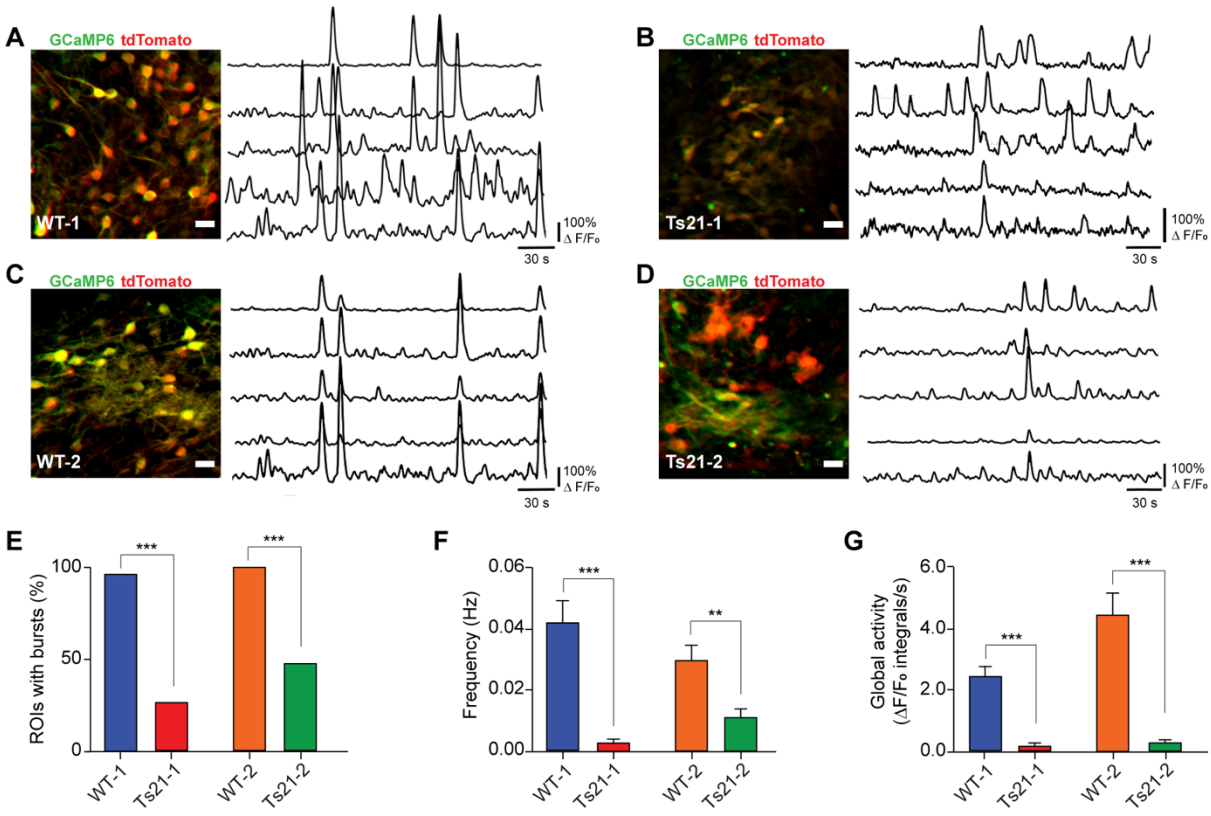

Figure 4.10 Ts21 neurons exhibit decreased burst activity.

(**A,B,C,D**) Left: representative images of cortical regions taken from WT-1 (A), Ts21-1 (B), WT-2 (C) and Ts21-2 (D) grafts in the somatosensory cortex of adult mice. Neurons express tdTomato (red) and GCaMP6s (green). Scale bars, 20 µm. Right: representative $\Delta F/F_0$ calcium traces from 5 active human neurons imaged in WT-1 (A), Ts21-1 (B), WT-2 (C) and Ts21-2 (D) grafts.

(**E**) Percentage of ROIs in WT-1 (50/52 ROIs, *n* = 6 animals), Ts21-1 (10/38 ROIs, *n* = 3 animals), WT-2 (34/34 ROIs, *n* = 3 animals) and TS21-2 (11/23 ROIs, *n* = 3 animals) grafts that exhibit bursts at 3-5 months after transplantation. *Z*-test, ****P* <0.001.

(**F**) Frequency of burst events in WT-1, Ts21-1, WT-2 and Ts21-2 grafts measured at 3-5 months after transplantation. Kruskal-Wallis test, ***P* < 0.01; ****P* < 0.001.

(**G**) Global ROI activity in WT-1, Ts21-1, WT-2 and Ts21-2 grafts measured at 3-5 months after transplantation. Kruskal-Wallis test, ****P* <0.001. Data are represented as mean ± SEM.

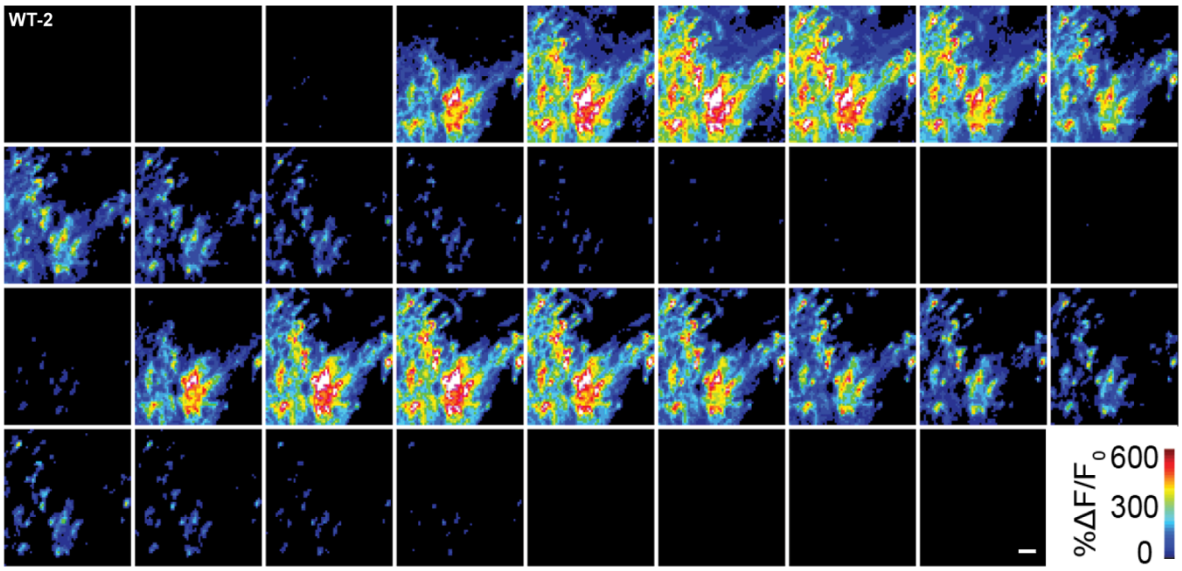

Figure 4.11 Reproducibility of calcium dynamics in an independent control line.

Image frames from a recurrent activity burst in a WT-2 graft at 112 days post-transplantation. Note the same stereotypical spatiotemporal pattern of neural activation across the region of interest. Scale bar, 20 μm.

Chapter 5. Discussion

Most of our understanding of human brain development and disease comes from studies using animal models. Despite the massive importance of these studies, it is an undeniable fact that the human brain is much more complex than that of any other animal, which limits the ability to translate findings from animal models to humans. In this context, the generation of human iPSCs is the first technology to provide unlimited access to human neurons that can be used to dissect mechanisms of neural development and disease. In this study, human iPSC-derived neurons transplanted into a mouse brain, with the aim of providing adequate cell-cell interactions and trophic support to foster neuronal growth and maturation, were used to study cellular mechanisms of human neuron development and early neural circuit formation, and to model a common neurodevelopmental disorder.

5.1 Transplanted human iPSC-derived neurons as a model system for the study of human neural development

Previous in vitro studies of human neuron development using pluripotent stem cells have been hampered by the reduced survival and maturation potential of neurons in culture (Korecka et al., 2016). More recently, three-dimensional culture systems of diverse brain regions have been developed that more closely resemble the developing human brain. Under optimal culture conditions, cerebral organoids can survive for several months in vitro, enabling the generation of neural tissue consisting of multiple cell types with complex cytoarchitecture, including layering of progenitor zones and neurons that is reminiscent of the organizational patterns observed in the early stages of human forebrain development (Lancaster et al., 2013; Mariani et al., 2015; Pasca et al., 2015; Qian et al., 2016). In addition, cerebral organoids have enhanced maturation compared to monolayer cultures, with functional and morphologically mature neurons capable of firing action potentials and establishing synaptic connectivity and neural network activity (Quadrato et al., 2017). However, even these more sophisticated model systems have important limitations, including the lack of a physiological microenvironment, vascularization and an immune system. Mansour and colleagues have recently shown that transplanted cerebral organoids derived from hESCs have a significantly increased viability when compared to 3D cultures, which was attributed to the infiltration of the organoids by the host's vasculature (Mansour et al., 2018). In addition, cellular maturation of neurons was accelerated in vivo compared to cerebral organoids cultured in vitro. Consistent with enhanced maturation, grafted organoids exhibited recurrent bursts of highly synchronized rhythmic neural activity, indicating the generation of functional neural networks.

In the present study, the transplantation of dissociated human NPCs and neurons derived from hiPSCs granted the presence of a myriad of host cells within the grafts and a well-developed vasculature that can support neurodevelopmental processes and the maturation of human neurons. In addition, there is evidence that host cells interact with the human cells within the graft, as demonstrated by the monosynaptic retrograde tracing experiments showing that host neurons input on the human neurons. It is a reasonable assumption that other host cell types, such as astrocytes and oligodendrocytes, will also interact with the human cortical neurons. In this regard, it has been previously established that co-culturing human NPCs with astrocytes greatly enhances cell survival and proliferation, as well as neural differentiation and synaptic maturation of human neurons derived from hiPSCs compared to regular culture conditions (Tang et al., 2013), which highlights the critical role of astrocytes in the morphological and functional maturation of human neurons derived from hiPSCs. Therefore, similarly to transplantation of human cerebral organoids, the transplantation of dissociated human neurons originates cortical tissue grafts that mimic a more physiological microenvironment, with a likely positive impact on neuronal survival and maturation.

This study has shown that human iPSC-derived cortical neural grafts recapitulate several aspects of human cortical development, highlighting the suitably of a such a system to model human neuron and cortical development. After transplantation, cells continued to undergo neurogenesis, generating excitatory cortical neurons of different layer identities and glial cells derived from the ectoderm, which were not present at the time of transplantation. This process, as others have observed after transplantation of hESC-derived neurons (Espuny-Camacho et al., 2013), followed a sequential temporal patterning and time course that matched human cortical neurogenesis (van den Ameele et al., 2014), suggesting that the regulation of neurodevelopmental processes is not only species-specific, but also cell-autonomous, as transplantation into a host where these processes are much shorter did not alter the time course of human neuron development. In addition, the cytoarchitecture within the grafts was reminiscent of the complex organization of the developing human cortex, including the presence of rosette-like structures evocative of a cortical ventricular zone, and modest spatial segregation of neurons with deep and upper cortical layer identities.

Transplantation studies of mouse ESC-derived cortical neurons and embryonic neurons into the visual cortex (V1) of adult mice have demonstrated that grafted neurons send long-range axonal projections and receive afferent inputs to and from the host brain in an area-specific pattern, similar to endogenous V1 cortical neurons (Falkner et al., 2016; Michelsen et al., 2015). Furthermore, transplanted neurons could also respond to visual stimuli in vivo, demonstrating functional integration of the transplanted neurons into the host circuitry.

Interestingly, in the study by Michelsen and colleagues, it was shown that the graft can only develop long-range axonal projections if a cortical lesion is performed in the host brain prior to cell injection (Michelsen et al., 2015). It was hypothesised that an *a priori* lesion is necessary to activate specific guidance cues that allow newly growing axons to reach their appropriate targets. Despite the absence of such a cortical lesion in the present study, bundles of human axons could also project extensively from the cortical neural grafts to distant target areas in the host adult brain, suggesting that human axons are either non-responsive to or can overcome the inhibitory signals to axon growth present in the adult cortex. The specificity of long-range axonal projections suggests human axons might be trailing pre-existing axonal paths in the host brain, or that conserved guidance cues could persist in the adult brain. However, functional connectivity patterns did not recapitulate the appropriate endogenous afferent connectivity to the somatosensory cortex. Indeed, monosynaptic retrograde tracing demonstrated that most afferent input to human neurons originated from other human neurons within the cortical neural graft, with limited input connectivity from mouse cells. Importantly, areas that are known to input extensively to the somatosensory cortex, such as the thalamus, were remarkably absent from the host input into the human cortical graft. It could well be that a lesion is not necessary for human iPSC-derived neurons to adequately survive and mature in an adult host brain, but that an *a priori* lesion is still necessary to achieve more physiological connectivity patterns and functional integration into the host neural circuitry, by providing the necessary cues for meaningful connections to be established.

A key advantage of the proposed model system is that it enables the longitudinal imaging of developing human neurons in an in vivo context, which can be used to acquire insights on neurite pruning, synaptic refinement and functional neural network formation in vivo. Pruning is the process of elimination of neuronal branches and synapses in the developing nervous system to ensure proper formation of a functional neural network, by elimination of exuberant or misguided connections. Neuronal processes can be pruned by small-scale retraction or long-range degeneration (Low and Cheng, 2006); an alternative pruning mechanism has been described exclusively at the developing neuromuscular junction, which involves axosome shedding (Bishop et al., 2004). Our knowledge of the cellular mechanisms of pruning in the central nervous system (CNS) derives almost exclusively from studies using animal models. One important study has used in vivo time-lapse two-photon microscopy of the intact neocortex to explore mechanisms of neurite growth and refinement during early postnatal development in mice (Portera-Cailliau et al., 2005). The authors observed that developing axons exhibit simultaneous growth and pruning, and that pruning occurs primarily by retraction rather than degeneration, which occurred in less than 5% of all observed pruning events. Analogous observations were made in the present study. In addition, both the speed and fraction of axons

growing and retracting is remarkably similar between developing mouse thalamocortical neurons and human cortical neurons, which is surprising given that human axons travel much longer distances to reach their final targets. In another critical time-lapse study looking into the structural maturation of transplanted mouse embryonic neurons, the authors described massive rearrangements of neurites, boutons forming in the vicinity of growth cones, an increase in dendritic spine density and reduction in spine turnover over time (Falkner et al., 2016). The same observations could be replicated in the present study in human cortical neurons, underscoring that many essential cellular mechanisms of developmental neuronal plasticity are conserved among species, despite the obvious time differences to achieve full maturation, which is much delayed in human neurons.

Finally, one of the main advantages of the present approach is that it can model early neuronal network development in populations of human neurons. The occurrence of spontaneous fluctuations in intracellular calcium levels at very early stages of development, even before synapse formation, is well described in multiple species and neuronal circuits (Spitzer, 2006). These early forms of activity have been linked to several neurodevelopmental processes, such as neuronal differentiation, migration, neurotransmitter specification and synaptogenesis (Blankenship and Feller, 2010). Later, when synaptic connections start to form and functional connectivity is established, the spontaneous activity becomes synchronized across groups of neighbouring neurons, which is thought to be essential for the development and refinement of neural circuits (Hanson and Landmesser, 2004; Kirkby et al., 2013; Yamamoto and López-Bendito, 2012). Indeed, the presence of synchronized oscillatory network activity has been described in the developing rodent hippocampus (Garaschuk et al., 1998; Leinekugel et al., 2002), retina (Cang et al., 2005; Wong et al., 1995), spinal cord (Hanson and Landmesser, 2003), thalamus (Moreno-Juan et al., 2017) and neocortex (Adelsberger et al., 2005; Corlew et al., 2004; Garaschuk et al., 2000). These early patterns of highly synchronized spontaneous network activity are eventually replaced postnatally by more sparse and uncorrelated activity patterns, which represent a more mature and efficient network state for neural coding (Golshani et al., 2009). In humans, EEG studies of preterm neonates have also demonstrated the presence of oscillatory rhythmic patterns of electrical activity that disappear with maturation (Khazipov and Luhmann, 2006). Importantly, the detection of synchronized patterns of spontaneous burst firing has been consistently detected in human PSC-derived neuronal populations (Kirwan et al., 2015; Kuijlaars et al., 2016; Mansour et al., 2018; Quadrato et al., 2017), including in the present study.

In the study by Kirwan and colleagues, cultures of hiPSC-derived cortical neurons displayed bursts of synchronized network activity within a limited time interval (from 64-100 days in vitro).

However, most evidence suggests that a transition to more mature, non-synchronized neuronal activity patterns occurs after birth. Thus, the oscillatory activity patterns described in this and other studies are in keeping with the young developmental age of the engrafted neurons. They also indicate the progressive generation of functional neuronal networks in human cortical grafts, highlighting the potential of this model system as an investigative tool to research neurodevelopmental disorders that affect cortical circuit formation.

5.2 Transplanted human iPSC-derived neurons as a model system for human neurodevelopmental disorders

Many biological processes are conserved between different species, which justifies the use of animal models to understand fundamental pathophysiological processes underlying human neurodevelopmental disorders. Contributions from animal studies have been critical for the advancement of biomedical knowledge and to inform drug development for a myriad of human conditions. However, fundamental differences between the human brain and that of animal models preclude a thorough understanding of human diseases affecting the central nervous system, and are one of the likely reasons for the systematic failure to translate findings from bench-to-bedside. The generation of neurons differentiated from patient-specific iPSCs offers a remarkable opportunity to investigate the pathophysiological mechanisms of human diseases. Specifically, human iPSC-derived neurons from patients can model neurodevelopment from very early stages, which can lead to the discovery of new disease phenotypes that would otherwise be inaccessible. This approach is particularly useful in genetically complex conditions such as DS, in which a wide-range of phenotypes likely results from the overexpression of several Hsa21 genes and their interactions, both with other Hsa21 genes and genes elsewhere in the genome. In the present study, this approach has led to the discovery that neurons from DS individuals have reduced synaptic turnover and network synchronicity. Given that several of the genes encoded by Hsa21 are involved in neurogenesis, neurite outgrowth and synaptic plasticity (Nikolaienko et al., 2005), it is unsurprising that several of these processes were shown to be affected in human cortical grafts derived from DS individuals.

Developmental neurite pruning does not seem to be affected in the early development of Ts21 neurons. However, synaptic remodelling was disturbed, with Ts21 neurons exhibiting less bouton and spine dynamics. Several human neurodevelopmental disorders have abnormal synaptic development and cortical connectivity. As an example, non-syndromic autism and fragile X syndrome have been shown in post-mortem studies to have increased dendritic spine density (Hutsler and Zhang, 2010; Irwin et al., 2001; Tang et al., 2014), which has been linked

to defective postnatal synaptic pruning (Tang et al., 2014). Other neurodevelopmental disorders, such as Rett syndrome, have reduced dendritic spine numbers (Belichenko et al., 1994). In DS, density of dendritic spines has been reported inconsistently. In some individuals, a decrease in spine density was observed while in others this was normal, which suggests that a reduction in spine density is not a universal feature of the disease. A Golgi study of cortical pyramidal neurons of autistic brains has revealed that increases in dendritic spine density were positively correlated with the severity of cognitive impairment (Hutsler and Zhang, 2010). Although cognitive impairment is a constant finding in DS individuals, the degree of this phenotype varies widely between individuals. It is plausible that a similar spectrum of dendritic spine dysgenesis exists in DS, which correlates with the severity of intellectual disability. Indeed, the discrepancy in dendritic spine numbers in studies of human neurons derived from distinct iPSC lines could be a true reflection of phenotypic variability between individuals (Shi et al., 2012c; Weick et al., 2013). In addition, the few post-mortem neuropathological reports documenting spine numbers seem to suggest that a reduction in spine density occurs only at later stages of development, but not in the foetal brain. Due to the scarcity of studies in post-mortem foetal tissue of similar age to the neurons in the present study, it is difficult to acknowledge if this phenotype is also present in individuals with DS at any point during brain development. However, given that the increase in spine density was present in two independent cell lines (albeit at significant levels in only one of these cell lines) and was rescued by a return to the euploid status, it is conceivable that this finding has biological significance. Whether this phenotype is linked to the significant decrease in oscillatory network activity in Ts21 neurons would be interesting to explore. The apparent contradiction between increased number of dendritic spines and reduced network synchronization could represent a compensatory mechanism to correct synaptic deficits in Ts21 neurons, perhaps resulting from a higher proportion of non-functional connections being formed (Kanner et al., 2018). Similarly, whether reduced synaptic remodelling in Ts21 neurons could have an impact on the establishment of proper neural connections remains elusive, as it is known that pruning, including synaptic disassembly, is fundamental to ensure the correct formation of a functional neural circuitry. Finally, we did not explore the cortical identity of the cells used for synaptic analysis. Considering the almost complete absence of upper cortical layer neurons in Ts21 grafts, it is possible that the cells used for synaptic analysis were intrinsically different in disease and control groups.

The marked reduction in synchronized burst activity in Ts21 cortical grafts suggests that individuals with DS may have an impaired ability to build functional cortical neuronal networks during early development. Stern and colleagues have found a similar reduction in network bursts in primary cultures of hippocampal neurons from two distinct DS mouse models, which

was attributed to changes in potassium currents in Ts21 neurons (Stern et al., 2015). A further clue to the underlying mechanism of the deficit in neural synchronization in Ts21 neurons came from the observation that hyperpolarization-activated currents (I_h), mediated by HCN channels, were significantly reduced in Ts21 neurons. HCN channels, which upon activation conduct a mixed Na^+/K^+ current, have been implicated in several neuronal functions, notably the generation of neuronal synchronization and network rhythmic oscillations in several brain regions (Wahl-Schott and Biel, 2009). Of note, HCN channel subtypes are differentially expressed at distinct developmental periods and contribute to the maturation of network connectivity (Bender and Baram, 2008). For instance, spontaneous burst activity normally originating from rat neonatal CA3 pyramidal cells has been shown to be reduced when HCN1 channels are pharmacologically blocked, resulting in disruption of hippocampal network activity (Bender et al., 2005), which suggests HCN channels might act as pacemakers to initiate spontaneous rhythmic neuronal firing. Presumably, a similar role for HCN-mediated currents on neuronal synchronization and generation of rhythmic network activity could be found in other developing brain regions. In cortical neurons, hyperpolarization-activated currents are mainly mediated by the HCN1 subtype. Interestingly, RNAseq from the four cell lines used in this study was performed in Rick Livesey's lab, which revealed significantly reduced expression of *HCN1* in both Ts21 cell lines (unpublished data). Several other membrane ion channels also had altered expression in Ts21 cell lines, but the reduced expression of *HCN1* is particularly interesting, given the significant decrease in the proportion of Ts21 neurons exhibiting hyperpolarization-activated currents mediated by HCN channels. Since spontaneous neural oscillations are a hallmark of a developing central nervous system and are involved in the maturation of cortical networks, it is conceivable that the defective generation of synchronized neural activity in Ts21 neurons early in foetal life could lead to permanent pathological changes in cortical circuits, ultimately contributing to the cognitive impairments observed in individuals with DS. Although the expression of several membrane ion channels was disturbed in Ts21 neurons (unpublished data), the reduced expression and activity of HCN1 channels provides a potential link to decreased synchronized burst activity in Ts21 neurons. In the future, it would be interesting to explore the relationship between HCN1 channel activity and the development of synchronous neural activity during cortical neural network formation.

5.3 Concluding remarks

This represents the first in vivo time-lapse study of human cortical neurons and has provided important insights regarding the cellular mechanisms of developmental plasticity of neuronal connections and neural circuit formation. However, several outstanding questions and hurdles remain. First, it is often difficult to compare results from different studies due to differences in

experimental protocols. It is therefore necessary to standardize protocols for the generation of iPSC cell lines, differentiation of neurons and transplantation procedures.

Second, genetic variability between individuals implies that it is often challenging to ascertain whether experimental findings are a truthful representation of biological / pathological processes, rather than a mere reflection of inter-individual differences. A recent study comparing global gene expression data from several independent isogenic trisomic/disomic iPSC pairs failed to find a common pattern of differentially expressed genes in all isogenic pairs, except for genes expressed on Hsa21 (Gonzales et al., 2018). This suggests it is unlikely that Ts21 iPSCs have a single non-Hsa21 transcriptome signature. Thus, the use of multiple cell lines from distinct individuals is normally required to address concerns of genetic variability and ensure that results are reproducible across individuals, which adds to the complexity of these studies.

Third, it remains to be established how much influence the host microenvironment exerts over the developing human neurons. Developmental processes described in this study are clearly protracted in time, suggesting human neurons are following an intrinsic species-specific programme. However, it cannot be excluded that the host microenvironment could be affecting cellular processes of engrafted human cells. Regarding the disease modelling paradigm, it is possible that the transplantation of Ts21 neurons in a normal host brain could mitigated some of the phenotypes associated with the disease. For example, cell-cell interactions with astrocytes have been shown to be fundamental to several aspects of the disease. Chen and colleagues have documented the negative effects of factors secreted by Ts21 astrocytes over Ts21 neurons, such as increased apoptosis and reduced neurogenesis (Chen et al., 2014). Although Ts21 astrocytes were abundantly present in the human cortical grafts, the additional presence of host astrocytes (and potentially other cell types) could compensate for some of the deleterious effects of the Ts21 astroglia. Nevertheless, the present study establishes the validity and pertinence of this model system to gain further insights into human-specific aspects of neural development and to uncover mechanisms of disease.

Finally, it needs to be recognized that animal models (particularly rodents) allow for a more integrative approach at the organism level, which is a limitation of cell-based models. While cell-based models that recapitulate the human trisomy constitute an obvious advantage for the study of cellular and molecular phenotypes in the context of a human genetic background, they are unable to probe complex phenotypes, such as craniofacial dysmorphia or the cognitive disability characteristic of DS. Thus, the ideal strategy to dissect the mechanisms of complex

disorders that affect multiple organ systems and molecular pathways, such as Down syndrome, probably requires the complementary use of animal and human PSC-based models.

References

Adelsberger, H., Garaschuk, O., and Konnerth, A. (2005). Cortical calcium waves in resting newborn mice. Nat. Neurosci. *8*, 988–990.

van den Ameele, J., Tiberi, L., Vanderhaeghen, P., and Espuny-Camacho, I. (2014). Thinking out of the dish: what to learn about cortical development using pluripotent stem cells. Trends Neurosci. *37*, 334–342.

Anderson, J.S., Nielsen, J.A., Ferguson, M.A., Burback, M.C., Cox, E.T., Dai, L., Gerig, G., Edgin, J.O., and Korenberg, J.R. (2013). Abnormal brain synchrony in Down Syndrome. NeuroImage. Clin. *2*, 703–715.

Antonarakis, S.E., Lyle, R., Dermitzakis, E.T., Reymond, A., and Deutsch, S. (2004). Chromosome 21 and down syndrome: from genomics to pathophysiology. Nat. Rev. Genet. *5*, 725–738.

Ardhanareeswaran, K., Mariani, J., Coppola, G., Abyzov, A., and Vaccarino, F.M. (2017). Human induced pluripotent stem cells for modelling neurodevelopmental disorders. Nat. Rev. Neurol. *12*, 265–278.

Avaliani, N., Sørensen, A.T., Ledri, M., Bengzon, J., Koch, P., Brüstle, O., Deisseroth, K., Andersson, M., and Kokaia, M. (2014). Optogenetics reveal delayed afferent synaptogenesis on grafted human-induced pluripotent stem cell-derived neural progenitors. Stem Cells *32*, 3088–3098.

Babiloni, C., Albertini, G., Onorati, P., Muratori, C., Buffo, P., Condoluci, C., Sarà, M., Pistoia, F., Vecchio, F., and Rossini, P.M. (2010). Cortical sources of EEG rhythms are abnormal in down syndrome. Clin. Neurophysiol. *121*, 1205–1212.

Ballard, C., Mobley, W., Hardy, J., Williams, G., and Corbett, A. (2016). Dementia in Down's syndrome. Lancet Neurol. *15*, 622–636.

Barnes, S.J., Sammons, R.P., Jacobsen, R.I., Mackie, J., Keller, G.B., and Keck, T. (2015). Subnetwork-Specific Homeostatic Plasticity in Mouse Visual Cortex In Vivo. Neuron *86*, 1290–1303.

Bartesaghi, R., Guidi, S., Ciani, E., Guide, S., and Ciani, E. (2011). Is it possible to improve neurodevelopmental abnormalities in Down syndrome? Rev. Neurosci. *22*, 419–455.

Becker, L.E., Armstrong, D.L., and Chan, F. (1986). Dendritic Atrophy in Children with Down's Syndrome. Ann. Neurol. *20*, 520–526.

Belichenko, N.P., Belichenko, P. V, Kleschevnikov, A.M., Salehi, A., Reeves, R.H., and Mobley, W.C. (2009). The "Down syndrome critical region" is sufficient in the mouse model to confer behavioral, neurophysiological, and synaptic phenotypes characteristic of Down syndrome. J. Neurosci. *29*, 5938–5948.

Belichenko, P. V., Masliah, E., Kleschevnikov, A.M., Villar, A.J., Epstein, C.J., Salehi, A., and Mobley, W.C. (2004). Synaptic structural abnormalities in the Ts65Dn mouse model of down syndrome. J. Comp. Neurol. *480*, 281–298.

Belichenko, P. V., Kleschevnikov, A.M., Salehi, A., Epstein, C.J., and Mobley, W.C. (2007). Synaptic and cognitive abnormalities in mouse models of down syndrome: Exploring genotype-phenotype relationships. J. Comp. Neurol. *504*, 329–345.

Belichenko, P. V, Oldfors, A., Hagberg, B., and Dahlström, A. (1994). Rett syndrome: 3-D confocal microscopy of cortical pyramidal dendrites and afferents. Neuroreport *5*, 1509–1513.

Benarroch, E.E. (2013). HCN channels: function and clinical implications. Neurology *80*, 304–310.

Bender, R.A., and Baram, T.Z. (2008). Hyperpolarization activated cyclic-nucleotide gated (HCN) channels in developing neuronal networks. Prog. Neurobiol. *86*, 129–140.

Bender, R.A., Galindo, R., Mameli, M., Gonzalez-Vega, R., Valenzuela, C.F., and Baram, T.Z. (2005). Synchronized network activity in developing rat hippocampus involves regional hyperpolarization-activated cyclic nucleotide-gated (HCN) channel function. Eur. J. Neurosci. *22*, 2669–2674.

Bishop, D., Nikić, I., Brinkoetter, M., Knecht, S., Potz, S., Kerschensteiner, M., and Misgeld, T. (2011). Near-infrared branding efficiently correlates light and electron microscopy. Nat. Methods *8*, 568–570.

Bishop, D.L., Misgeld, T., Walsh, M.K., Gan, W.-B., and Lichtman, J.W. (2004). Axon branch removal at developing synapses by axosome shedding. Neuron *44*, 651–661.

Blankenship, A.G., and Feller, M.B. (2010). Mechanisms underlying spontaneous patterned activity in developing neural circuits. Nat. Rev. Neurosci. *11*, 18–29.

Bloomfield, P.S., Bonsall, D., Wells, L., Dormann, D., Howes, O., and Paola, V. De (2018). The effects of haloperidol on microglial morphology and translocator protein levels: An in vivo study in rats using an automated cell evaluation pipeline. J. Psychopharmacol. *32*, 1264–1272.

Briggs, J.A., Mason, E.A., Ovchinnikov, D.A., Wells, C.A., and Wolvetang, E.J. (2013a). Concise Review: New Paradigms for Down Syndrome Research Using Induced Pluripotent Stem Cells: Tackling Complex Human Genetic Disease. Stem Cells Transl. Med. *2*, 175–184.

Briggs, J.A., Sun, J., Shepherd, J., Ovchinnikov, D.A., Chung, T.-L., Nayler, S.P., Kao, L.-P., Morrow, C.A., Thakar, N.Y., Soo, S.-Y., et al. (2013b). Integration-Free Induced Pluripotent Stem Cells Model Genetic and Neural Developmental Features of Down Syndrome Etiology. Stem Cells *31*, 467–478.

Callaway, E.M., and Luo, L. (2015). Monosynaptic Circuit Tracing with Glycoprotein-Deleted Rabies Viruses. J. Neurosci. *35*, 8979–8985.

Camp, J.G., Badsha, F., Florio, M., Kanton, S., Gerber, T., Wilsch-Bräuninger, M., Lewitus, E., Sykes, A., Hevers, W., Lancaster, M., et al. (2015). Human cerebral organoids recapitulate gene expression programs of fetal neocortex development. Proc. Natl. Acad. Sci. *112*, 15672–15677.

Cang, J., Rentería, R.C., Kaneko, M., Liu, X., Copenhagen, D.R., and Stryker, M.P. (2005). Development of Precise Maps in Visual Cortex Requires Patterned Spontaneous Activity in the Retina. Neuron *48*, 797–809.

Chakrabarti, L., Galdzicki, Z., and Haydar, T.F. (2007). Defects in embryonic neurogenesis and initial synapse formation in the forebrain of the Ts65Dn mouse model of Down syndrome. J. Neurosci. *27*, 11483–11495.

Chambers, S.M., Fasano, C.A., Papapetrou, E.P., Tomishima, M., Sadelain, M., and Studer, L. (2009). Highly efficient neural conversion of human ES and iPS cells by dual inhibition of SMAD signaling. Nat. Biotechnol. *27*, 275–280.

Chen, C., Jiang, P., Xue, H., Peterson, S.E., Tran, H.T., McCann, A.E., Parast, M.M., Li, S., Pleasure, D.E., Laurent, L.C., et al. (2014). Role of astroglia in Down's syndrome revealed by patient-derived human-induced pluripotent stem cells. Nat. Commun. *5*, 180–197.

Chen, T.-W., Wardill, T.J., Sun, Y., Pulver, S.R., Renninger, S.L., Baohan, A., Schreiter, E.R., Kerr, R.A., Orger, M.B., Jayaraman, V., et al. (2013). Ultrasensitive fluorescent proteins for imaging neuronal activity. Nature *499*, 295–300.

Chin, M.H., Mason, M.J., Xie, W., Volinia, S., Singer, M., Peterson, C., Ambartsumyan, G., Aimiuwu, O., Richter, L., Zhang, J., et al. (2009). Induced pluripotent stem cells and embryonic stem cells are distinguished by gene expression signatures. Cell Stem Cell *5*, 111–123.

Choi, J., Lee, S., Mallard, W., Clement, K., Tagliazucchi, G.M., Lim, H., Choi, I.Y., Ferrari, F., Tsankov, A.M., Pop, R., et al. (2015). A comparison of genetically matched cell lines reveals the equivalence of human iPSCs and ESCs. Nat. Biotechnol. *33*, 1173–1181.

Chou, S.T., Byrska-Bishop, M., Tober, J.M., Yao, Y., VanDorn, D., Opalinska, J.B., Mills, J.A., Choi, J.K., Speck, N.A., Gadue, P., et al. (2012). Trisomy 21-associated defects in human primitive hematopoiesis revealed through induced pluripotent stem cells. Proc. Natl. Acad. Sci. *109*, 17573–17578.

Contestabile, A., Fila, T., Ceccarelli, C., Bonasoni, P., Bonapace, L., Santini, D., Bartesaghi, R., and Ciani, E. (2007). Cell Cycle Alteration and Decreased Cell Proliferation in the Hippocampal Dentate Gyrus and in the Neocortical Germinal Matrix of Fetuses With Down Syndrome and in Ts65Dn Mice. Hippocampus *17*, 665–678.

Corlew, R., Bosma, M.M., and Moody, W.J. (2004). Spontaneous, synchronous electrical activity in neonatal mouse cortical neurones. J. Physiol. *560*, 377–390.

Cramer, N.P., Xu, X., F Haydar, T., and Galdzicki, Z. (2015). Altered intrinsic and network properties of neocortical neurons in the Ts65Dn mouse model of Down syndrome. Physiol. Rep. *3*, e12655.

Davisson, M.T., Schmidt, C., and Akeson, E.C. (1990). Segmental trisomy of murine chromosome 16: a new model system for studying Down syndrome. Prog. Clin. Biol. Res. *360*, 263–280.

Delabar, J.M., Theophile, D., Rahmani, Z., Chettouh, Z., Blouin, J.L., Prieur, M., Noel, B., and Sinet, P.M. (1993). Molecular mapping of twenty-four features of Down syndrome on chromosome 21. Eur. J. Hum. Genet. *1*, 114–124.

Dierssen, M. (2012). Down syndrome: the brain in trisomic mode. Nat. Rev. Neurosci. *13*, 844–858.

Dierssen, M., and Ramakers, G.J.A. (2006). Dendritic pathology in mental retardation: From molecular genetics to neurobiology. Genes, Brain Behav. *5*, 48–60.

Dimos, J.T., Rodolfa, K.T., Niakan, K.K., Weisenthal, L.M., Mitsumoto, H., Chung, W., Croft, G.F., Saphier, G., Leibel, R., Goland, R., et al. (2008). Induced Pluripotent Stem Cells Generated from Patients with ALS Can Be Differentiated into Motor Neurons. Science *321*, 1218–1221.

Dossi, E., Vasile, F., and Rouach, N. (2018). Human astrocytes in the diseased brain. Brain Res. Bull. *136*, 139–156.

Dubbs, A., Guevara, J., and Yuste, R. (2016). moco: Fast Motion Correction for Calcium Imaging. Front. Neuroinform. *10*, 6.

Edwards, L.J., Kirilina, E., Mohammadi, S., and Weiskopf, N. (2018). Microstructural imaging of human neocortex in vivo. Neuroimage *182*, 184–206.

Espuny-Camacho, I., Michelsen, K.A.A., Gall, D., Linaro, D., Hasche, A., Bonnefont, J.J., Bali, C., Orduz, D., Bilheu, A.A.A., Herpoel, A.A., et al. (2013). Pyramidal neurons derived from human pluripotent stem cells integrate efficiently into mouse brain circuits in vivo. Neuron *77*, 440–456.

Espuny-Camacho, I., Arranz, A.M., Fiers, M., Snellinx, A., Ando, K., Munck, S., Bonnefont, J., Lambot, L., Corthout, N., Omodho, L., et al. (2017). Hallmarks of Alzheimer's Disease in Stem-Cell-Derived Human Neurons Transplanted into Mouse Brain. Neuron *93*, 1–16.

Falkner, S., Grade, S., Dimou, L., Conzelmann, K.-K., Bonhoeffer, T., Götz, M., and Hübener, M. (2016). Transplanted embryonic neurons integrate into adult neocortical circuits. Nature *539*, 248–253.

Franklin, K.B.J., and Paxinos, G. (2008). The mouse brain in stereotaxic coordinates (Boston). Gaillard, A., Gaillard, F., and Roger, M. (1998). Neocortical grafting to newborn and adult rats: developmental, anatomical and functional aspects. Adv. Anat. Embryol. Cell Biol. *148*, 1–86.

Gaillard, A., Prestoz, L., Dumartin, B., Cantereau, A., Morel, F., Roger, M., and Jaber, M. (2007). Reestablishment of damaged adult motor pathways by grafted embryonic cortical neurons. Nat. Neurosci. *10*, 1294–1299.

Garaschuk, O., Hanse, E., and Konnerth, A. (1998). Developmental profile and synaptic origin of early network oscillations in the CA1 region of rat neonatal hippocampus. J. Physiol. *507*, 219–236.

Garaschuk, O., Linn, J., Eilers, J., and Konnerth, A. (2000). Large-scale oscillatory calcium waves in the immature cortex. Nat. Neurosci. *3*, 452–459.

Gardiner, K., Fortna, A., Bechtel, L., Davisson, M.T., and Bernardi, G. (2003). Mouse models of Down syndrome: how useful can they be? Comparison of the gene content of human chromosome 21 with orthologous mouse genomic regions. Gene *318*, 137–147.

Gardiner, K., Herault, Y., Lott, I.T., Antonarakis, S.E., Reeves, R.H., and Dierssen, M. (2010). Down Syndrome: From Understanding the Neurobiology to Therapy. J. Neurosci. *30*, 14943–14945.

Giger, R.J., Hollis, E.R., and Tuszynski, M.H. (2010). Guidance Molecules in Axon Regeneration. Cold Spring Harb. Perspect. Biol. *2*, a001867.

Gimeno, A., García-Giménez, J.L., Audí, L., Toran, N., Andaluz, P., Dasí, F., Viña, J., and Pallardó, F. V (2014). Decreased cell proliferation and higher oxidative stress in fibroblasts from Down Syndrome fetuses. Preliminary study. Biochim. Biophys. Acta *1842*, 116–125.

Ginhoux, F., Lim, S., Hoeffel, G., Low, D., and Huber, T. (2013). Origin and differentiation of microglia. Front. Cell. Neurosci. *7*, 45.

Golden, J.A., and Hyman, B.T. (1994). Development of the Superior Temporal Neocortex Is Anomalous in Trisomy 21. J. Neuropathol. Exp. Neurol. *53*, 513–520.

Golshani, P., Gonçalves, J.T., Khoshkhoo, S., Mostany, R., Smirnakis, S., and Portera-Cailliau, C. (2009). Internally mediated developmental desynchronization of neocortical network activity. J. Neurosci. *29*, 10890–10899.

Gonzales, P.K., Roberts, C.M., Fonte, V., Jacobsen, C., Stein, G.H., and Link, C.D. (2018). Transcriptome analysis of genetically matched human induced pluripotent stem cells disomic or trisomic for chromosome 21. PLoS One *13*, e0194581.

Grienberger, C., and Konnerth, A. (2012). Imaging calcium in neurons. Neuron *73*, 862–885.

Griffin, W.S., Sheng, J.G., McKenzie, J.E., Royston, M.C., Gentleman, S.M., Brumback, R.A., Cork, L.C., Del Bigio, M.R., Roberts, G.W., and Mrak, R.E. (1998). Life-long overexpression of S100beta in Down's syndrome: implications for Alzheimer pathogenesis. Neurobiol. Aging *19*, 401–405.

Grillo, F.W., Song, S., Teles-Grilo Ruivo, L.M., Huang, L., Gao, G., Knott, G.W., Maco, B., Ferretti, V., Thompson, D., Little, G.E., et al. (2013). Increased axonal bouton dynamics in the aging mouse cortex. Proc. Natl. Acad. Sci. U. S. A. *110*, E1514-23.

Gropp, A., Kolbus, U., and Giers, D. (1975). Systematic approach to the study of trisomy in the mouse. II. Cytogenet. Genome Res. *14*, 42–62.

Guenther, M.G., Frampton, G.M., Soldner, F., Hockemeyer, D., Mitalipova, M., Jaenisch, R., and Young, R.A. (2010). Chromatin structure and gene expression programs of human embryonic and induced pluripotent stem cells. Cell Stem Cell *7*, 249–257.

Guidi, S., Bonasoni, P., Ceccarelli, C., Santini, D., Gualtieri, F., Ciani, E., and Bartesaghi, R. (2008). Neurogenesis impairment and increased cell death reduce total neuron number in the hippocampal region of fetuses with Down syndrome. Brain Pathol. *18*, 180–197.

Guidi, S., Ciani, E., Bonasoni, P., Santini, D., and Bartesaghi, R. (2011). Widespread proliferation impairment and hypocellularity in the cerebellum of fetuses with down syndrome. Brain Pathol. *21*, 361–373.

Guihard-Costa, A.-M., Khung, S., and Delbecque, K. (2006). Biometry of Face and Brain in Fetuses with Trisomy 21. Pediatr Res *59*, 33–38.

Gupta, M., Dhanasekaran, A.R., and Gardiner, K.J. (2016). Mouse models of Down syndrome: gene content and consequences. Mamm. Genome *27*, 538–555.

Hanson, M.G., and Landmesser, L.T. (2003). Characterization of the circuits that generate spontaneous episodes of activity in the early embryonic mouse spinal cord. J. Neurosci. *23*, 587–600.

Hanson, M.G., and Landmesser, L.T. (2004). Normal Patterns of Spontaneous Activity Are Required for Correct Motor Axon Guidance and the Expression of Specific Guidance Molecules. Neuron *43*, 687–701.

Harris, K.M., and Weinberg, R.J. (2012). Ultrastructure of synapses in the mammalian brain. Cold Spring Harb. Perspect. Biol. *4*, a005587.

Heikkilä, T.J., Ylä-Outinen, L., Tanskanen, J.M.A., Lappalainen, R.S., Skottman, H., Suuronen, R., Mikkonen, J.E., Hyttinen, J.A.K., and Narkilahti, S. (2009). Human embryonic stem cell-derived neuronal cells form spontaneously active neuronal networks in vitro. Exp. Neurol. *218*, 109–116.

Hibaoui, Y., and Feki, A. (2015). Concise Review: Methods and Cell Types Used to Generate Down Syndrome Induced Pluripotent Stem Cells. J. Clin. Med. *4*, 696–714.

Hibaoui, Y., Grad, I., Letourneau, A., Sailani, M.R., Dahoun, S., Santoni, F.A., Gimelli, S., Guipponi, M., Pelte, M.F.M.M.F., Béna, F., et al. (2014). Modelling and rescuing neurodevelopmental defect of Down syndrome using induced pluripotent stem cells from monozygotic twins discordant for trisomy 21. EMBO Mol. Med. *6*, 259–277.

Holtmaat, A., Bonhoeffer, T., Chow, D.K., Chuckowree, J., De Paola, V., Hofer, S.B., Hübener, M., Keck, T., Knott, G., Lee, W.-C.A., et al. (2009). Long-term, high-resolution imaging in the mouse neocortex through a chronic cranial window. Nat. Protoc. *4*, 1128–1144.

Huo, H.-Q., Qu, Z.-Y., Yuan, F., Ma, L., Yao, L., Xu, M., Hu, Y., Ji, J., Bhattacharyya, A., Zhang, S.-C., et al. (2018). Modeling Down Syndrome with Patient iPSCs Reveals Cellular and Migration Deficits of GABAergic Neurons. Stem Cell Reports *10*, 1251–1266.

Hutsler, J.J., and Zhang, H. (2010). Increased dendritic spine densities on cortical projection neurons in autism spectrum disorders. Brain Res. *1309*, 83–94.

Irwin, S.A., Patel, B., Idupulapati, M., Harris, J.B., Crisostomo, R.A., Larsen, B.P., Kooy, F., Willems, P.J., Cras, P., Kozlowski, P.B., et al. (2001). Abnormal dendritic spine characteristics in the temporal and visual cortices of patients with fragile-X syndrome: A quantitative examination. Am. J. Med. Genet. *98*, 161–167.

Israel, M.A., Yuan, S.H., Bardy, C., Reyna, S.M., Mu, Y., Herrera, C., Hefferan, M.P., Van Gorp, S., Nazor, K.L., Boscolo, F.S., et al. (2012). Probing sporadic and familial Alzheimer's disease using induced pluripotent stem cells. Nature *482*, 216–220.

Jiang, J., Jing, Y., Cost, G.J., Chiang, J.-C., Kolpa, H.J., Cotton, A.M., Carone, D.M., Carone, B.R., Shivak, D.A., Guschin, D.Y., et al. (2013). Translating dosage compensation to trisomy 21. Nature *500*, 296–300.

Kanner, S., Goldin, M., Galron, R., Ben Jacob, E., Bonifazi, P., and Barzilai, A. (2018). Astrocytes restore connectivity and synchronization in dysfunctional cerebellar networks. Proc. Natl. Acad. Sci. U. S. A. *115*, 8025–8030.

Katada, A., Hasegawa, S., Ohira, D., Kumagai, T., Harashima, T., Ozaki, H., and Suzuki, H. (2000). On chronological changes in the basic EEG rhythm in persons with Down syndrome – with special reference to slowing of alpha waves. Brain Dev. *22*, 224–229.

Khazipov, R., and Luhmann, H.J. (2006). Early patterns of electrical activity in the developing cerebral cortex of humans and rodents. Trends Neurosci. *29*, 414–418.

Kim, J.-E., O'Sullivan, M.L., Sanchez, C.A., Hwang, M., Israel, M.A., Brennand, K., Deerinck, T.J., Goldstein, L.S.B., Gage, F.H., Ellisman, M.H., et al. (2011). Investigating synapse formation and function using human pluripotent stem cell-derived neurons. Proc. Natl. Acad. Sci. U. S. A. *108*, 3005–3010.

Kirkby, L.A., Sack, G.S., Firl, A., and Feller, M.B. (2013). A Role for Correlated Spontaneous Activity in the Assembly of Neural Circuits. Neuron *80*, 1129–1144.

Kirwan, P., Turner-Bridger, B., Peter, M., Momoh, A., Arambepola, D., Robinson, H.P.C., and Livesey, F.J. (2015). Development and function of human cerebral cortex neural networks from pluripotent stem cells in vitro. Development *142*, 3178–3187.

Kleschevnikov, A.M., Belichenko, P. V, Villar, A.J., Epstein, C.J., Malenka, R.C., and Mobley, W.C. (2004). Hippocampal Long-Term Potentiation Suppressed by Increased Inhibition in the Ts65Dn Mouse, a Genetic Model of Down Syndrome. J. Neurosci. *24*, 8153–8160.

Korbel, J.O., Tirosh-Wagner, T., Urban, A.E., Chen, X.-N., Kasowski, M., Dai, L., Grubert, F., Erdman, C., Gao, M.C., Lange, K., et al. (2009). The genetic architecture of Down syndrome phenotypes revealed by high-resolution analysis of human segmental trisomies. Proc. Natl. Acad. Sci. *106*, 12031–12036.

Korecka, J.A.A., Levy, S., and Isacson, O. (2016). In vivo modeling of neuronal function, axonal impairment and connectivity in neurodegenerative and neuropsychiatric disorders using induced pluripotent stem cells. Mol. Cell. Neurosci. *73*, 3–12.

Korenberg, J.R., Chen, X.N., Schipper, R., Sun, Z., Gonsky, R., Gerwehr, S., Carpenter, N., Daumer, C., Dignan, P., and Disteche, C. (1994). Down syndrome phenotypes: the consequences of chromosomal imbalance. Proc. Natl. Acad. Sci. U. S. A. *91*, 4997–5001.

Kuijlaars, J., Oyelami, T., Diels, A., Rohrbacher, J., Versweyveld, S., Meneghello, G., Tuefferd, M., Verstraelen, P., Detrez, J.R., Verschuuren, M., et al. (2016). Sustained synchronized neuronal network activity in a human astrocyte co-culture system. Sci. Rep. *6*, 36529.

Kurt, M.A., Kafa, M.I., Dierssen, M., and Davies, D.C. (2004). Deficits of neuronal density in CA1 and synaptic density in the dentate gyrus, CA3 and CA1, in a mouse model of Down syndrome. Brain Res. *1022*, 101–109.

Lancaster, M.A., Renner, M., Martin, C.-A., Wenzel, D., Bicknell, L.S., Hurles, M.E., Homfray, T., Penninger, J.M., Jackson, A.P., and Knoblich, J.A. (2013). Cerebral organoids model human brain development and microcephaly. Nature *501*, 373–379.

Larsen, K.B., Laursen, H., Graem, N., Samuelsen, G.B., Bogdanovic, N., and Pakkenberg, B. (2008). Reduced cell number in the neocortical part of the human fetal brain in Down syndrome. Ann Anat *190*, 421–427.

Lee, H.-C., Tan, K.-L., Cheah, P.-S., and Ling, K.-H. (2016). Potential Role of JAK-STAT Signaling Pathway in the Neurogenic-to-Gliogenic Shift in Down Syndrome Brain. Neural Plast. *2016*, 1–12.

Leinekugel, X., Khazipov, R., Cannon, R., Hirase, H., Ben-Ari, Y., and Buzsáki, G. (2002). Correlated bursts of activity in the neonatal hippocampus in vivo. Science *296*, 2049–2052.
Lejeune, J., Gautier, M., and Turpin, R. (1959). [Study of somatic chromosomes from 9 mongoloid children]. C. R. Hebd. Seances Acad. Sci. *248*, 1721–1722.

Letourneau, A., Santoni, F.A., Bonilla, X., Sailani, M.R., Gonzalez, D., Kind, J., Chevalier, C., Thurman, R., Sandstrom, R.S., Hibaoui, Y., et al. (2014). Domains of genome-wide gene expression dysregulation in Down's syndrome. Nature *508*, 345–350.

Li, L.B.B.B., Chang, K.-H., Wang, P.-R., Hirata, R.K.K.K., Papayannopoulou, T., and Russell, D.W.W.W. (2012). Trisomy Correction in Down Syndrome Induced Pluripotent Stem Cells. Cell Stem Cell *11*, 615–619.

Liang, N., Trujillo, C.A., Negraes, P.D., Muotri, A.R., Lameu, C., and Ulrich, H. (2018). Stem cell contributions to neurological disease modeling and personalized medicine. Prog. Neuro-Psychopharmacology Biol. Psychiatry *80*, 54–62.

Liu, C., Belichenko, P. V, Zhang, L., Fu, D., Kleschevnikov, A.M., Baldini, A., Antonarakis, S.E., Mobley, W.C., and Yu, Y.E. (2011). Mouse models for Down syndrome-associated developmental cognitive disabilities. Dev. Neurosci. *33*, 404–413.

Low, L.K., and Cheng, H.-J. (2006). Axon pruning: an essential step underlying the developmental plasticity of neuronal connections. Philos. Trans. R. Soc. B *361*, 1531–1544.

Lu, J., Esposito, G., Scuderi, C., Steardo, L., Delli-Bovi, L.C., Hecht, J.L., Dickinson, B.C., Chang, C.J., Mori, T., and Sheen, V. (2011). S100B and APP Promote a Gliocentric Shift and Impaired Neurogenesis in Down Syndrome Neural Progenitors. PLoS One *6*, e22126.

Lu, J., Lian, G., Zhou, H., Esposito, G., Steardo, L., Delli-Bovi, L.C., Hecht, J.L., Lu, Q.R., and Sheen, V. (2012). OLIG2 over-expression impairs proliferation of human Down syndrome neural progenitors. Hum. Mol. Genet. *21*, 2330–2340.

Lui, J.H.H., Hansen, D.V. V, and Kriegstein, A.R.R. (2011). Development and Evolution of the Human Neocortex. Cell *146*, 18–36.

Luo, C., Lancaster, M.A., Castanon, R., Nery, J.R., Knoblich, J.A., and Ecker, J.R. (2016). Cerebral Organoids Recapitulate Epigenomic Signatures of the Human Fetal Brain. Cell Rep. *17*, 3369–3384.

Maclean, G.A., Menne, T.F., Guo, G., Sanchez, D.J., Park, I.-H., Daley, G.Q., and Orkin, S.H. (2012). Altered hematopoiesis in trisomy 21 as revealed through in vitro differentiation of isogenic human pluripotent cells. Proc. Natl. Acad. Sci. U. S. A. *109*, 17567–17572.

Mansour, A.A., Gonçalves, J.T., Bloyd, C.W., Li, H., Fernandes, S., Quang, D., Johnston, S., Parylak, S.L., Jin, X., and Gage, F.H. (2018). An in vivo model of functional and vascularized human brain organoids. Nat. Biotechnol. *36*, 432–441.

Mariani, J., Simonini, M.V., Palejev, D., Tomasini, L., Coppola, G., Szekely, A.M., Horvath, T.L., and Vaccarino, F.M. (2012). Modeling human cortical development in vitro using induced pluripotent stem cells. Proc. Natl. Acad. Sci. U. S. A. *109*, 12770–12775.

Mariani, J., Coppola, G., Zhang, P., Abyzov, A., Provini, L., Tomasini, L., Amenduni, M., Szekely, A., Palejev, D., Wilson, M., et al. (2015). FOXG1-Dependent Dysregulation of GABA/Glutamate Neuron Differentiation in Autism Spectrum Disorders. Cell *162*, 375–390.

Marin-Padilla, M. (1976). Pyramidal cell abnormalities in the motor cortex of a child with Down's syndrome. A Golgi study. J. Comp. Neurol. *167*, 63–81.

Mayshar, Y., Ben-David, U., Lavon, N., Biancotti, J.-C., Yakir, B., Clark, A.T., Plath, K., Lowry, W.E., and Benvenisty, N. (2010). Identification and classification of chromosomal aberrations in human induced pluripotent stem cells. Cell Stem Cell *7*, 521–531.

Michelsen, K.A., Acosta-Verdugo, S., Benoit-Marand, M., Espuny-Camacho, I., Gaspard, N., Saha, B., Gaillard, A., and Vanderhaeghen, P. (2015). Area-specific reestablishment of damaged circuits in the adult cerebral cortex by cortical neurons derived from mouse embryonic stem cells. Neuron *85*, 982–997.

Mito, T., and Becker, L.E. (1993). Developmental changes of S-100 protein and glial fibrillary acidic protein in the brain in Down syndrome. Exp. Neurol. *120*, 170–176.

Molliver, M.E., Kostovic´, I., and Van Der Loos, H. (1973). The development of synapses in cerebral cortex of the human fetus. Brain Res. *50*, 403–407.

Molyneaux, B.J., Arlotta, P., Menezes, J.R.L., and Macklis, J.D. (2007). Neuronal subtype specification in the cerebral cortex. Nat. Rev. Neurosci. *8*, 427–437.

Morawski, M., Kirilina, E., Scherf, N., Jäger, C., Reimann, K., Trampel, R., Gavriilidis, F., Geyer, S., Biedermann, B., Arendt, T., et al. (2018). Developing 3D microscopy with CLARITY on human brain tissue: Towards a tool for informing and validating MRI-based histology. Neuroimage *182*, 417–428.

Moreno-Juan, V., Filipchuk, A., Antón-Bolaños, N., Mezzera, C., Gezelius, H., Andrés, B., Rodríguez-Malmierca, L., Susín, R., Schaad, O., Iwasato, T., et al. (2017). Prenatal thalamic waves regulate cortical area size prior to sensory processing. Nat. Commun. *8*, 14172.

Mou, X., Wu, Y., Cao, H., Meng, Q., Wang, Q., Sun, C.C.C., Hu, S., Ma, Y., Zhang, H., Olson, L., et al. (2012). Generation of disease-specific induced pluripotent stem cells from patients with different karyotypes of Down syndrome. Stem Cell Res. Ther. *3*, 14.

Murray, A., Letourneau, A., Canzonetta, C., Stathaki, E., Gimelli, S., Sloan, F., Bena, –, Abrehart, R., Goh, P., Lim, S., et al. (2015). Brief report: Isogenic induced pluripotent stem cell lines from an adult with mosaic down syndrome model accelerated neuronal ageing and neurodegeneration. Stem Cells *33*, 2077–2084.

Nicholas, C.R., Chen, J., Tang, Y., Southwell, D.G., Chalmers, N., Vogt, D., Arnold, C.M., Chen, Y.-J.J., Stanley, E.G., Elefanty, A.G., et al. (2013). Functional Maturation of hPSC-Derived Forebrain Interneurons Requires an Extended Timeline and Mimics Human Neural Development. Cell Stem Cell *12*, 573–586.

Niclis, J.C., Gantner, C.W., Alsanie, W.F., McDougall, S.J., Bye, C.R., Elefanty, A.G., Stanley, E.G., Haynes, J.M., Pouton, C.W., Thompson, L.H., et al. (2017). Efficiently Specified Ventral Midbrain Dopamine Neurons from Human Pluripotent Stem Cells Under Xeno-Free Conditions Restore Motor Deficits in Parkinsonian Rodents. Stem Cells Transl. Med. *6*, 937–948.

Nikolaienko, O., Nguyen, C., Crinc, L.S., Cios, K.J., and Gardiner, K. (2005). Human chromosome 21/Down syndrome gene function and pathway database. Gene *364*, 90–98.

O'Doherty, A., Ruf, S., Mulligan, C., Hildreth, V., Errington, M.L., Cooke, S., Sesay, A., Modino, S., Vanes, L., Hernandez, D., et al. (2005). An Aneuploid Mouse Strain Carrying Human Chromosome 21 with Down Syndrome Phenotypes. Science *309*, 2033–2037.

Ohi, Y., Qin, H., Hong, C., Blouin, L., Polo, J.M., Guo, T., Qi, Z., Downey, S.L., Manos, P.D., Rossi, D.J., et al. (2011). Incomplete DNA methylation underlies a transcriptional memory of somatic cells in human iPS cells. Nat. Cell Biol. *13*, 541–549.

Park, I.-H., Arora, N., Huo, H., Maherali, N., Ahfeldt, T., Shimamura, A., Lensch, M.W., Cowan, C., Hochedlinger, K., and Daley, G.Q. (2008). Disease-Specific Induced Pluripotent Stem Cells. Cell *134*, 877–886.

Pasca, A.M., Sloan, S.A., Clarke, L.E., Tian, Y., Makinson, C.D., Huber, N., Kim, C.H., Park, J.Y., O'Rourke, N.A., Nguyen, K.D., et al. (2015). Functional cortical neurons and astrocytes from human pluripotent stem cells in 3D culture. Nat. Methods *12*, 671–678.

Peron, S., Chen, T.-W., and Svoboda, K. (2015). Comprehensive imaging of cortical networks. Curr. Opin. Neurobiol. *32*, 115–123.

Petanjek, Z., Judaš, M., Šimić, G., Rašin, M.R., Uylings, H.B.M., Rakic, P., and Kostović, I. (2011). Extraordinary neoteny of synaptic spines in the human prefrontal cortex. Proc. Natl. Acad. Sci. *108*, 13281–13286.

Petit, T.L., Leboutillier, J.C., Alfano, D.P., and Becker, L.E. (1984). Synaptic Development in the Human Fetus: A Morphometric Analysis of Normal and Down's Syndrome Neocortex. Exp. Neurol. *83*, 13–23.

Pinter, J.D., Eliez, S., Eric Schmitt, J., George Capone, B.T., and Reiss, A.L. (2001). Neuroanatomy of Down's Syndrome: A High-Resolution MRI Study. Am J Psychiatry *158*, 1659–1665.

Portera-Cailliau, C., Weimer, R.M., De Paola, V., Caroni, P., and Svoboda, K. (2005). Diverse Modes of Axon Elaboration in the Developing Neocortex. PLoS Biol. *3*, e272.

Prè, D., Nestor, M.W., Sproul, A.A., Jacob, S., Koppensteiner, P., Chinchalongporn, V., Zimmer, M., Yamamoto, A., Noggle, S.A., and Arancio, O. (2014). A Time Course Analysis of the Electrophysiological Properties of Neurons Differentiated from Human Induced Pluripotent Stem Cells (iPSCs). PLoS One *9*, e103418.

Pujol, J., Del Hoyo, L., Blanco-Hinojo, L., De Sola, S., Maci, D., Martínez-Vilavella, G., Amor, M., Deus, J., Rodríguez, J., Farr, M., et al. (2015). Anomalous brain functional connectivity contributing to poor adaptive behavior in Down syndrome. Cortex *64*, 148–156.

Qian, X., Nguyen, H.N., Song, M.M., Hadiono, C., Ogden, S.C., Hammack, C., Yao, B., Hamersky, G.R., Jacob, F., Zhong, C., et al. (2016). Brain-Region-Specific Organoids Using Mini-bioreactors for Modeling ZIKV Exposure. Cell *165*, 1238–1254.

Quadrato, G., Nguyen, T., Macosko, E.Z., Sherwood, J.L., Yang, S.M., Berger, D.R., Maria, N., Scholvin, J., Goldman, M., Kinney, J.P., et al. (2017). Cell diversity and network dynamics in photosensitive human brain organoids. Nature *545*, 48–53.

Raveau, M., Polygalov, D., Boehringer, R., Amano, K., Yamakawa, K., and McHugh, T.J. (2018). Alterations of in vivo CA1 network activity in Dp(16)1Yey Down syndrome model mice. Elife *7*, e31543.

Raz, N., Torres, I.J., Briggs, S.D., Spencer, W.D., Thornton, A.E., Loken, W.J., Gunning, F.M., McQuain, J.D., Driesen, N.R., and Acker, J.D. (1995). Selective neuroanatomic abnormalities in Down's syndrome and their cognitive correlates: evidence from MRI morphometry. Neurology *45*, 356–366.

Real, R., Peter, M., Trabalza, A., Khan, S., Smith, M.A., Dopp, J., Barnes, S.J., Momoh, A., Strano, A., Volpi, E., et al. (2018). In vivo modeling of human neuron dynamics and Down syndrome. Science *362*, eaau1810.

Roper, R.J., and Reeves, R.H. (2006). Understanding the Basis for Down Syndrome Phenotypes. PLoS Genet. *2*, 231–236.

Ruiz, S., Diep, D., Gore, A., Panopoulos, A.D., Montserrat, N., Plongthongkum, N., Kumar, S., Fung, H.-L., Giorgetti, A., Bilic, J., et al. (2012). Identification of a specific reprogramming-associated epigenetic signature in human induced pluripotent stem cells. Proc. Natl. Acad. Sci. U. S. A. *109*, 16196–16201.

Shi, Y., Kirwan, P., Smith, J., Robinson, H.P.C., and Livesey, F.J. (2012a). Human cerebral cortex development from pluripotent stem cells to functional excitatory synapses. Nat. Neurosci. *15*, 477–486.

Shi, Y., Kirwan, P., and Livesey, F.J. (2012b). Directed differentiation of human pluripotent stem cells to cerebral cortex neurons and neural networks. Nat. Protoc. *7*, 1836–1846.

Shi, Y., Kirwan, P., Smith, J., MacLean, G., Orkin, S.H., Livesey, F.J., Selkoe, D.J., Hardy, J., Bertram, L., Tanzi, R.E., et al. (2012c). A human stem cell model of early Alzheimer's disease pathology in Down syndrome. Sci. Transl. Med. *4*, 124ra29.

Siarey, R.J., Villar, A.J., Epstein, C.J., and Galdzicki, Z. (2005). Abnormal synaptic plasticity in the Ts1Cje segmental trisomy 16 mouse model of Down syndrome. Neuropharmacology *49*, 122–128.

Smetters, D., Majewska, A., and Yuste, R. (1999). Detecting Action Potentials in Neuronal Populations with Calcium Imaging. Methods *18*, 215–221.

Soldner, F., Hockemeyer, D., Beard, C., Gao, Q., Bell, G.W., Cook, E.G., Hargus, G., Blak, A., Cooper, O., Mitalipova, M., et al. (2009). Parkinson's Disease Patient-Derived Induced Pluripotent Stem Cells Free of Viral Reprogramming Factors. Cell *136*, 964–977.

Song, M., Mohamad, O., Chen, D., and Yu, S.P. (2013). Coordinated development of voltage-gated Na+ and K+ currents regulates functional maturation of forebrain neurons derived from human induced pluripotent stem cells. Stem Cells Dev. *22*, 1551–1563.

Song, S., Grillo, F.W., Xi, J., Ferretti, V., Gao, G., and De Paola, V. (2016). EPBscore: a Novel Method for Computer-Assisted Analysis of Axonal Structure and Dynamics. Neuroinformatics *14*, 121–127.

Sosa, L.J., Postma, N.L., Estrada-Bernal, A., Hanna, M., Guo, R., Busciglio, J., and Pfenninger, K.H. (2014). Dosage of amyloid precursor protein affects axonal contact guidance in Down syndrome. FASEB J. *28*, 195–205.

Spitzer, N.C. (2006). Electrical activity in early neuronal development. Nature *444*, 707–712.
Stagni, F., Giacomini, A., Emili, M., Guidi, S., and Bartesaghi, R. (2018). Neurogenesis impairment: An early developmental defect in Down syndrome. Free Radic. Biol. Med. *114*, 15–32.

Steinbeck, J.A., Koch, P., Derouiche, A., and Brüstle, O. (2012). Human embryonic stem cell-derived neurons establish region-specific, long-range projections in the adult brain. Cell. Mol. Life Sci. *69*, 461–470.

Steinbeck, J.A., Choi, S.J., Mrejeru, A., Ganat, Y., Deisseroth, K., Sulzer, D., Mosharov, E. V, and Studer, L. (2015). Optogenetics enables functional analysis of human embryonic stem cell–derived grafts in a Parkinson's disease model. Nat. Biotechnol. *33*, 204–209.

Stern, S., Segal, M., and Moses, E. (2015). Involvement of Potassium and Cation Channels in Hippocampal Abnormalities of Embryonic Ts65Dn and Tc1 Trisomic Mice. EBioMedicine *2*, 1048–1062.

Suetsugu, M., and Mehraein, P. (1980). Spine distribution along the apical dendrites of the pyramidal neurons in Down's syndrome. A quantitative Golgi study. Acta Neuropathol. *50*, 207–210.

Takahashi, K., Tanabe, K., Ohnuki, M., Narita, M., Ichisaka, T., Tomoda, K., and Yamanaka, S. (2007). Induction of Pluripotent Stem Cells from Adult Human Fibroblasts by Defined Factors. Cell *131*, 861–872.

Takashima, S., Becker, L.E., Armstrong, D.L., and Chan, F.F.-W. (1981). Abnormal neuronal development in the visual cortex of the human fetus and infant with down's syndrome. A quantitative and qualitative golgi study. Brain Res. *225*, 1–21.

Takashima, S., Iida, K., Mito, T., and Arima, M. (1994). Dendritic and histochemical development and ageing in patients with Down's syndrome. J. Intellect. Disabil. Res. *38*, 265–273.

Tang, G., Gudsnuk, K., Kuo, S.-H., Cotrina, M.L., Rosoklija, G., Sosunov, A., Sonders, M.S., Kanter, E., Castagna, C., Yamamoto, A., et al. (2014). Loss of mTOR-Dependent Macroautophagy Causes Autistic-like Synaptic Pruning Deficits. Neuron *83*, 1131–1143.

Tang, X., Zhou, L., Wagner, A.M., Marchetto, M.C.N., Muotri, A.R., Gage, F.H., and Chen, G. (2013). Astroglial cells regulate the developmental timeline of human neurons differentiated from induced pluripotent stem cells. Stem Cell Res. *11*, 743–757.

Thevenaz, P., Ruttimann, U.E., and Unser, M. (1998). A pyramid approach to subpixel registration based on intensity. IEEE Trans. Image Process. *7*, 27–41.

Tornero, D., Tsupykov, O., Granmo, M., Rodriguez, C., Grønning-Hansen, M., Thelin, J., Smozhanik, E., Laterza, C., Wattananit, S., Ge, R., et al. (2017). Synaptic inputs from stroke-injured brain to grafted human stem cell-derived neurons activated by sensory stimuli. Brain *140*, 692–706.

Wahl-Schott, C., and Biel, M. (2009). HCN channels: Structure, cellular regulation and physiological function. Cell. Mol. Life Sci. *66*, 470–494.

Weick, J.P., Liu, Y., and Zhang, S.-C. (2011). Human embryonic stem cell-derived neurons adopt and regulate the activity of an established neural network. Proc. Natl. Acad. Sci. *108*, 20189–20194.

Weick, J.P., Held, D.L., Bonadurer, G.F., Doers, M.E., Liu, Y., Maguire, C., Clark, A., Knackert, J.A., Molinarolo, K., Musser, M., et al. (2013). Deficits in human trisomy 21 iPSCs and neurons. Proc. Natl. Acad. Sci. *110*, 9962–9967.

Weitzdoerfer, R., Dierssen, M., Fountoulakis, M., and Lubec, G. (2001). Fetal life in Down syndrome starts with normal neuronal density but impaired dendritic spines and synaptosomal structure. J. Neural Transm. Suppl. *61*, 59–70.

Wickersham, I.R., Finke, S., Conzelmann, K.-K., and Callaway, E.M. (2007a). Retrograde neuronal tracing with a deletion-mutant rabies virus. Nat. Methods *4*, 47–49.

Wickersham, I.R., Lyon, D.C., Barnard, R.J.O., Mori, T., Finke, S., Conzelmann, K.-K., Young, J.A.T., and Callaway, E.M. (2007b). Monosynaptic Restriction of Transsynaptic Tracing from Single, Genetically Targeted Neurons. Neuron *53*, 639–647.

Wiseman, F.K., Alford, K.A., Tybulewicz, V.L.J., and Fisher, E.M.C. (2009). Down syndrome--recent progress and future prospects. Hum. Mol. Genet. *18*, R75–R83.

Wisniewski KE (1990). Down syndrome children often have brain with maturation delay, retardation of growth, and cortical dysgenesis. Am J Med Genet Suppl. *7*, 274–281.

Wong, R.O.L., Chernjavsky, A., Smith, S.J., and Shatz, C.J. (1995). Early functional neural networks in the developing retina. Nature *374*, 716–718.

Yabut, O., Domogauer, J., and D 'arcangelo, G. (2010). Cellular/Molecular Dyrk1A Overexpression Inhibits Proliferation and Induces Premature Neuronal Differentiation of Neural Progenitor Cells. J. Neurosci. *30*, 4004–4014.

Yamamoto, N., and López-Bendito, G. (2012). Shaping brain connections through spontaneous neural activity. Eur. J. Neurosci. *35*, 1595–1604.

Yu, D.X., Di Giorgio, F.P., Yao, J., Marchetto, M.C., Brennand, K., Wright, R., Mei, A., McHenry, L., Lisuk, D., Grasmick, J.M., et al. (2014). Modeling hippocampal neurogenesis using human pluripotent stem cells. Stem Cell Reports *2*, 295–310.

Yu, J., Vodyanik, M.A., Smuga-Otto, K., Antosiewicz-Bourget, J., Frane, J.L., Tian, S., Nie, J., Jonsdottir, G.A., Ruotti, V., Stewart, R., et al. (2007). Induced pluripotent stem cell lines derived from human somatic cells. Science *318*, 1917–1920.

Yu, T., Li, Z., Jia, Z., Clapcote, S.J., Liu, C., Li, S., Asrar, S., Pao, A., Chen, R., Fan, N., et al. (2010). A mouse model of Down syndrome trisomic for all human chromosome 21 syntenic regions. Hum. Mol. Genet. *19*, 2780–2791.

Zakiewicz, I.M., Bjaalie, J.G., and Leergaard, T.B. (2014). Brain-wide map of efferent projections from rat barrel cortex. Front. Neuroinform. *8*, 5.

Zdaniuk, G., Wierzba-Bobrowicz, T., Szpak, G.M., and Stępień, T. (2011). Astroglia disturbances during development of the central nervous system in fetuses with Down's syndrome. Folia Neuropathol. *49*, 109–114.

Ziv, O., Zaritsky, A., Yaffe, Y., Mutukula, N., Edri, R., and Elkabetz, Y. (2015). Quantitative Live Imaging of Human Embryonic Stem Cell Derived Neural Rosettes Reveals Structure-Function Dynamics Coupled to Cortical Development. PLOS Comput. Biol. *11*, e1004453.

Appendix

The supplementary figures presented in the Appendix are an integral part of the publication that supports this thesis and result from work performed by Dr Alessio Strano at The Gurdon Institute, University of Cambridge, UK. They are shown here with the purpose of characterising the new induced pluripotent stem cell lines and the population of differentiated cells that were used in this study.

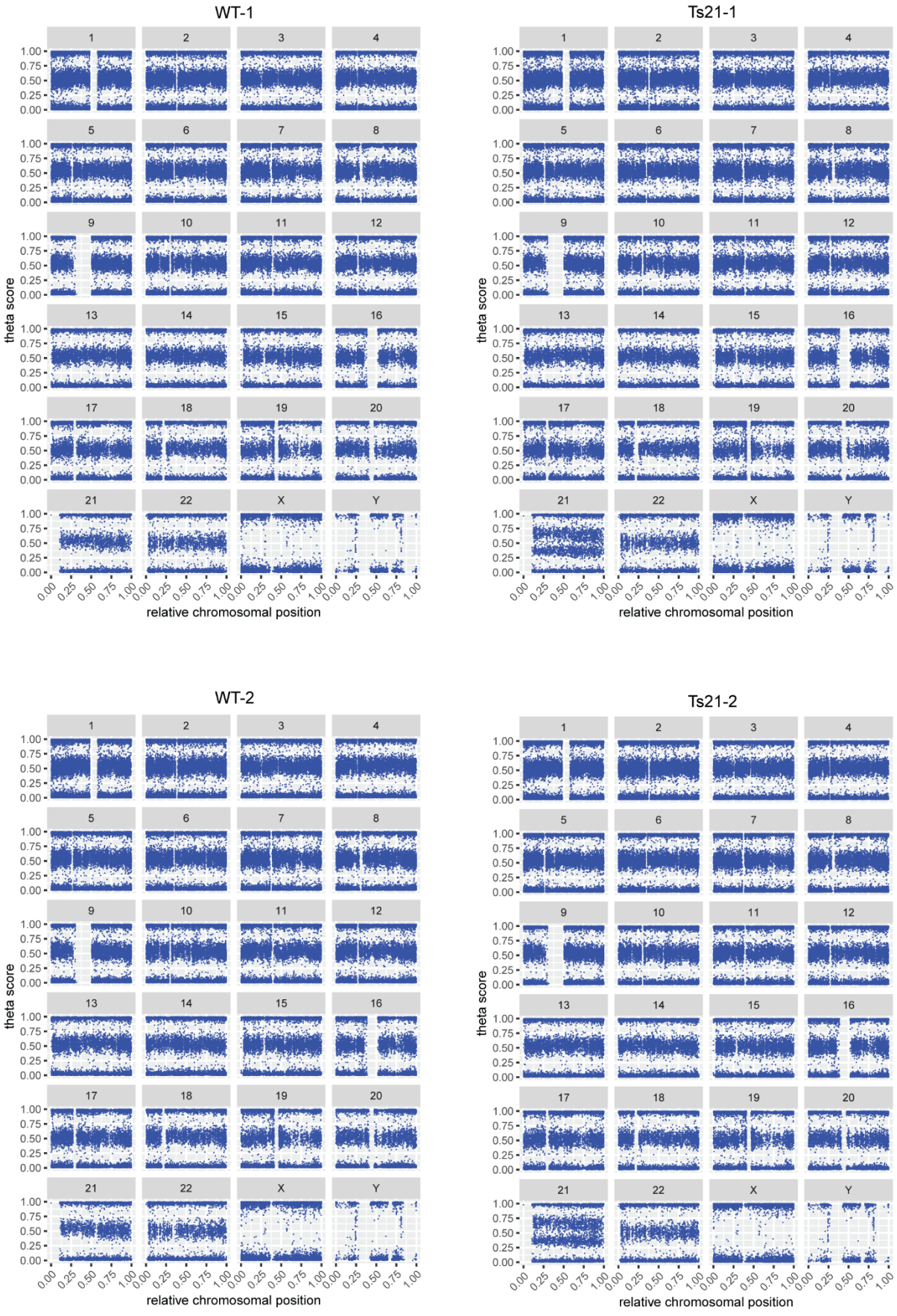

(figure legend on next page)

Supplementary Figure 1. Genome-wide single nucleotide polymorphism array

A genome-wide SNP array was performed using the Illumina Infinium HumanCytoSNP-12 BeadChip array, except for the WT-1 sample, which was run on the CytoSNP850K platform. Data was processed using GenomeStudio 2.0 software, and analysed for copy number variants (CNV) using the CNV-region-report-v2.1 plugin. The B allele frequency plots are shown for all chromosomes. No CNVs were detected in any of the lines used in this study, except for the duplication of Hsa21 in Ts21-1 and Ts21-2. Note reversal of trisomy of chromosome 21 in the revertant disomic cell line, WT-2.

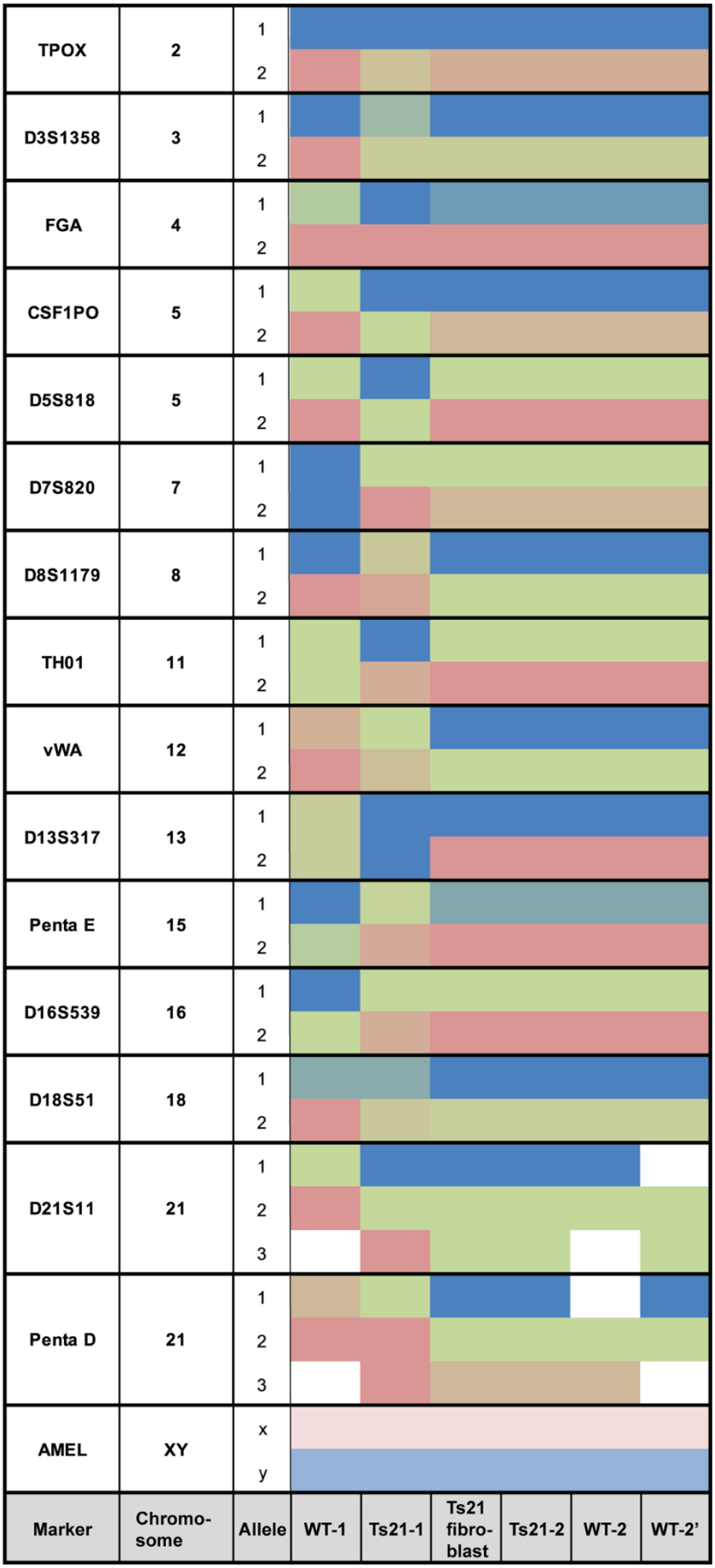

(figure legend on next page)

Supplementary Figure 2. Short tandem repeat assay

A microsatellite short-tandem repeat (STR) assay for DNA typing was performed using the Promega PowerPlex® 16 HS System on all cell lines used in this study, the fibroblasts that originated the Ts21-2 cell line, and on a cell line originating from a second independent revertant disomic subclone of Ts21-2, designated WT-2'. Within the 16 loci analysed, varying repeat lengths are discriminated by alternating colour and are used to define the identity of each cell line. Note that there is no mosaicism in the parental fibroblast population from which the Ts21-2 cell line originated. WT-2 and WT-2' are disomic for different pairs of Hsa21, but otherwise identical to the originating fibroblasts and the Ts21-2 cell line, indicating they are revertant disomic cell lines that originated from a spontaneous loss of a copy of Hsa21 *in vitro*.

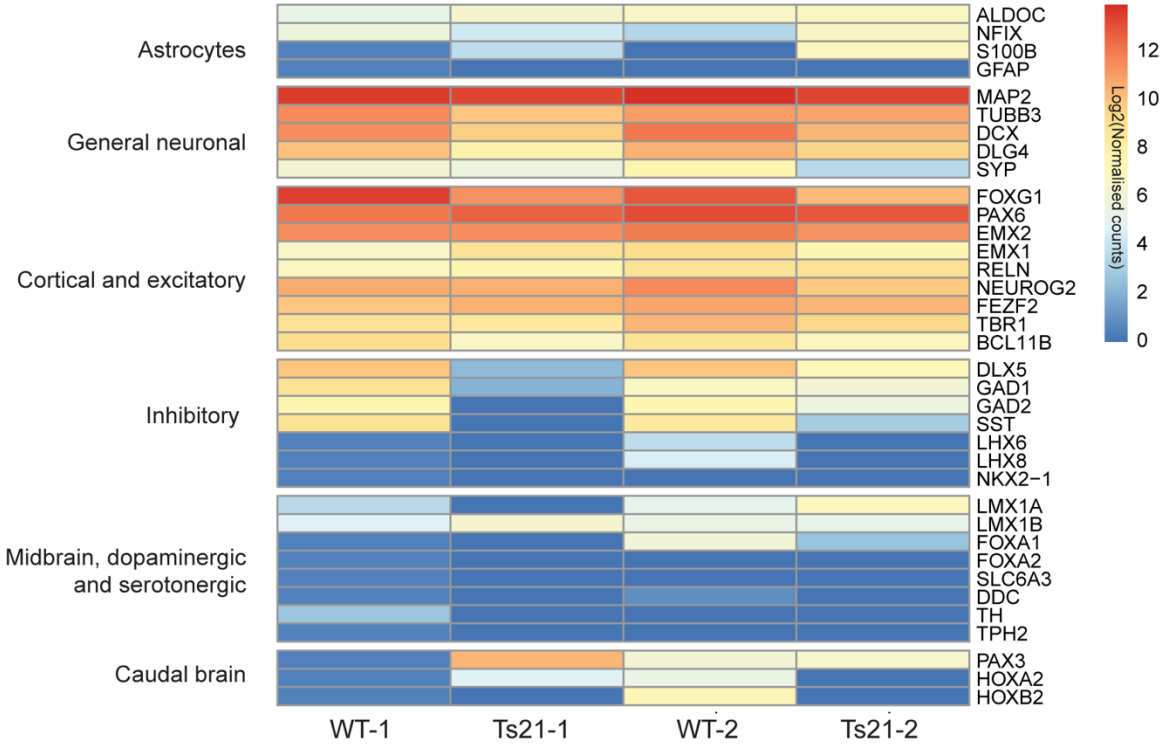

Supplementary Figure 3. Gene expression analysis of hiPSC-derived neuronal cells *in vitro*

A gene expression analysis was performed using a custom NanoString gene expression panel of approximately 250 genes. The heatmap of log2 normalised counts for a panel of selected genes (right) that are expressed in the indicated brain regions and cell types (left) highlights that at day 35-36 (i.e., immediately before transplantation) cultures are enriched in neurons with excitatory cortical identity.